Fakultät für Medizin

Institut für Strahlenbiologie

Role of miR-21 in determining sensitivity of mammary epithelial cells to radiation treatment

Vanja Radulović

Vollständiger Abdruck der von der Fakultät für Medizin der Technischen Universität München zur Erlangung des akademischen Grades eines

Doktors der Naturwissenschaften (Dr. rer. nat.)

genehmigten Dissertation.

Vorsitzender:	**Prof. Dr. Gabriele Multhoff**
Prüfer der Dissertation:	**1. Prof. Dr. Michael J. Atkinson**
	2. Prof. Dr. Aphrodite Kapurniotu

Die Dissertation wurde am 25.04.2017 bei der Technischen Universität München eingereicht und durch die Fakultät für Medizin am 06.12.2017 angenommen.

Dedicated To My Family

CONTENTS

ABSTRACT

Breast cancer represents the most common malignancy in women and the second leading cause of cancer related deaths. Diverse molecular approaches are being developed to improve existing strategies for diagnosis, prognosis and treatments of breast cancer and therefore increase survival of patients.

MicroRNAs involved in breast cancer are potential therapeutic targets. Mir-21, declared as oncomiR, controls almost all aspects of carcinogenesis such as invasion, metastasis, proliferation, and apoptosis. Due to its role, inhibition of miR-21 presents a potential biological strategy for breast cancer therapy. The evidence of this treatment effects on breast cancer cells exist but the effect on the adjacent, normal tissue still needs to be investigated. Thus, in this study we addressed this issue.

We evaluated the response of non-transformed mammary epithelial cells (MCF-10A) and breast cancer cells (MDA-MB-361) to anti-miR-21 treatment alone and in combination with radiation, as radiotherapy presents standard approach for breast cancer patients. We showed that this combined treatment led to significant increase in apoptosis, reduced growth, and cell viability of cancer cells compared to normal cells whose proliferation was not significantly affected.

The proteome of MCF-10A cells was analysed to further extend characterization of this treatment on normal cells. As a novelty, the absence of JNK1/2 phosphorylation was observed in this study with lower expression of total JNK1/2 proteins after miR-21 knockdown in MCF-10A cells. Significant changes of ERK1/2 proteins, members of MAPK signaling pathway, were not detected. Additionally, the variations in protein expression were detected for Nrf2 transcription factor and its downstream pathway with central role in oxidative stress regulation.

Our findings encourage the potential use of anti-miR-21 treatment in combination with radiation, as a novel breast cancer therapeutical strategy as the cellular response to combined treatment was different between cancer and non-cancer cells. Inhibition of miR-21 in breast cancer cells might hold a significant therapy improvement for the breast cancer patients.

ZUSSAMMENFASSUNG

Mammakarzinom ist die häufigste Krebserkrankung der Frau. Zudem sterben an Brustkrebs mehr Frauen sterben als an irgendeiner anderen Krebsform. Deshalb werden zahlreiche neue molekulare Therapieansätze entwickelt, um die Diagnose, Prognose und die Therapie für Mammakarzinom zu verbessern und damit das Überleben der Patienten zu steigern.

MiR-21, die zu der Gruppe der oncomiRs gehört, reguliert viele wichtige Aspekte der Karzinogenese, wie zum Beispiel Invasion, Metastasierung, Proliferation und Apoptose. Daher bietet die Inhibition von miR-21 einen interessanten biologischen Ansatz für die Therapie von Mammakarzinomen. Ein Beweis für die effektive Wirkung dieser Behandlungsform auf Brustkrebszellen existiert bereits. Jedoch gibt es keine ausreichenden Studien über die Wirkung einer anti-miR-21 Therapie auf das angrenzende gesunde Brustgewebe.

Daher wurde die Wirkung von einer anti-miR-21 Behandlung auf nicht-transformierte Brustepithelzellen (MCF-10A) und auf Brustkrebszellen (MDA-MB-361) untersucht. Zudem wurde der Effekt der Therapie in Kombination mit Bestrahlung überprüft, da Strahlentherapie in der Regel standardgemäß zur Behandlung von Brustkrebs eingesetzt wird. Unsere Ergebnisse zeigen, dass die kombinierte Behandlung in Krebszellen zu einem signifikanten Anstieg in Apoptose, reduziertem Wachstum und Zellvitalität führen, während die Proliferation von gesunden Brustzellen nicht signifikant beeinträchtigt wurde. Zum ersten Mal wurde anschließend auch das Proteom von MCF-10A Zellen nach Inhibition von miR-21 untersucht. Es konnte gezeigt werden, dass nach Behandlung JNK1/2 nicht nur geringer exprimiert wird, sondern auch nicht mehr phosphoryliert wird. ERK1/2 Proteine, Mitglieder des MAPK Signalwegs, wurden jedoch nicht beeinträchtigt.

Zusätzlich konnte eine Veränderung in der Menge an dem Nrf2 Transkriptionsfaktor festgestellt werden, welcher eine zentrale Rolle in der oxidativen Stressantwort übernimmt. Zusammenfassend erweist sich die kombinierte Therapie von miR-21 Inhibition mit Strahlentherapie als empfehlenswert, da die Brustkrebstherapie signifikant verbessert werden könnte ohne das normale Brustkrebsgewebe weiter zu schädigen.

ABBREVIATIONS

°C - Celsius degree

µg - microgram (unit of mass)

µl - microliter (unit of volume)

A260 - Absorption at 260nm

A280 - Absorption at 280nm

Ab - Antibody

bp - Base pair

BSA - Bovine Serum Albumin

cDNA - Complementary deoxyribonucleic acid

circRNA - Circular RNA

Cs^{137} - Caesium-137

Ct - Cycle threshold

Da - Dalton

DMEM - Dulbecco's Modified Eagle's Medium

DMSO - Dimethyl sulfoxide

DNA - Deoxyribonucleic acid

DTT - Dithiothreitol

ECL - Enhanced chemiluminescence

EDTA - Ethylenediaminetetraacetic acid

EGF - Epidermal growth factor

eRNA - Enhancer RNA

EV - Empty vector

FACS - Fluorescent activated cell sorting

FCS - Fetal Calf Serum

FSRT - Fractionated Stereotactic Radiotherapy

GAPDH - Glyceraldehyde 3-phosphate dehydrogenase

g - Gram (unit of mass)

Gy - Gray

h - Hours

HRP - Horseradish peroxidase

IMRT - Intensity Modulated Radiotherapy

IR - Ionising radiation

kDa - Kilo Dalton

l - Liter

M - Molar

Min - Minutes

mRNA - Messenger RNA

miRNA - microRNA

ml - milliliter

mm - millimeter

mV - millivolt

ncRNA - Non-coding RNA

PAGE - Polyacrylamide gel electrophoresis

PBS - Phosphate buffered saline

PCR - Polymerase chain reaction

PI - Propidium iodide

piRNA - Piwi-interacting RNA

RNA - Ribonucleic acid

RNase - Ribonuclease

rpm - Revolutions per minute

rRNA – Ribosomal RNA

RT- Room temperature

RT-PCR - Real-time PCR

SDS - Sodium dodecyl sulfate

s - Seconds

siRNA - Small interfering RNA

snRNA - Small nuclear ribonucleic acid

snoRNA - Small nucleolar RNA

SYBR green - Synergy brand green dye

TBP - TATA-binding protein

T-PER - Tissue Protein Extraction Reagent

tRNA - Transfer RNA

Tris - Tris(hydroxymethyl)aminomethane

TU - Transduction units

V - Volt

WB - Western blot

% v/v – Percent volume per volume

% w/v – Percent weight per volume

1 INTRODUCTION

1.1 MicroRNAs – regulators of gene expression

Protein-coding genes are probably the most well-studied sequences in the human genome yet they represent only 2% of the genome. In the last 20 years, two research consortia ENCODE (Encyclopedia of DNA elements) [1] and FANTOM (Functional Annotation of the Mammalian Genome) [2, 3] were set in order to identify all functional elements in the human genome sequence [4]. Their results revealed that the non-protein coding part of the transcriptome, named ncRNAs, also has important functional role in biological processes fundamental for normal development and physiology as for disease also [5].

The classification system of ncRNAs is still evolving, therefore they are generally described according to their mature length, location and orientation respective to the nearest protein-coding gene. Besides classic tRNAs and rRNAs, a number of additional ncRNA types can be classified according to their size into - short ncRNAs (18-200 nt) and long ncRNAs (200 nt to >100 kb in size). Short ncRNAs are further sub-grouped, according to their attributes, into: microRNAs (miRNAs) [6], Piwi-interacting RNAs (piRNAs) [7], small interfering RNAs (siRNAs) [8], small nuclear (snRNAs) and small nucleolar RNAs (snoRNAs) [9], enhancer RNAs (eRNAs) [10, 11] and circular RNAs (circRNAs) [12]. Long ncRNAs (lncRNAs) represent the most prevalent and functionally quite diverse class of ncRNAs [13, 14]. Unlike well-studied short ncRNAs (such as miRNAs and snoRNAs), lncRNAs are poorly conserved across species and are expressed at low levels. Despite this, it is shown that they also have a significant role in a wide variety of important biological processes which qualify them as future important research topic [15].

With ~ 2000 identified human miRNAs [16], they represent today probably the best studied group of ncRNAs. The miRNAs regulate a large number of essential biological functions in normal development. It is estimated that 60% of the human genome may be under regulation of miRNAs [17].

MiRNAs present a family of short (21–25 nucleotides), endogenously expressed, highly conserved, single stranded RNA molecules involved in post-transcriptional regulation of gene expression and therefore have the ability to control diverse cellular and metabolic pathways. This post-transcriptional regulation is based on miRNA target recognition according to the sequence complementarity to positions 2–8 at the 5' end of miRNA, named the seed sequence. Binding of the mature miRNA seed sequence to the 3’ untranslated region (3'UTR) of the messenger RNA (mRNA), can lead to either mRNA degradation (by more precise binding) or translation repression (by less precise binding) mechanism [18-20]. More precise binding presents binding where miRNA and its mRNA target are extensively base-paired (including seed sequence and positions 10-11 of the miRNA) that leads to mRNA degradation by Ago2. Less precise binding is present when imperfect base-pairing at complementary sites occurs, creating bulges that disable activity of Ago2 and repress translation of the targeted mRNA [21, 22]. Binding sites of miRNA targets involved in a translation regulation are mostly located in 3' untranslated region (3'UTR), but can also be located in 5' untranslated region (5'UTR) and coding DNA sequence (CDS) regions [23, 24]. One miRNA can regulate several different mRNA targets but also multiple miRNAs can cooperatively regulate a single mRNA target creating a complex and dynamic regulative system [18, 25].

In order to undertake this regulative role, the mature miRNAs must be processed from a precursor transcript. Their biogenesis represents a complex spatial-controlled process involving two cleavage events performed by ribonuclease III (RNAse III) enyzmes - Drosha and Dicer [26]. The transcription of miRNA genes is performed by RNA polymerase II forming long primary miRNA transcript - pri-miRNA (> 1 kb) with an internal hairpin structure where the mature miRNA sequences are to be found [27]. Nuclear microprocessor complex, formed by Drosha and its cofactor DGCR8, initiates initial maturation by precise cropping of the hairpin structure, leading to the release of a small hairpin RNA – pre-miRNA (~ 65 nt) [27, 28]. Pre-miRNA is then transported into the cytoplasm by the interaction of exportin-5 and Ran-GTP prior to final maturation [29]. The pre-miRNA loop is cleaved in the cytoplasm by Dicer, which cuts near to the

hairpin loop resulting in a short RNA duplex (~ 22 nt) comprised of mature miRNA guide strand (5'-3') and the miRNA passenger strand (3'-5') (Figure 1). Nomenclature of miRNAs originating from 5' arm of the pre-miRNA hairpin structure will contain suffix -5p in their name while the ones originating from 3' arm will be labeled with -3p suffix.

In order to exert their effects, mature miRNAs require formation of a ribonucleoprotein complex with target mRNA - the RNA-induced silencing complexes (RISC). For this purpose, mature single-stranded miRNAs interact with Argonaute proteins (Ago) in RISC complexes and are now able to bind to the target sequence of their mRNA targets, while the passenger strand is degraded (Figure 1) [30-32]. Each of the steps in this process is a potential point of regulation which adds to the complexity of the miRNA-gene regulation [33, 34].

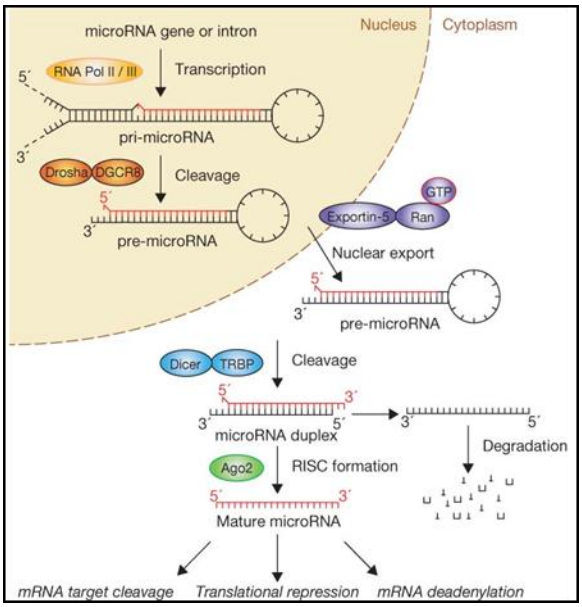

Figure 1. Canonical pathway of miRNA biogenesis. MiRNA genes are transcribed by RNA polymerase II forming long primary miRNA transcript - primary miRNA (pri-miRNA). Nuclear microprocessor complex, formed by Drosha and its cofactor DGCR8, initiates maturation which leads to the release of precursor miRNA (pre-miRNA). They are transported by exportin 5 into the cytoplasm where they are further processed by Dicer and loaded in RISC complex in order to target mRNAs.

MiRNAs in normal cells maintain a balance between cellular processes such as proliferation, cell signaling, differentiation, stress responses, cell adhesion, cell survival and cell death. Since individual miRNAs are able to regulate expression of multiple

genes, any dysregulation of their function could possibly have serious consequences on maintaining this cellular balance [35].

MiRNAs expression signatures are unique to any cancer type and this feature qualifies miRNAs to potentially be used for disease classification as well as both diagnostic and prognostic therapeutic biomarkers [36, 37].

1.2 Biology of breast cancer and incidence

Breast cancer is the most common malignancy in women and the second leading cause of cancer related deaths right after lung cancer worldwide in 2016 [38, 39]. Breast cancers exhibit a group of highly heterogeneous solid tumors of the epithelial tissue with striking genetic and phenotypic diversity which makes them a challenge to diagnose and treat. Diverse histopathological and biological features of breast cancer require considering different therapeutic strategies and treatments [40].

Accurate determination of the breast cancer type is important for selecting the most effective therapeutic treatment. Immunohistochemistry markers (ER, PR and HER2) are used, together with clinicopathological characteristics (tumor size, tumor grade and nodal involvement) for this purpose. At the molecular level, based on gene expression, six intrinsic subtypes of breast cancers can be defined: luminal A, luminal B, HER2-enriched, basal-like, claudin-low and normal-like. The most favorable survival prognosis is for luminal A tumours and the least favorable for HER2 enriched and basal-like breast cancers [41-43]. Triple-negative breast cancers (lacking the expression of all three hormone receptors) are particularly difficult to define and treat due to their lack of response to hormonal therapies and therefore are associated with poor prognosis [44, 45].

Breast tumors arise after the accumulation of somatic mutations in a genetically normal precursor leading to oncogenesis. These mutations can occur either spontaneously or be induced by different factors such as radiation, viruses, free radicals, exposure to toxic environment, chemicals etc. The nature of these genetic mutations or the identities of the initiating cells are both possible mechanisms that determine the breast cancer

heterogeneity (cell-of-origin concept) [46]. Recently, the cancer stem cell (CSC) concept has defined the cell that can maintain tumorigenicity and seed metastases responsible for the tumor initiation, but not for all tumors can be shown to contain them. Breast cancer stem cells (BCSCs) were the first isolated cancer stem cells presenting small population of cells with high proliferation rate able to generate heterogenic types of cancer cells. They have specific phenotype - $CD44^{+}/CD24^{-}$, where highly expressed CD44 has important role in adhesion, migration, invasion, cell proliferation and tumor angiogenesis and low levels of CD24 increase the tumor ability to metastasize [47-49].

1.3 Radiotherapy in treatment of breast cancer

The main therapeutical approaches used for breast cancer are surgery, radiation therapy (radiotherapy), chemotherapy, hormonal therapy as well as recently introduced gene therapies that should suppress the expression of oncogenes (like *HER2*) or restore the activity of tumor-suppressor genes (p53). In order to increase the chance of a successful treatment these are usually combined.

Radiation therapy currently presents the most effective treatment available for localized solid cancers. The goal of this therapy is to depose high energy of radiation into the cancer cells. High-energy photons (X-rays and γ-rays) are mostly used in external beam treatments. Understanding of various molecular mechanisms involved in the radiosensitivity and radioresistance of cancer cells improved the radiation therapy over the past years [50]. Breast conserving surgery followed by external beam radiation therapy represents the standard of care for the majority of breast cancer patients [51]. Whilst adjuvant radiotherapy can improve the overall survival [52] it may induce moderate-to-intense skin reaction in 85-95% of patients [53, 54], and less frequently second cancer development [55]. Prediction of radiotherapy toxicity still represents a problem and till nowadays no suitable method for the assessment of the patient radiosensitivity is established [56]. It is estimated that less than 10% of phase I cancer clinical trials combine chemical and radiation therapy [57] and it is of great importance to elucidate potential side-effects of new targeted therapies applying comprehensive preclinical analysis. The challenge of radiotherapy is to maximize radiation doses to cancer cells while minimizing damage to surrounding healthy tissue [58]. This therapy is applied in a course of multiple fractions over several weeks in order to diminish normal

cell toxicity and to reduce or prevent late side effects of the therapy [59]. Modern high-precision RT techniques are developed (such as FSRT and IMRT) for the delivery of doses to tumors while minimizing the risk of surrounding tissue toxicity [60]. In fractionated stereotactic radiotherapy (FSRT) regimen, the total irradiation dose is fractioned to lower energy doses while in the intensity-modulated radiation therapy (IMRT) regimen the irradiation dose distributed to the tumor is conformed to its shape. Both of the techniques are lowering the risk of tissue toxicity compared to the single-dose radiation regimen.

There is a need for a novel treatment strategy or agent to protect normal tissues from radiation therapy damage, without compromising or enhancing the killing effect of radiation on tumours which includes development of radiosensitizers [61].

Strategies that combine radiation and molecular targeting represent future modalities that will enable increase in cancer cell radiosensitivity and make them prone to effects of radiation [62].

1.4 MiRNAs as markers for radiation biodosimetry

Radiotherapy, as treatment against cancer, is based on the idea that targeted exposure to ionizing radiation destroys the cancer cells while the surrounding normal tissue can stand this exposure and recover from it. Recently, increasing amount of data showed the changes in expression of miRNAs after radiation exposure in different cell types and their specific role in cellular radiosensitivity. It has been suggested that several miRNAs are associated with tumor radioresistance [63-65]. The expression of miR-210, miR-17-92 cluster, miR-31, miR-221 and miR-222 is usually dysregulated in radioresistant cancer cells and promote cancer radioresistance. Normal tissue also represent critical radiotherapy target, therefore few studies on how miRNAs are contributing to the normal tissue radiation responses were performed. MiRNA expression profile changes in endothelial cells after irradiation showed that some of the miRNAs are severely dysregulated, affecting different cellular processes especially inflammatory ones. MiRNAs can also contribute to the radioresistance and radiosensitivity of both normal tissues and cancers, and could potentially predict the risk for normal tissue toxicity. Radiation effects might be modified or associated with differential regulations of miRNA

levels and used in anticancer treatments [66]. Despite the great potential of clinical use of miRNAs, not so many studies have been performed for the establishment of the connection between miRNAs and ionizing radiation exposure [67, 68].

1.5 Role of miRNAs in breast cancer

MiRNAs participate in the regulation of processes vital for maintaining normal cell function. Any dysregulation of these pathways, following alteration of miRNA expression, can contribute to the pathogenesis of cancer. Aberrant targeting of miRNAs may influence translation of several cancer-related genes and lead to cancer initiation, progression, metastasis or drug resistance [69]. Upregulated expression of mir-21 in cancers promotes EMT through targeting the tumor suppressor gene – PTEN [70]. Significantly overexpressed miR-10b [71] and miR-373/520c in breast cancers stimulate cancer cell migration and invasion both *in vitro* and *in vivo* and are known as pro-metastatic miRNAs [72].

In cancers, miRNAs can repress or contribute to its phenotype by inhibition of oncogenes or expression of tumor suppressors, respectively. Oncogenic miRNAs (oncomiRs) are mostly overexpressed while tumor suppressor miRNAs are downregulated in cancers compared to normal tissues. Both reduced and enhanced miRNA expression can promote tumorigenesis depending on their role in this process [73, 74].

The link between altered miRNA expression profiles and development of breast cancer is observed either via the loss of tumor suppressor miRNAs (let-7 family, miR-30a, miR-31, miR-125 family, miR-200 family, miR-342) or the overexpression of oncomiRs (miR-10b, miR-21, miR-155, miR-221, miR-222, miR-373, and miR-520c) in breast cancer cells. OncomiRs exert their oncogenic activity by targeting tumor-suppressor genes and activating oncogenic transcription factors [75, 76]. MiRNA expression profiles can be used to distinguish the molecular breast cancer subtypes [77, 78].

Expanding knowledge of how miRNAs control gene expression in cancers makes them ideal candidates for therapeutic applications. Several miRNAs are described as putative

therapeutic targets in diverse breast cancer therapies: hormone therapies (miR-375 [79], miR-342 [80], miR-221/222 [81]), targeted therapies (miR-210 [82]), therapies associated with response to chemotherapeutic agents (miR-125b [83], miR-21 [84]) or radiation therapy (miR-34a [85]).

MiR-221 and miR-222 are two highly homologous miRNAs, overexpressed in some breast cancers [86], and they have been identified as regulators of epithelial-to-mesenchymal transition (EMT) and its promoting signaling pathway - RAS-RAF-MEK [87]. MiR-125a is a miRNA that is significantly downregulated [88, 89] in breast cancer tissue samples and has been demonstrated to be involved in malignant proliferation and invasion [90]. MiR-335 has been shown to suppress breast cancer cell migration but its expression is either lost or severely downregulated in breast cancers and associated with poor patient prognosis [91]. MiR-1226 is a miRNA with tumor suppressor function in preventing the malignant phenotype by targeting MUC1. Due to the fact that its expression is downregulated in breast cancer cells, its function may be revoked [92].

MiR-21 has important biological role in development [93], morphogenesis [94], differentiation [70] and is overexpressed in breast cancer and positively associated with tumor size, stage and grade of the tumor [95]. It is associated with invasive and metastatic breast cancers [96] and correlates with cancers expressing ER- and HER2+ [97]. It also regulates epithelial-to-mesenchymal transition (EMT) and inhibits tumor-suppressor proteins like PTEN, TPM1, PDCD4 and maspin [98, 99]. Since it is upregulated in breast cancers, targeting miR-21 can restore the expression of genes regulated by it which define miR-21 as a potential target in breast cancer therapy.

Functional studies in breast cancer cells *in vitro* showed that knockdown of miR-21 resulted in reduced proliferation and growth of MCF-7 cells [95] and significantly reduced invasion and lung metastasis *in vivo* of MDA-MB-231 cells [99]. It clearly implicates the importance of miR-21 role in breast cancers and its role in carcinogenesis.

1.6 MiR-21 inhibition (anti-miR-21) as a therapeutic approach in breast cancer treatment

Tumors dependent on overexpression of a miRNA demonstrate oncomiR addiction [100]. MiRNAs and anti-miRNA constructs are already being tested in couple of clinical trials [101, 102]. Targeting miRNAs can also be used as a method to enhance other forms of cancer therapies such as chemotherapy (helping to reduce the drug resistance properties of cancer cells) [103, 104] or radiotherapy (influencing cellular sensitivity to radiation) [105, 106].

Using antisense oligomers (anti-miRs) for the inhibition of oncomiRs present a promising therapeutical strategy [35]. One of the risks of this approach is affecting RNA species other than the intended miRNA target. The assessment of potential off-target effects is important for anti-miR-based studies and the development of miRNA therapeutics. Efficient delivery of anti-miR oligonucleotides is another factor that needs to be taken into consideration for successful development of miRNA-based therapeutic modalities [107, 108].

Suppression of miR-21 is linked to reduced cell proliferation and increased apoptosis in breast cancer cell lines [109]. MiR-21 inhibition studies led to the discovery of candidate targets of miR-21. Although it clearly represent an important miRNA, only a handful of targets (PDC4 and maspin [99], TMP1 [110], PTEN [111] and MMP3 [98]) have been validated, despite *in silico* predictions revealing hundreds (even thousands) of possible targets [112, 113].

1.7 Signalling pathways in cancer (MAPK)

Cellular signaling pathways are mutually interconnected and form complex signaling networks. Regulation of diverse fundamental cellular processes such as growth, proliferation, differentiation, migration and apoptosis depends on information cells receive from different growth factor receptors, cell-matrix and cell-cell interactions. Usually many of the same molecules are engaged in the control of different processes which makes their regulation even more complex [114, 115].

MAPK pathways (mitogen-activated protein kinase) are evolutionarily conserved serine-threonine kinase pathways that respond to extracellular and intracellular stimulations including peptide growth factors, cytokines, hormones, and various cellular stressors such as oxidative stress. Their direct or indirect dysregulation is often implicated in the pathogenesis of cancer [114, 116, 117].

In mammalian cells we can distinguish three branches of the MAPK cascade: the extracellular signal regulated kinase (ERK), the c-Jun N-terminal kinase (JNK) also known as stress-activated protein kinase (SAPK) and p38 MAP kinase (Figure 2). ERK primarily responds to growth factors promoting cell growth while JNK and p38 respond to different stimuli and thus can have multiple effects [118, 119].

Several isoforms of each of these kinases are detected: ERK1/2, ERK3/4, ERK5, ERK7/8; p38-α, -β, -γ (ERK6), and -δ; and JNK 1/2/3 [120, 121]. When the cell receives the stimulus at the plasma membrane, the activation of MAPK signaling axis starts. This is followed by activation of a MAP kinase kinase kinase (MAP3K or MEKK), which activates MAP kinase kinase (MAP2K or MKK) which leads to the final activation of MAP kinase (MAPK). Activated MAPKs phosphorylate various substrate proteins [122].

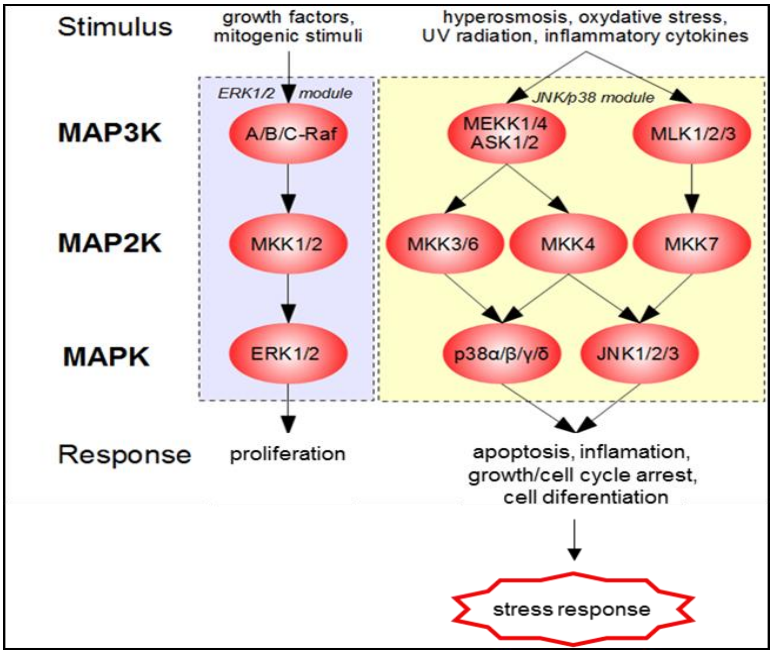

Figure 2. Overview of ERK1/2, JNK and p38 pathways. ERK1/2, JNK and p38 pathways represent three branches of important MAPK cascade in mammalians.

Two MAPK signalling cascades, that are implicated in breast cancer and have function in mammary epithelial cells, were particularly in our focus of interest: the ERK1/2 pathway and the JNK pathway [123].

1.7.1 The ERK1/2 pathway

The ERK1/2 signaling pathway is highly conserved in all eukaryotes and its deregulation is often involved in human disease, including cancers. It has been shown that this pathway is deregulated in 30% of human breast cancers but the nature of the deregulation varies between tumours and cancer subtypes [124].

Most lesions/mutations leading to constitutive activation of this signaling pathway occur early in the pathway, such as overexpression of the receptor tyrosine kinases [125, 126]. ERK1/2 is activated upon phosphorylation by MEK (MEK1 and MEK2), which is itself activated when phosphorylated by Raf. Dysregulatation in ERK1/2 signaling alone is usually not sufficient for the initiation of carcinogenesis and is often accompanied by expression changes of the genes coding for HER2 receptor, c-myc or p53 [127]. Higher ERK1/2 activity can influence metastasis and patient's response to treatment can be dependent on its activity [125, 128].

1.7.2 Correlative regulation between miR-21 and ERK1/2 signaling pathway

MiRNAs and RNA-binding proteins present two main regulators of ERK1/2 signaling pathway [129]. Recent data suggested that the mechanism via miR-21 promote proliferation, migration and inhibition of apoptosis in cancers is performed by activation of this pathway [130]. In HER2 breast cancer cells miR-21 is being upregulated via same pathway thus promoting cell invasion [131]. Directly targeting PTEN, overexpression of miR-21 can lead to the activation of AKT and ERK1/2 pathways and thus promote tumor growth and metastasis [132]. MiR-21 overexpression, characteristic of breast cancer cells, may be a common feature of oncogene pathways associated with activation of ERK1/2 pathway. MiR-21 can regulate and control ERK1/2 signaling pathway even though ERK1/2 is not the direct target of this miRNA.

1.7.3 The JNK pathway

Members of the JNK family are activated in response to cellular stresses including heat shock, ionizing radiation, oxidative stress, DNA-damage, and growth factor deprivation [133-136]. JNK1/2 are expressed in every tissue including breast, while JNK3 is primarily localized in neuronal tissues, testis, and cardiac myocytes [137]. The role of JNKs is mostly pro-apoptotic [138, 139], but they also support processes involved in tumorigenesis like enhancement of cell survival and proliferation [140]. The opposing role of JNKs lies in their ability to activate quite large number of different substrates depending on the stimuli received.

Activation of JNK requires phosphorylation on tyrosine and threonine residues which is catalyzed by upstream MEK4 and MEK7 (these are themselves substrates of MAP3Ks). Following activation, JNK is usually relocated to the nucleus. It is known that JNK phosphorylates the transcription factor c-Jun which can lead to promotion of cell proliferation (Figure 3). This has been already reported in a number of breast cancer cells *in vitro*. Inhibition of JNK has a result in G2/M cell cycle arrest which led to decreased proliferation and apoptosis [123, 141].

Persistent activation of JNK1/2 is involved in cancer development and progression [139, 142]. JNK has a wide range of opposing functions within cells but is best known for its role in triggering apoptosis either through the upregulation of pro-apoptotic genes via activation of transcription factors such as c-Jun or directly modulating the activities of mitochondrial pro- and anti-apoptotic proteins[139].

Inhibitors of JNK are currently used in clinical trials for different cancers where JNK is overexpressed [141].

Potential correlation between JNK1/2 and miR-21 is suggested as blocking JNK1 cause a reduction in the expression of pre-miR-21 which results in decreased cell proliferation. It is proposed that the JNK-1/miR-21 pathway (via c-jun) contributes to chemoresistance of ovarian cancer cells [143]. Recent studies showed that one of the mitogen-activated protein kinase kinases, MAP2K3, is downregulated in breast cancer epithelial cells and

that its upregulation promotes cell senescence. It has been shown in hepatocellular carcinoma cells that MAP2K3 is a novel target for miR-21 [144, 145].

a.

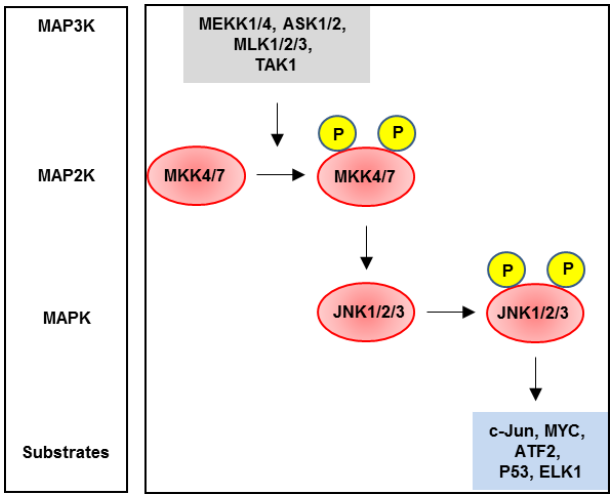

b.

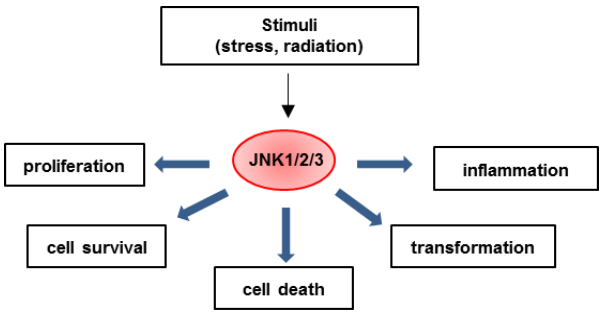

Figure 3. Activation of JNK/1/2/3 pathway. Different stimuli can lead to the activation of this pathway and its downstream substrates (a) [146] which can have effect on diverse cellular processes (b) [142].

1.7.4 Integrins - part of signaling pathway activated upon radiation treatment

Integrins represent a family of cell surface-adhesion receptors (composed of α and β subunits that are noncovalently associated as transmembrane glycoproteins) [147, 148]. Most integrin receptors have the ability to bind a variety of extracellular matrix (ECM) proteins (enabling cell adhesion, tissue maintenance and repair) and to transmit a signal into the cell via association with intracellular kinases (determining cellular responses such as migration, survival, differentiation and motility) [149].

Clustering of ligand bound integrins can activate intracellular signaling pathways. Many of their signaling functions depend on cytoplasmic protein tyrosine kinases named focal adhesion kinase (FAK). FAK is a cytoplasmic protein tyrosine kinase activated by integrins or extracellular stimuli, such as growth factors, which regulates the movement, proliferation and survival of cells (Figure 4). It is recruited to adhesions by intracellular anchor proteins such as *talin* or *paxillin,* where the cross-phosphorylation takes part and enables further intracellular signal transduction [150]. Integrins and signaling receptors can activate Ras/MEK/MAPK pathway and enable promotion of cell growth, cell survival, and cell proliferation [151-153].

FAK is involved in cellular processes important for cancer progression and tumour angiogenesis (apoptosis, adhesion, migration and invasion). Increased FAK expression is shown in several solid cancer types (colon, breast, lung and cervical cancer). FAK promotes tumour progression and metastasis effecting not only cancer cells but also the cells of the tumour microenvironment [154-156].

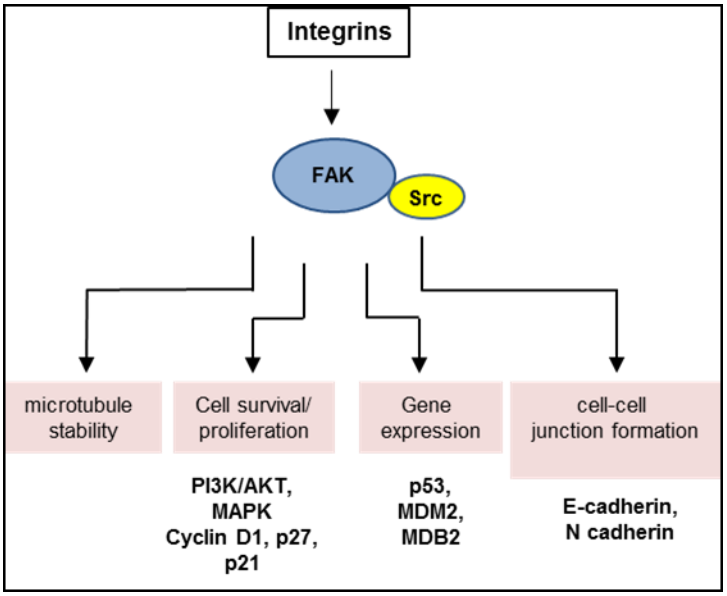

Figure 4. Schematic overview of FAK cellular functions. FAK is activated by integrin family members and regulates the movement, proliferation and survival of cells.

Recent data confirmed that modulation of mir-21 activity can alter the phosphorylation of FAK, established downstream target of PTEN (miR-21 direct target) [157] and

expression of further downstream targets - two metalloproteinases with major role in cell behavior (MMP2 and MMP9) [158, 159].

1.8 Role of reactive oxygen species (ROS) in cancer

Reactive oxygen species (ROS) are highly reactive radicals that can be categorized into two groups: free (superoxide anion (O_2^-) and hydroxyl radical (HO•)) or non-free (hydrogen peroxide (H_2O_2)) radicals of oxygenated molecules. Endogenous levels of ROS are usually generated in the process of mitochondrial oxidative phosphorylation while majority of exogenous may arise after exposure to pollutants, drugs, and xenobiotics [160]. Exposure to ionizing radiation, via radiolysis, also generates ROS species [161].

Under normal physiological conditions, the intracellular levels of ROS are maintained at low levels to prevent cellular damage. Detoxification of ROS is facilitated by non-enzymatic molecules (vitamins A, C and E), endogenous antioxidant molecules (glutathione, coenzyme Q, ferritin, l-carnitine) or through endogenous antioxidant enzymes which scavenge specifically for species of ROS (superoxide dismutase (SOD), catalase (CAT), glutathione peroxidases (GPXs)) [162].

An imbalance of this system, producing elevated levels of ROS, results in oxidative stress. This results in development of different chronic diseases such as cardiovascular diseases [163], diabetes [164] and cancer [165]. Oxidative stress leads to direct or indirect ROS-mediated damage of nucleic acids and proteins [166] and has important role in the initiation of breast cancer progression [162, 167]. Signaling pathways influenced by ROS are persistently elevated in cancers where they have important role in cell growth, proliferation, differentiation, protein synthesis, cell survival, and inflammation [168].

MAPK/ERK1/2 pathway can be activated by ROS generated as a byproduct during estrogen metabolism what leads to increased cell proliferation. ROS generated by estrogens affect pro-proliferative (cyclin D1, Cdc2), prosurvival (AKT), antiapoptotic (Bcl2) and pro-inflammatory (NF-κB) molecules that lead to the activation of several signaling pathways involved in the breast cancer cell survival and proliferation, resulting in the progression of breast cancer. Activation of ERK1/2 through ROS that increases

cell survival and motility is also shown in various cancers including breast cancer. Treatment of breast cancer cells with ROS scavangers or inhibitors of ERK1/2 or MEK promotes apoptosis and cell adhesion [103, 169-171].

Cancer cells usually maintain higher levels of ROS compared to normal cells and this aspect might make them more susceptible to further accumulation of ROS what can be used as a promising therapeutic solution to selectively kill these cells [166, 172]. Better redox status characterization of different breast cancer subtypes are needed in order to prevent potential side effects of higher ROS presence in normal cells.

1.9 NF-E2-related factor-2 (Nrf2) pathway

This pathway has an important role in cellular redox homeostasis and its activation represents one of the main defense systems against oxidative stress. It is also considered as a cell-survival pathway since it represents cellular attempt to defend itself from stressful conditions [173].

Induction of cytoprotective enzymes require three essential components: (1) antioxidant responsive elements (AREs), (2) the redox-sensitive transcription factor (Nrf2) that heterodimerizes with Maf (musculoaponeurotic fibrosarcoma) transcription factors and enables the transcription machinery for expression of ARE-related genes and (3) cytosolic repressor protein - Kelch-like ECH-associated protein 1 (Keap1). Keap1 regulates activation by binding to Nrf2 and promoting its proteosomal degradation. Activation of the pathway leads to production of phase II detoxifying enzymes such as glutathione S-transferase (GST), heme oxygenase 1 (HMOX1), NADPH quinine oxidoreductase 1 (NQO-1), peroxiredoxin (PRX), sulfiredoxin (SRXN), thioredoxin (Trx) [174]. Under basal conditions, repressor Keap1 is bound to Nrf2 promoting its cytoplasmatic position as well as its ubiquitination. Under stress conditions, such as oxidative stimulus, Nrf2 is released from Keap1 and translocated into the nucleus where it binds ARE elements in the promotor regions of gene inducing their transcription [175-177]. The KEAP1–NRF2 complex therefore presents an intracellular sensor able to detect electrophiles or ROS.

The expression of more than 500 genes is modulated by this pathway. These include *NQO1*, *HMOX1*, glutamate-cysteine ligase (*GCL*) and *GST*, each with important role in protection against oxidative stress [178].

Protein kinases can also modulate this pathway post-transcriptionally where the role of each kinase is dependent on the cell type. MAPKs (ERKs and JNKs) have been proposed to regulate Nrf2 but their role and underlying mechanisms are still poorly understood. Nrf2 contains many serine, threonine and tyrosine residues, that may be potential sites for phosphorylation by different kinases such as MAPK cascades, PI3K/AKT pathway, protein kinase C (PKC), GSK3β pathway, JNK, and ERK signaling pathways [179, 180] enabling the release of Nrf2 from Keap1 and activating its nuclear translocation (Figure 5).

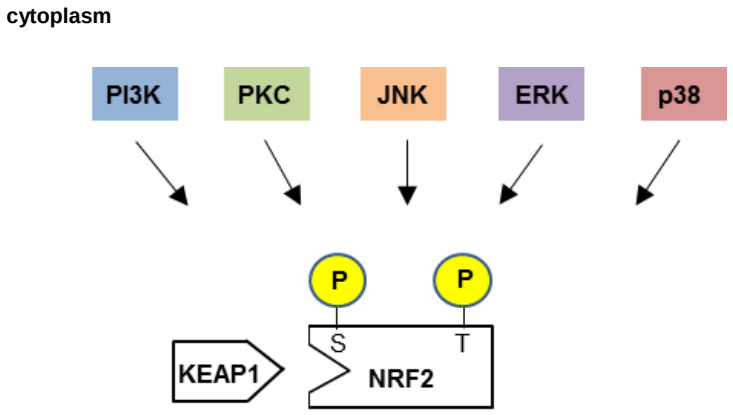

Figure 5. Activation of NRF2 by phosphorylation. Phosphorylation of NRF2 at serine (S) and threonine (T) residues by PI3K, PKC, JNK and ERK also present the way of NRF2 activation leading to its dissociation from KEAP1 and translocation to the nucleus. p38 is known to either stimulate and inhibit the NRF2 nuclear translocation.

Nrf2 is usually considered as a tumor suppressor, where Nrf2-deficient mice are more sensitive to carcinogenesis [181] and Nrf2 loss is correlated with enhanced metastasis [182]. Recently, its role as an oncogene is also suggested. Activation of Nrf2 can promote not only the survival of normal but also cancer cells leading to the promotion of cancer [183]. Upregulated levels of Nrf2 are observed in different types of malignancies, such as lung cancer [184], breast cancer, [185] and head and neck cancers [186]. Hyperactivation of Nrf2 can change the tumor surrounding and favor the survival of

cancer cells (protecting them from excessive oxidative stress by expressing antioxidant target genes, by direct promotion of survival and proliferation) [187]. Nrf2 can contribute to the chemoresistance of cancer cells by preventing the intracellular accumulation of drugs in cancer cells thus protecting them from apoptosis [188]. Inhibition of Nrf2 as therapeutic approach depends on the type of cancer and factors that contribute to the activation of Nrf2. Nrf2 represents potential therapeutic cancer target as well as prognostic molecular marker for the determination of the cancer progression [189].

1.10 Hypothesis

Main hypothesis of this thesis assumes that treatment with anti-miR-21 will make breast cancer cells more sensitive (susceptible) to radiation treatment while the non-cancerous cells will be able to sustain this therapy combination.

In order to test this hypothesis we aim to:

- Identify the differences in cellular response between non-transformed mammary epithelial (MCF-10A) and breast cancer (MDA-MB-361) cell lines to the combined treatment of anti-miR-21 and low (0.25 Gy) and medium (2.5 Gy) dose of irradiation
- Characterize the influence of miR-21 knockdown on MCF-10A proteome, without and in combination with radiation
- Discover and verify new potential targets of miR-21

2 MATERIALS

2.1 Chemicals

2- mercaptoethanol, Sigma-Aldrich, Steinheim, Germany

5x First Strand Buffer, Invitrogen, Darmstadt, Germany

Acid-Phenol:Chloroform, 5:1 Solution pH 4.5, Thermo Fisher Scientific, Darmstadt, Germany

Bovine serum albumin (BSA), Sigma-Aldrich, Steinheim, Germany

Bradford reagent, Sigma-Aldrich, Steinheim, Germany

Bromphenol blue, Roche molecular diagnostics, Mannheim, Germany

Cholera Toxin from *Vibrio cholera*, Sigma-Aldrich, Steinheim, Germany

di-Sodiumhydrogen-phospate, Merck, Darmstadt, Germany

DMEM, high glucose, GlutaMAX™ Supplement, Gibco, Karlsruhe, Germany

DMEM/F12, Gibco, Karlsruhe, Germany

DMSO (Dimethylsulfoxid), Sigma-Aldrich, Steinheim, Germany

DTT, Invitrogen, Darmstadt, Germany

ECL™ Select Western Blotting Detection Reagent, GE Healthcare, Munich, Germany

EDTA (Ethylenediaminetetraacetic acid), Sigma-Aldrich, Steinheim, Germany

EGF (Animal-Free Recombinant Human EGF), Peprotech, Hamburg, Germany

Ethanol absolute, Merck, Darmstadt, Germany

Ethidium bromide (EtBr), Merck, Darmstadt, Germany

Fetal Calf Serum Gold (FCS), PAA Laboratories GmbH, Cölbe, Germany

Glycine, Merck, Darmstadt, Germany

Horse serum, Thermo Fisher Scientific, Darmstadt, Germany

Hydrocortisone, Sigma-Aldrich, Steinheim, Germany

Hydrogen chloride, 1 mol/l (1 N), Merck, Darmstadt, Germany

Insulin from bovine pancreas, Sigma-Aldrich, Steinheim, Germany

Isopropanol, Merck, Darmstadt, Germany

Lipofectamin™ 2000, Invitrogen, Karlsruhe, Germany

Magnesium chloride, Sigma-Aldrich, Steinheim, Germany

Methanol, Merck, Darmstadt, Germany

NuPAGE® MES SDS Running Buffer (20X), Thermo Fisher Scientific, Darmstadt, Germany

OligodT primers, Invitrogen, Darmstadt, Germany

Opti-MEM medium, Gibco Darmstadt, Germany

Paraformaldehyde, Merck, Darmstadt, Germany

PEG-it™ Virus Precipitation Solution (5X), BioCat GmbH, Heidelberg, Germany

Phenol/chloroform, Sigma-Aldrich, Steinheim, Germany

Phosphate buffered saline (PBS), Invitrogen, Darmstadt, Germany

PhosSTOP (Phosphatase Inhibitor Coctail), Roche Diagnostics, Mannheim, Germany

Ponceau-S-Red, Sigma-Aldrich, Steinheim, Germany

Powdered milk, Carl Roth GmbH, Karlsruhe, Germany

Propidium iodide, Sigma-Aldrich, Steinheim, Germany

Protease inhibitor cocktail tablets, Roche Diagnostics, Mannheim, Germany

Puromycin dihydrochloride, Sigma-Aldrich, Steinheim, Germany

Random primers, Promega. Mannheim, Germany

Reverse transcriptase SuperScript® II, Invitrogen, Darmstadt, Germany

RNase OUT, Invitrogen, Darmstadt,Germany

Sodium chloride, Merck, Darmstadt, German

Sodium hydroxide, Merck, Darmstadt, Germany

Soybean Trypsin Inhibitor, Thermo Fisher Scientific, Darmsdtadt, Germany

SYBR Green Master Mix 2x, Applied Biosystems, Darmstadt, Germany

T-PER, Thermo Scientific, Darmstadt, Germany

Tris, Merck, Darmstadt, Germany

Trypsin, Invitrogen, Darmstadt, Germany

Tween 20, Sigma-Aldrich, Steinheim, Germany

X-Gal, Thermoscientific, Darmstadt, Germany

2.2 Instruments and consumables

7900HT Fast Real-Time PCR System, Applied Biosystems, Darmstadt, Germany

96-well plates, Nunclon™ Delta Surface, Thermo Fisher Scientific, Darmsdtadt, Germany

96-well White opaque Tissue Culture Plate, Corning Incorporated, Wiesbaden, Germany

Alpha Innotech ChemiImager System FluorChem HD2, Biozym, Hessisch Oldendorf, Germany

Blotting paper, extra tick, Protean®, Bio-Rad Laboratories, Munich, Germany

Cell culture flasks (T125, T75, T25) Greiner BioOne GmbH, Frickenhausen, Germany

Cell Culture plates multi – wells, Corning Incorporated, Wiesbaden, Germany

Centrifuge Biofuge pico, Heraeus Instruments, Osterode, Germany

Centrifuge Eppendorf 5424R, Eppendorf, Hamburg, Germany

Centrifuge Rotina 420R, Andreas Hettich, Tuttlingen, Germany

Centrifuge tubes (15 ml and 50 ml), Greiner BioOne GmbH, Frickenhausen, Germany

Centrifuge/vortex combi-spin FVL 2400, PeqLab, Erlangen, Germany

Cryotube™ vials (1 ml), Kisker Biotech GmbH, Steinfurt, Germany

Cs^{137}- γ-source, HWM-D 2000 machine, Wälischmiller Engineering, Markdorf, Germany

Dispenser Multipette® plus, Eppendorf, Hamburg, Germany

Electrophoresis Cell, Novex mini cell, Invitrogen, Darmstadt, Germany

Electrophoresis Power Pac Basic, Bio-Rad Laboratories, Munich, Germany

Electrophoresis Transfer Blot, Bio-Rad Laboratories, Munich, Germany

Freezer -20°C, Liebherr, Ehingen(Donau), Germany

Freezer -80 °C, New Brunswick, Nurtingen, Germany

GravityPLUS™ plates, InSphero AG, Schlieren, Switzerland

Giemsa, Merck, Darmstadt, Germany

Heating block, Thermomixer comfort 1.5 ml, Eppendorf, Hamburg, Germany

Heating block, Thermomixer comfort 2ml, Eppendorf, Hamburg, Germany

Incubator, Sanyo, Bad Nenndorf, Germany

LSR II flow cytometer BD, BD Biosciences, Heidelberg, Germany

Magnet plate, NeoLab, Heidelberg, Germany

Magnets stirrer, NeoLab, Heidelberg, Germany

Microplate reader Infinite® M200, Tecan, Switzerland

Microscope Axiovert 25, Carl Zeiss, Jena, Germany

Microscope KEYENCE BZ-9000 series, Keyence, Frankfurt, Germany

Multiple plate reader, TECAN Infinity M200, Tecan, Crailsheim, Germany

Nalgene Cryo Freezing Container, Sigma-Aldrich, Steinheim, Germany

Nitrocellulose blotting membrane, Amersham™ Protran™ 0.2 µm, GE Healthcare, Munich, Germany

Nonidet™ P-40, Sigma-Aldrich, Steinheim, Germany

Optical Adhesive Film, MicroAmp, RQ-PCR, Applied Biosystems, Darmstadt, Germany

Parafilm® Carl Roth, Karlsruhe, Germany

Petri dishes, Greiner Labortechnik GmbH, Fickenhausen, Germany

pH meter, InoLab, Walheim,Germany

Pipette tips Graduated Filter Tips, TipOne Starlab, Ahrensburg, Germany

Pipettes 10, 20, 100, 200, 1000µl, Eppendorf, Hamburg, Germany

Reaction tubes 1.5 ml, 2.0ml, Eppendorf, Hamburg, Germany

Reaction tubes 15ml, 50ml, Falcon Blue Max BD Biosciences, Heidelberg, Germany

Sonicator B12, Branson, Ultrasonic, Danbury, USA

StepOnePlus ™ Real-Time PCR System, Applied Biosystems, Darmstadt, Germany

Stericup® 0.45 mm filters, Millipore Merck, Darmstadt, Germany

Sterile laminar flow work bench, BDK Luft und Reinraumtechnik, Sonnenbühl-Genkingen, Germany

Z1 Coulter Particle counter, Beckman Coulter, Fullerton, USA

2.3 Buffers and solutions

Laemlli buffer (4x)

Tris-HCl, pH 6.8	240 mM
SDS	8 % w/v
Glycerine	40 % v/v
Bromphenolblue	0.08 % w/v
β-mercaptoethanol	20 % v/v

TBS-T (10x)

Tris	4.24 g
Tris-HCl	26 g
NaCl	80 g
miliQ water	900 ml (dissolve the salts)
Tween 20	10 ml

Towbin buffer

Tris	3.03 g
Glycine	14.4 g
Destilled water	700 ml
Ethanol	200 ml
Destilled water	up to 1 liter

Ponceau-S-Red solution

Ponceau-S-Red	0.2 % w/v
Acetic acid	5 % v/v
Destilled water	500 ml

Western blot (Blocking buffer)

Powdered milk	8 g
TBS-T (1x)	100 ml

FACS – Solution I

NaCl	10 mM
Na-citrate	4 mM
RNase	10 µg/ml
Nonidet P-40	0.3 % v/v
PI	50 µg/ml

FACS – Solution II

Citric acid	70 mM
Sucrose	250 mM
PI	50 µg/ml

2.4 Commercial kits

CellTiter-Glo® Luminescent Cell Viability assay	Promega, Mannheim, Germany
Chemiluminescent Detection Reagents	GE Healthcare, Munich, Germany
Lipofectamine® 2000	Invitrogen, Darmstadt, Germany
Megaplex RT primer Human pool A	Applied Biosystems, Darmstadt, Germany
*mir*Vana™ miRNA Isolation Kit	Thermo Fisher Scientific, Darmsdtadt, Germany
Precision Plus Protein™ Standard Marker Dual Color	Bio-Rad Laboratories, Munich, Germany
Restore™ PLUS Western Stripping Buffer	Thermo Fisher Scientific, Darmsdtadt, Germany
TaqMan Universal PCR Master Mix, no AmpErase® UNG	Applied Biosystems, Darmstadt, Germany
TaqMan® MicroRNA Assay	Applied Biosystems, Darmstadt, Germany
TaqMan® MicroRNA Reverse Transcription Kit	Applied Biosystems, Darmstadt, Germany
WST-1 cell proliferation reagent	Roche Diagnostics, Mannheim, Germany

2.5 Cell lines

2.5.1 Human non-transformed breast epithelial cell line (MCF-10A)

MCF-10A cells derived from a patient with fibrocystic disease and the subline of immortalized MCF-10A line arose spontaneously in culture with normal calcium levels (1.05 mM) [190]. This cell line is characterized with a stable, near-diploid karyotype with genetic modifications typical for culture-adapted breast epithelial cells such is the loss of the p16 locus [191]. This cell line was purchased from ATCC (ATCC® CRL-10317™) and maintained in DMEM/F12 medium with supplements as described in Section 3.1.1

2.5.2 Breast cancer cell line (MDA-MB-361)

The MDA-MB-361 cell line was established from a patient with breast adenocarcinoma. The cell line was purchased from ATCC (ATCC® HTB-27™) and maintained in DMEM medium (high glucose content) supplemented with 20 % FCS.

2.5.3 Human embryonic kidney cell line (HEK293T)

HEK293T cell line derived from parental HEK293 cells, and they express Large T antigen important for replicating plasmids with SV40 origin of replication necessary for the lentiviral production. The cell line was purchased from ATCC (ATCC® CRL-3216™) and maintained in DMEM medium (high glucose content) supplemented with 10 % FCS.

2.6 Antibodies for Western blot

All primary and respective secondary antibodies with corresponding dilutions used in Western blot are shown in Table 1. All secondary antibodies were purchased from Santa Cruz.

Table 1: List of Antibodies (*present the predicted molecular weight and ** observed one)

Antigen	Molecular weight (kDA)	Source	Catalog Number	Company	Primary antibody	Secondary antibody
FAK	125	Rabbit	3285	Cell Signalling	1:1000	1:20000
Phospho-FAK	125	Rabbit	8556	Cell Signalling	1:1000	1:20000
ERK1/2	42, 44	Rabbit	4695	Cell Signalling	1:1000	1:20000
Phospho-ERK1/2	42, 44	Rabbit	9101	Cell Signalling	1:1000	1:20000
JNK1/2	46, 54	Rabbit	9252	Cell Signalling	1:1000	1:20000
Phospho-JNK1/2	46, 54	Mouse	9255	Cell Signalling	1:1000	1:20000
PTEN	54	Rabbit	9559	Cell Signalling	1:1000	1:20000
NRF2	68	Rabbit	ab31163	Abcam	1:1000	1:20000
Phospho-NRF2	68*, 90**	Rabbit	ab76026	Abcam	1:1000	1:20000
GAPDH	37	Mouse	sc-47724	Santa Cruz	1:5000	1:50000

2.7 Plasmids and reference DNA/ Nucleic acids

pGreenPuro^{TM} (MZIP000-PA-1-GVO-SBI) and pmiRZIP-21 plasmid (MZIP21-PA-1-GVO-SBI) are purchased from BioCat GmbH, Heidelberg, Germany.

2.8 Softwares and databases

Table 2. List of software and databases used for different analyses

Software	Source
Ingenuity Pathway Analysis	www.ingenuity.com/
TotalLab TL100	TotalLab, Sigma, Steinheim, Germany
Flowing Software 2	Cell Imaging Core, Turku Centre for Biotechnology
PANTHER	www.pantherdb.org
STRING	string-db.org
GraphPad Prism 7	www.graphpad.com/scientific-software/prism/
microRNA.org	www.microrna.org/microrna/home.do
DIANA Tools (microT-CDS)	diana.imis.athena-innovation.gr/DianaTools/index.php?r=microT_CDS/index
miRDB	www.mirdb.org/miRDB/
TargetScan Human 7.1	www.targetscan.org/vert_71

3 METHODS

3.1 Cell culture

3.1.1 Cell culture maintenance of human non-transformed mammary epithelial cell line (MCF-10A), human breast adenocarcinoma cell line (MDA-MB-361) and human embryonic kidney HEK293T cell line

MCF-10A cells were cultured in T75 cell culture flasks in DMEM/F-12 medium (Dulbecco's Modified Eagle Medium/Nutrient Mixture F-12) supplemented with 5% horse serum, 0.5 mg/ml hydrocortisone, 20 ng/ml EGF, 10 µg/ml insulin and 100 ng/ml cholera toxin.

MDA-MB-361 cells were cultured in DMEM (Dulbecco Modified Eagles medium) supplemented with 20% fetal bovine serum while HEK293T cells were cultured in DMEM with GlutaMAX (Dulbecco Modified Eagles medium) supplemented with 10% fetal bovine serum. All cell lines were maintained in culture at 37 °C in a 5% carbon dioxide (CO_2) substituted incubator.

After starting the cell lines from stocks, they were kept in culture for a maximum of 4 weeks. In order to maintain exponential growth phase during this time cells were passaged at least twice per week. For passaging, medium was aspirated from the cell culture plates and the cell monolayer was rinsed with 5 ml of pre-warmed PBS. After removing the PBS, 2 ml of 0.05% Trypsin-EDTA (1x) solution was added and incubated at 37 °C for up to 10 min. In order to ensure that all cells are detached from the culture plates the flasks were monitored under the microscope. In the case of MCF-10A cells, the trypsinisation was stopped by adding 2 ml of Trypsin Soybean inhibitor (1X) which was followed by the addition of 10 ml of pre-warmed complete medium. For MDA-MB-361 and HEK293T cells trypsin activity was stopped by adding 5ml of growth medium containing 20% or 10% serum, respectively. The number of cells was counted with a Z1 Coulter Particle counter® and the cell suspension was briefly centrifuged at 300 x g for 5 min at room temperature. The supernatant was discarded and cell pellet resuspended in 10-15 ml of fresh complete media (depending on the cell number) and split at the ratio of 1:3 into new flasks.

3.1.2 Authentication of the cell lines

All cell lines used were authenticated by genetic profiling service (Eurofins MWG Operon, Ebersberg, Germany). The pellets of 1 x 10^6 cells of each cell line was made and frozen to -20 °C before sending to the company. For each sample then the DNA was isolated and the genetic characteristics were determined by PCR-single-locus-technology. For this purpose PowerPlex® 21 System was used and it allowed investigation of 21 independent loci (20 STR loci and Amelogenin). Obtained profiles were subsequently verified by the online STR matching analysis database (DSMZ, Heidelberg, Germany).

3.1.3 Cryopreservation

All cell lines were cryopreserved by slowly cooling to -80 °C and then stored at -196 °C in liquid nitrogen. A cryoprotectant (DMSO) was used to prevent the damage during the freezing and thawing processes. For all cell lines, ~ 2 x 10^6 cells at the exponential phase of growth were harvested by trypsinisation followed by centrifugation at 300 x g for 5 min. After discarding the supernatant, the cell pellet was resuspended in 1 ml of growth medium (containing serum, percentage depending on cell line) supplemented with 10% DMSO. This cell suspension was transferred into a cryogenic storage vial and placed in a Nalgene Cryo Freezing Container (cooling rate of -1 °C/min) in a -80 °C freezer overnight. The vials were then stored at -196 °C in liquid nitrogen.

3.1.4 Thawing cryopreserved cells

The procedure of thawing is stressful to frozen cells since they become sensitive to cryoprotectant (DMSO). Cells were therefore quickly thawed, centrifuged and DMSO was removed. Cryogenic storage vials with frozen cells were taken out of liquid nitrogen tank and placed in a 37°C water bath for couple of minutes till the cell suspension is completely melted. Pre-warmed medium containing serum (9 ml) was placed in a 15 ml centrifuge tubes and 1 ml of cell suspension from cryogenic storage vial was transferred to the same centrifuge tube and everything was then centrifuged at 300 x g for 5 min. The supernatant containing DMSO was discarded and the cell pellet was resuspended in 10-15 ml of fresh medium and transferred to a T75 culture flask.

3.1.5 Irradiation of cells

Irradiation of cell cultures was performed with a HWM D-2000 Cs^{137} γ-source irradiator. The dose was 0.46 Gy per minute. The irradiator contains a circular shielded irradiation chamber which is 10cm in height and 33cm in diameter. Cells were irradiated in cell T75 culture flasks (plating efficiency – 5 x 10^5 cells) or 6-well plates (plating efficiency - 2x 10^5 cells per well) at room temperature using a single exposure of 0.25 Gy or 2.5 Gy. Control cells were sham-irradiated (0 Gy) by treating them in the same way as the irradiated cells, except that the cells were placed outside the lead shielding of the irradiator. After radiation treatment, both sham-irradiated and irradiated cells were returned to 37 °C, for indicated time points of analyses (4, 24 or 48 hours).

3.2 Lentivirus transfer vectors

Lentiviruses used in this study are HIV-1 based gene delivery vehicles that are capable of infecting a wide variety of both dividing and non-dividing mammalian cell types. They enable the stable integration of DNA into the host genome, which results in long-term expression of a transgene [192].

In order to downregulate the miRNA expression the miRZip™ shRNA expression lentivector was used. This vector is based upon improved third generation of SBI's pGreenPuro™ lentivector (pGP) that was used as vector transduction control and therefore termed empty vector (EV). For the downregulation of miR-21 pmiRZIP-21 (further named – anti-miR-21) plasmid was used. Both lentiviral vectors (pGP and pmiRZIP-21) contain copGFP gene and a puromycin resistance gene transcribed from an internal cytomegalovirus (CMV) promoter. CopGFP gene is a fluorescent reporter while puromycin is used for stable drug selection of cells that were stably transduced.

3.2.1 Lentivirus production

Replication-defective lentiviral particles were produced by transient transfection of 5 x 10^6 HEK293T cells in a 10 cm Petri dish as previously described [193-195]. The change of medium in Petri dishes is done at least 1 hour before transfection. In 500 µl of Opti-MEM® (1X) reduced serum medium the three packaging plasmids pMDLg/pRRE (16 µg), pRSV.Rev (8 µg) and pMD2.G (5 µg) and 10 µg of pGP or pmiRZIP-21 vectors were combined (Figure 6). A mixture of 20 µl Lipofectamine® 2000 transfection reagent

and 480 µl Opti-MEM® (1X) medium was prepared and incubated at room temperature for 5 min.

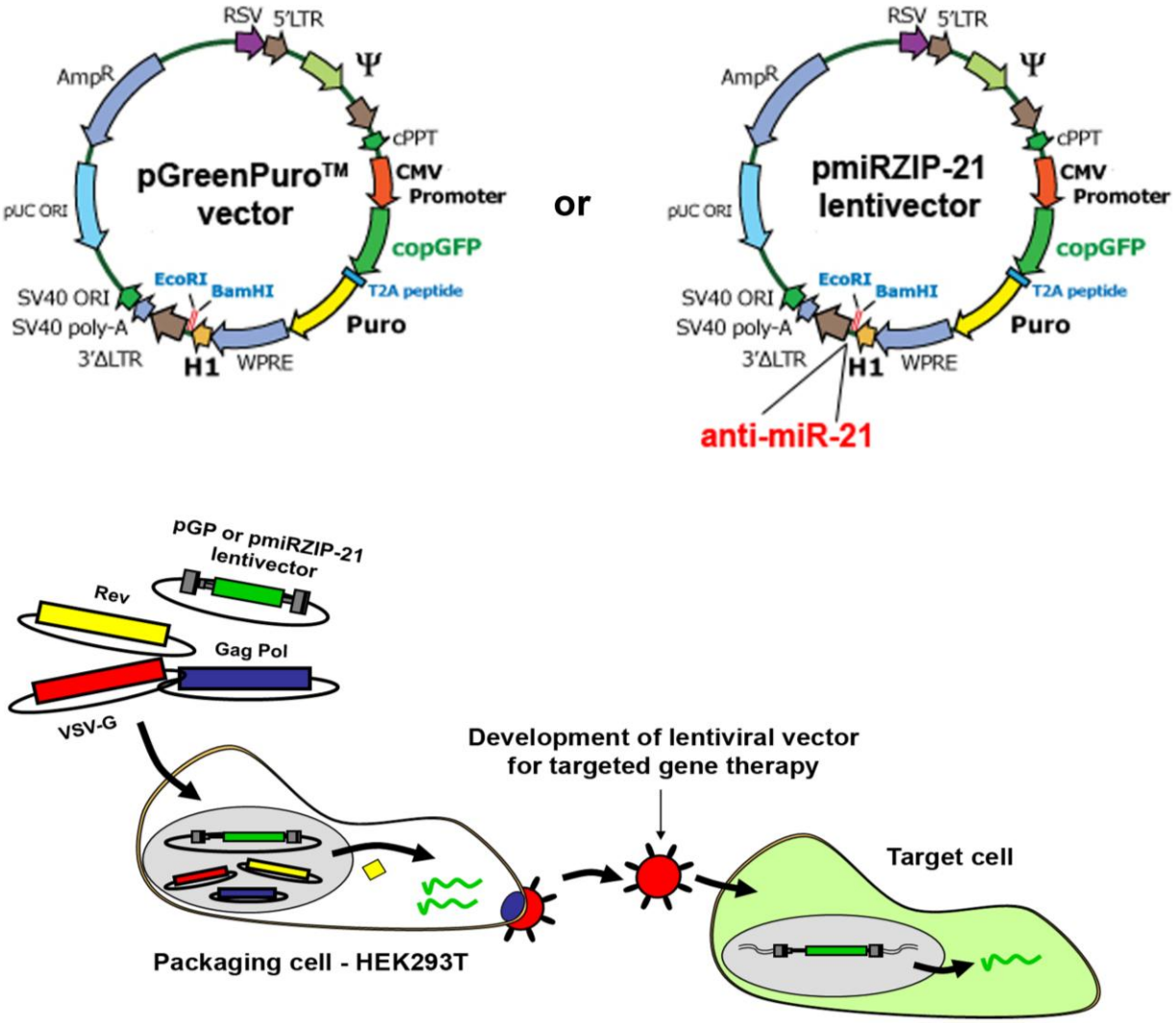

Figure 6. Lentivirus production and transduction of target cells. Production of EV and anti-miR-21 lentiviruses using pGP (upper left) and pmiRZip-21 lentivectors (upper right). Production of replication-defective lentiviral particles starts (using blue- pMDL/pRRE (expresses HIV gag/pol), yellow - pRSV-Rev (express HIV REV), red - pMD2.G (express VSV glycoprotein) and green (pGP or pmiRZIP-21) colored plasmids) by transient transfection of HEK293T for the development of lentiviral vectors. After 48 hours, virus particles are harvested and concentrated, after which the virus is ready for the lentiviral transduction of target cells.

The solutions were mixed together, vortexed vigorously for 15 s and then incubated at room temperature for 20 min. A final volume of 1 ml of previously mixed solution is then added to the cells drop-wise across the plate. The plates were incubated at 37 °C for 48 hours after which the virus particles were harvested, cleared of cell debris by low-speed (100 x g for 5 min) centrifugation and filtered with Stericup® filters. The lentivirus was concentrated using PEG-it™ Virus Precipitation Solution (5X) according to the manufacturer's instructions and stored at -80 °C in aliquots of 50 µl.

3.2.2 Lentivirus titer determination

To titrate lentiviral vector expressing GFP (fluorescent protein) the flow cytometric method (FACS) was used. The titration was performed in HEK293T, MCF-10A and MDA-MB-361 cell lines. For titration, 1 x 10^5 cells were plated in 6-well plates and the transduction of the cells was performed. Briefly, in the first well 1 ml of medium containing no virus was used as a control. In the other wells 1 ml of medium with 3 µl of virus and dilutions (-1, -2, -3 and -4) was used. After 24 hours of incubation the medium was changed and cells were incubated for an additional 48 hours in medium containing puromycin. The cells were trypsinized, cell pellets collected and analysed with FACS. The virus titer (transduction units/ ml) was calculated according to the formula:

$$TU/ml = (F \times N \times D \times 1000)/V$$

Where F - percentage of fluorescent (GFP) cells, N – starting number of cells at the time of transduction, D – fold dilution of lentiviral vector used for transduction and V – volume of diluted vector sample added into each well for transduction [196].

3.2.3 Lentiviral transduction of cell lines

Viral transduction of breast epithelial cells with EV and anti-miR-21 lentiviral vectors was done according to the protocols previously described [169, 170]. Briefly, 2 x 10^5 cells were plated per well in 6-well plates day before the transduction. Cells were infected with 3 x 10^5 lentiviral transduction units (TU) according to the virus titer, with the addition of poloxamer synperonic F108 (100 µg/ml) and polybrene (10 µg/ml) as adjuvants that further enhance lentiviral transduction rates. After 24 hours of incubation at 37 °C with 5%

CO2 the medium was changed and cells were incubated for an additional 48 hours in medium with the inclusion of puromycin (0.3 μg/ml) before further analysis.

3.3 Functional analysis

3.3.1 Clonogenic assay

The clonogenic assay is an *in vitro* assay of cell survival in radiation biology. It is based on the ability of single cell to grow into a colony, since only a fraction of cells retains the capacity to produce colonies after irradiation [197-199]. It is used to assess the differences in reproductive viability between untreated cells and cells that have been under different treatments of ionizing radiation and to conclude about the effects of anti-cancer strategy (knockdown of miR-21) on colony forming ability. The clonogenic assay consisted of three parts:

- Making the single cell suspensions out of lentiviral treated cells (EV and anti-miR-21) as well as control cells (without virus) and plating cells at a range of dilutions (500–12.000 cells per well dependent on the predicted survival at each radiation dose used) per well in a 6-well plate before treatment.
- After 24 hours the cells in 6-well plates were either sham-irradiated or exposed to different doses of radiation (0.2, 2, 4, 6 and 8 Gy).
- Colony formation capacity was assessed after 7-21 days depending on the cell line. Fixation of the colonies was performed with 100% ethanol and subsequently they were stained with Giemsa (diluted 1:10 in PBS). The colonies with more than 30 cells were counted with stereo microscope (Olympus SZX12) and the survival curve was plotted.

All clonogenic assays were performed with at least three biological replicates and each treatment was performed with two technical replicates.

3.3.2 Cell viability and cell attachment assays

For determining cell viability after the combined treatment with anti-miR-21 and radiation we used two commercially available assays: CellTiter-Glo® Luminescent Cell Viability assay and WST-1 colorimetric assay.

3.3.2.1 CellTiter-Glo® Luminescent Cell Viability assay

CellTiter-Glo® assay is based on quantitation of ATP, a signal of metabolically active cells that is detected as a luminescent signal. The lentiviral-transduced cells were plated in technical triplicates 3 days after transduction in opaque-walled 96-well plate. The number of plated cells was 1000 cells per well for MCF-10A cells and 5000 cells per well for MDA-MB-361 in a final volume of 100 µl. Culture medium was used as the background control. The cells were incubated for 72 hours, before radiation, in a humidified atmosphere at 37 °C with 5% CO_2. The cell viability of sham-irradiated and cells exposed to 0.25 Gy and 2.5 Gy was measured 4, 24 and 48 hours after radiation. 100 µl of CellTiter-Glo® Reagent was added to each well followed by orbital shaking for 2 min for the induction of cell lysis. The plates were incubated for 10 min at room temperature for stabilization of luminescent signal which was afterwards recorded using microplate reader Infinite® M200 with integration time of 1 second per well. Assay was performed for three biological replicates.

3.3.2.2 WST-1 colorimetric assay

The WST-1 colorimetric assay detects the amount of formazan dye formed from WST-1 reagent, which is in correlation with the metabolic activity of the cells. The lentiviral-transduced cells were plated in technical triplicates 3 days after transduction in flat bottom transparent polystyrol plate. The number of plated cells was 1000 cells per well for MCF-10A cells and 5000 cells per well for MDA-MB-361 in a final volume of 100 µl. Culture medium was used as the background control. The cells were incubated for 72 hours, before radiation, in a humidified atmosphere at 37 °C with 5% CO_2. The cell viability of sham-irradiated and cells exposed to 0.25 Gy and 2.5 Gy was measured 4, 24 and 48 hours after radiation. 10 µl of the WST-1 reagent was added per well and incubated for 1 hour at 37 °C and 5% CO_2. The plates were shaken for 1 minute after what the absorbance was measured (measurement wavelength – 450 nm; reference wavelength – 650nm) in microplate reader Infinite® M200. Assay was performed for three biological replicates.

3.3.2.3 Cell attachment assay

For detecting if miR-21 knockdown and radiation treatment influenced cell attachment a cell attachment assay was performed. Lentivirally-transduced MCF-10A and MDA-MB-361 cells were plated at 1 x 10^5 per well in 6-well plates 24 hours prior to irradiation. Cell detachment was monitored by counting the number of cells in the supernatant 24 and 48 hours after exposure to radiation. The number of attached cells was measured 48 hours after irradiation by trypsinizing, collecting and counting the cells using Z1 Coulter Particle counter ®. All assays were performed in biological triplicates, each with three technical replicates.

3.3.3 Cell cycle analysis

Cell cycle distribution was analysed 24 hours after irradiation of MCF-10A and MDA-MB-361 cells that were lentivirally transduced. 24 hours prior to radiation, 2 x 10^5 of cells were plated per well of 6-well plate. Treated cells were trypsinized and the pellets were collected by centrifugation at 300 x g for 5 min, after which the supernatant was carefully removed and washed once with PBS. The cell pellet was resuspended in 500 µl of solution I (10 mM NaCl, 4 mM Na-citrate, 10 µg/ml RNase, 0.3% Nonidet P-40, and 50 µg/ml propidiumiodide (PI)) and incubated in the dark at room temperature for 60 min. This was followed by the addition of 500 µl of solution II (70 mM citric acid, 250 mM sucrose and 50 µg/ml PI) [195, 200]. Cell cycle distribution analysis were performed using a FACScan LSR II (excitation wavelength: 488 nm; emission wavelength: 610 nm – for PI detection) and the BD FACSDiva™ software (BD Biosciences, Heidelberg, Germany). All obtained data were afterwards analysed with Flowing software. Cells with DNA content lower than that of cells in the G1 phase of the cell cycle were defined as the subG1 fraction and were considered to be apoptotic. All samples were done in biological triplicates.

3.3.4 3D microtissue analysis

Multicellular 3D spheroid models are suggested to be better representation of the *in vivo* situations since they are morphologically and functionally closer to native tissue or organ structures than 2D. Unlike in 2D, cells in a 3D system produce native extracellular matrix (ECM) which facilitates an integrated cellular response to environmental stimuli.

We have used hanging drop 3D-microtissue technology - GravityPLUS™ 3D Culture and Assay Platform.

The GravityPLUS™ 3D Culture and Assay Platform consists of two steps to form a 3D-microtissue (Figure 7). Briefly, the first step is seeding the desired number of cells in GravityPLUS™ plates in which the 3D-microtissues are created in the hanging drop over 3 days. The resulting 3D-microtissue was then transferred into the GravityTRAP™ plates in which the assays can be performed [201, 202]. The lentivirally transduced cells (MCF-10A and MDA-MB-361) and corresponding controls were seeded with 2000 cells per drop into scaffold-free 96-well InSphero culture GravityPLUS™ plates.

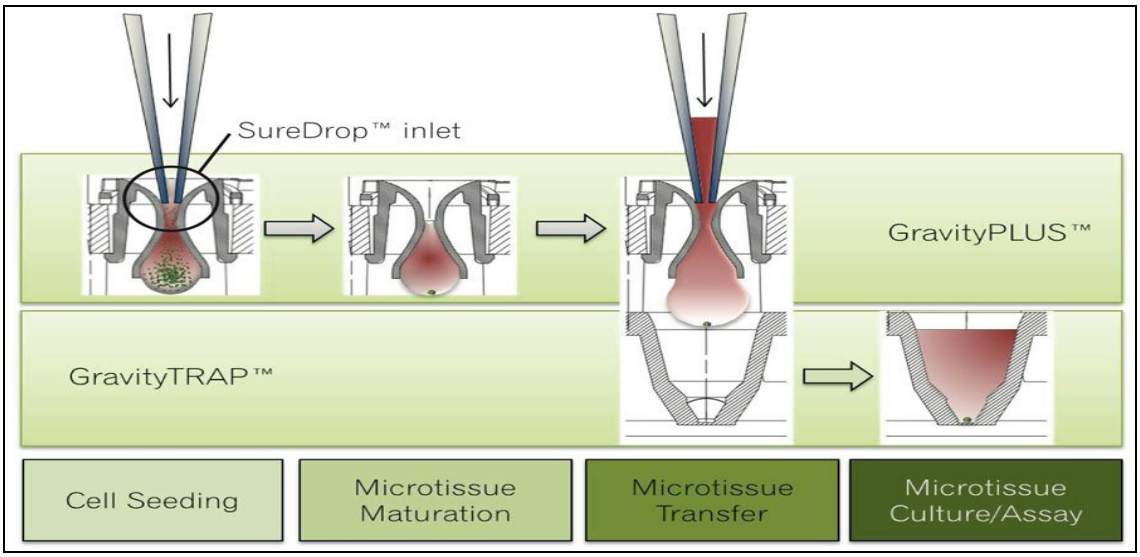

Figure 7. GravityPLUS™ platform design for 3D-microtissue formation. A 4-step process starts with cells seeding and microtissue maturation (in GravityPLUS™ plate) for 3 days. On the fourth day microtissue is transferred to GravityTRAP™ plate where it is further cultured and 3D-microtissue can then be used for analysis.

After 24 hours in the GravityTRAP™ plates (defined as day 0 of treatment), the 3D microtissues were sham-irradiated (0 Gy) or irradiated with a single dose of radiation (0.25 Gy or 2.5 Gy). Growth of eight 3D-microtissues per treatment was monitored every 3 days using a high content screening system Operetta (Perkin Elmer, Waltham, MA) and the maximal area of GFP expressing microtissue (μm^2) was quantified using the Harmony analysis Software (Perkin Elmer) [201, 202].

3.4 Semi-quantitative RT-PCR analysis of targeted miRNA expression

Quantitative real-time PCR represent the most sensitive and reproducible method to quantify gene expression. The expression levels of individual miRNAs were analysed using a specific single TaqMan™ microRNA assay. The differences in miRNA expressions between samples were calculated using the $2^{-\Delta\Delta Ct}$ method (Section 3.4.5) [203].

3.4.1 RNA extraction

Cell pellets for the isolation of total RNA were collected 4 and 24 hours after radiation treatment. Cell monolayer was rinsed with PBS, trypsinized, collected by centrifugation at 2000 rpm for 5 min, and washed twice with 1 ml of PBS. The pellets were kept either on ice or were stored at -20 °C for later extraction. Total RNA was isolated from the cells using the mirVana™ miRNA isolation kit according to the manufacturer's instructions. Cell pellets were lysed using 600 µl of Lysis/Binding buffer. The extraction of RNA was done with 600 µl of Acid-Phenol:Chloroform, vortexed and then centrifuged at 13 000 x g for 7 min to separate the aqueous and organic phases. To the aqueous phase containing nucleic acids 1.25 volumes of 100% ethanol was added and mixed, and afterwards filtered and washed with appropriate solutions provided in a kit. Total RNA was then eluted from filter cartridge in 50 µl of pre-heated to 95 °C nuclease-free water.

3.4.2 Quantification of nucleic acids

The concentration of total RNA was determined with the Nanodrop spectrophotometer (PeqLab Biotechnology, Germany). The RNA purity was assessed by using the ratio of the absorbance at 260 and 280 nm (A260/280). The quality of RNA was accepted when it was in range 1.8 - 2.0.

3.4.3 cDNA synthesis for miRNA analysis

cDNA for the TaqMan™ microRNA assay was made by using the TaqMan® MicroRNA Reverse Transcription Kit. The RNA concentration of each sample was adjusted to 20 ng/µl and 3 µl was used for the cDNA synthesis (in total 60 ng of each RNA sample was used in this reaction). 12 µl of reverse transcription mix was prepared according to Table 3 and was added to the RNA template. The mixture was gently mixed, spun down briefly and incubated on ice for 5 min before starting the program for reverse transcription reaction (Table 4). Before further analysis newly synthesized cDNA was stored at -20 °C. The snoRNA RNU44 was used as endogenous control for all the reaction with miRNAs.

Table 3: Reverse transcription mix (for 1 reaction)

Component	Volume (µl)
dNTP mix (100 mM)	0.15
MultiScribe™ RT enzyme (50U/µL)	0.70
RNase inhibitor (20U/µL)	0.19
10X RT Buffer	1.50
TaqMan RT primer (5x)	2.00
Nuclease free water	7.46
Total volume	**12**

Table 4: Program for cDNA synthesis

Number of cycles	Cycle	Temperature	Time
1	Primer annealing	16 °C	30 min
1	Elongation	42 °C	30 min
1	Inactivation	85 °C	5 min
1	Storage	4 °C	hold

3.4.4 Real-time PCR

Real-time PCR reactions were performed on reverse transcribed cDNA using the StepOnePlus™ Real-time PCR System in 96-well plates with a final reaction volume of

10 µl. Each reaction contained 2 µl of previously synthesized cDNA template and 8 µl of PCR master mix (Table 5). Each sample was quantified in three technical replicates. Before starting the real-time PCR reaction, the reaction plate was sealed and spun down at 1000 rpm for 2 min. The real-time PCR reaction was performed as presented in Table 6. As a negative control, 2 µl of nuclease - free water was used as template.

Table 5: Real-time PCR Master Mix (for 1 reaction)

Components	Volume (µl)
TaqMan Universal PCR Master Mix, no	5.0
TaqMan assay specific primer (20x)	0.5
Nuclease free water	2.5
Total	**8**

Table 6: Thermal cycler program for real-time PCR reaction

Number of cycles	Cycle	Temperature	Time
1	Activation	50 °C	2 min
1	Initial denaturation	95 °C	10 min
40	Denaturation	95 °C	15 sec
	Annealing/elongation	60 °C	1 min

3.4.5 Analysis of real-time PCR amplifications

The amplification of the specific miRNA in each sample was determined by the detection of the TaqMan® probe fluorescent signal. The initial cycles of PCR with low change in fluorescence signal were used to establish the baseline. The threshold level was set in the linear phase of the amplification curve and according to its intersection with the amplification curve, C_t value of individual miRNA can be detected (Figure 8). The Ct (cycle threshold) is defined as the PCR cycle where the product concentration exceeds the threshold value. The Ct value for each miRNA target was calculated as the mean of the 3 technical replicates. The fold changes of target miRNA expression was calculated and presented using the $2^{-\Delta\Delta Ct}$ method as previously described [203]. Briefly, for the calculation of miRNA expression changes following steps were used:

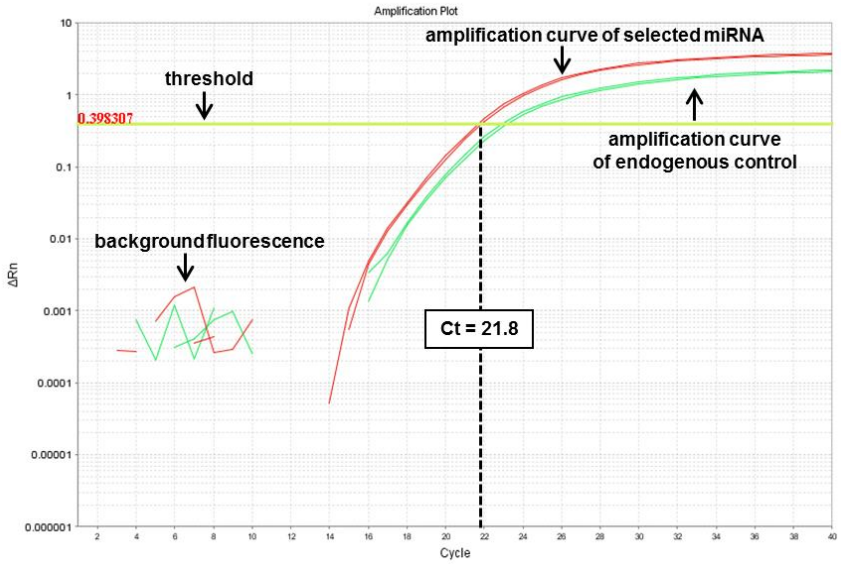

Figure 8. Graphical presentation of real-time PCR data. Red color presents amplification curve of selected miRNA and green color amplification curve of endogenous control (both done in technical duplicates). The threshold for selected miRNA was set at 0.39 within the exponential phase of amplification curve (ΔRn – relative fluorescence). The Ct value is detected at 22nd cycle as interception of threshold and amplification curve.

1. The target miRNA expression level (control or treated cells) was first normalized to the expression levels of the endogenous control RNU44 and is presented as ΔCt

$$\Delta C_t = C_t \text{ (miRNA)} - C_t \text{ (RNU44)}$$

2. The difference in expression level between normalized miRNA expressions in sample of interest (e.g. irradiated cells) relative to the expression level of normalized miRNA expressions in the control cells

$$\Delta\Delta C_t = \Delta C_t \text{ (irradiated cells)} - \Delta C_t \text{ (control cells)}$$

3. The change of selected miRNA expression value between samples was calculated as the $2^{-\Delta\Delta Ct}$

$$\text{Expression value} = 2^{-(\Delta Ct \text{ (irradiated cells)} - \Delta Ct \text{ (control cells)})} = 2^{-\Delta\Delta Ct}$$

Statistical analysis was performed as explained in section 3.10.

3.4.6 RT^2 Profiler PCR Assay – oxidative stress

This real-time RT-PCR based assay present a highly sensitive method for gene expression analysis. The Human Oxidative Stress RT^2 Profiler PCR assays used can profile the expression of 84 genes related to oxidative stress such as peroxidases and genes involved in reactive oxygen species (ROS). Five housekeeping genes are included for control purposes: actin, beta (*ACTB*), beta-2-microglobulin (*B2M*), glyceraldehyde-3-phosphate-dehydrogenase (*GAPDH*), hypoxanthine phosphoribosyl-transferase 1 (*HPRT1*) and ribosomal protein, large, P0 (*RLP0*).

The changes in gene expression were monitored in lentivirally transduced MCF-10A cells 4 and 24 hours after the exposure to a radiation dose of 2.5 Gy. cDNA synthesis was performed using the RT^2 First Strand Kit according to the manufacturers' instructions. Briefly, 500 ng of total RNA from each sample was used for the reverse transcription. For each sample the genomic elimination mix was prepared (Table 7).

Table 7: Genomic DNA elimination mix (for 1 reaction)

Component	Amount
Total RNA	0.5 µg
Buffer GE	2 µl
Nuclease free water	variable
Total volume	**10 µl**

The mixture was then incubated at 42 °C for 5 min and then placed on ice for at least 1 min. To a 10 µl volume of genomic DNA elimination mix 10 µl of reverse-transcription mix (Table 8) was added for each sample. Everything was then incubated at 42 °C for

15 min and the reaction was immediately stopped by incubation at 95 °C for 5 min. To each sample 91 µl of nuclease free water was added and stored at -20 °C prior to real-time PCR.

Table 8: Reverse-transcription mix (for 1 reaction)

Component	Volume (µl)
5x Buffer BC3	4
Control P2	1
RE3 Reverse Transcriptase Mix	2
Nuclease free water	3
Total volume	**10**

For the real-time PCR procedure the cDNA was mixed with RT^2 SYBR Green Mastermix (Table 9).

Table 9: Real-time PCR mix (per sample)

Component	Volume (µl)
2x RT^2 SYBR Green Mastermix	1350
cDNA	102
Nuclease free water	1248
Total volume	**2700**

The Real-time PCR mix was then dispensed into the RT^2 Profiler PCR Assay by adding 25 µl to each well. After sealing with optical adhesive film the plate was centrifuged at room temperature for 1 min at 1000 x g to remove bubbles. The PCR reaction was performed using the StepOnePlus™ Real-time PCR System using cycling program (Table 10).

The fold changes of genes on the array were calculated using the $2^{-\Delta\Delta Ct}$ method (see 3.4.5) with GAPDH used as endogenous control.

Table 10: Cycling program for real-time PCR

Number of cycles	Temperature	Time
1	95 °C	10 min
40	95 °C	15 sec
	60°C	1 min

3.4.7 TaqMan® Gene Expression Assay

According to the fold changes of genes detected in Human Oxidative Stress RT^2 Profiler PCR Assay, five genes were selected (*NRF2, HMOX1, TXNRD1, TXNRD2, HSPA1A*) for validation with the single TaqMan® Gene Expression Assays. The first step was reverse transcription using SuperScript™ II Reverse Transcriptase kit. For each sample 1 µg of total RNA was used. The reverse transcription mix is made by combining mixture I (blue) and mixture II (yellow) indicated in Table 11. cDNA synthesis was started with mixture I for each sample according to cycling program (Table 12). After finishing the cycling stage at 25 °C the program was stopped and 9 µl of mixture II was added for each sample and the program was further continued. The cDNAs of each sample were then diluted in ratio 1:4 with nuclease-free water. The mix for the real-time PCR reaction was done according to Table 13.

The real-time PCR reaction was performed on StepOnePlus™ Real-time PCR System using cycling program according to Table 4. The fold changes of genes were calculated using the $2^{-\Delta\Delta Ct}$ method (see 3.4.5) with TBP as endogenous control.

Table 11: Reverse transcription mix for TaqMan gene expression assay (for 1 reaction)

Component	Amount
Total RNA	1 µg
Nuclease free water	Variable
Oligo(dT)$_{12-18}$ Primer	1.5 µl
Random Primers	1.5 µl
5x First-Strand Buffer	4 µl
0.1 M DTT	2 µl
dNTP Mix	1 µl
RNaseOUT™	1 µl
SuperScript® II Reverse Transcriptase	1 µl
Total volume	**20 µl**

Table 12: Program for cDNA synthesis

Number of cycles	Temperature	Time
1	70 °C	2 min
1	25 °C	10 min
1	42 °C	60 min
1	95 °C	5 min

Table 13: Real-time PCR mix for TaqMan® Gene Expression Assay

Component	Volume (µl)
cDNA	4
TaqMan® probe	1
TaqMAn Universal PCR Master Mix, no	10
Nuclease free water	5
Total volume	**20**

3.5 Low density arrays

For detecting which miRNAs are changed 4 and 24 hours after exposure to 0.25 Gy and 2.5 Gy dose of irradiation the TaqMan® Low Density Array was used. TaqMan® Human MicroRNA Array A was loaded with 384 unique PCR primer sets, out of which 377 are specific to human miRNAs and 4 present control assays (3 endogenous templates and 1 negative control assay). With this specific array we set our focus on detecting changes in highly characterized and well-known miRNAs. These arrays were used in conjunction with Megaplex™ RT Primer Human Pool A that contain stem-looped reverse-transcription (RT) primers which enable simultaneous synthesis of cDNA for mature miRNAs.

3.5.1 cDNA synthesis and loading the Low density arrays

The starting material for the total RNA that was isolated as described in RNA extraction. For this step the TaqMan® MicroRNA Reverse Transcription Kit and Megaplex™ RT Primers were used to synthesize single-stranded cDNA from the total RNA. The final volume of 15 µl of reverse transcription (RT) reaction was made of 6 µl of total RNA (total of 300 ng) and 9 µl of reverse transcription mix (Table 14) for each sample. The final mixture of RT mix and RNA was gently mixed, spun down briefly and incubated on ice for 5 min. Program for the cDNA synthesis is shown in Table 15. cDNA was stored at -20 °C.

Prior to loading, the arrays were brought to on room temperature. The TaqMan® Low density arrays were run on the TaqMan 7900HT Real-time PCR system with a final reaction volume of 900 µl. Each reaction contained 15 µl of previously synthesized cDNA and 885 µl of master mix (450 µl of TaqMan Universal PCR Master Mix, no AmpErase® UNG and 435 µl of nuclease free water). 100 µl of the mixture was loaded into each of 8 fill reservoirs on the array. The arrays were centrifuged 2 times for 1 min at 1200 rpm in order to distribute the cDNA samples into all of the reaction wells. After verifying that the filling was complete, the array was sealed and the fill reservoirs were cut off according to the manufacturers' instructions.

Table 14: Low density array reverse transcription (RT) mix (for 1 reaction)

Component	Volume (µl)
MegaPlex RT primers (10X)	1.6
dNTP mix (100 mM)	0.4
MultiScribe™ RT enzyme (50U/µL)	3.0
10X RT Buffer	1.6
RNase inhibitor (20U/µL)	0.2
$MgCl_2$ (25 mM)	1.8
Nuclease free water	0.4
Total volume	**9**

Table 15: Thermal cycler program for Low density array RT reaction

Number of cycles	Cycle	Temperature	Time
40	Primer annealing	16 °C	2 min
	Elongation	42 °C	1 min
	Elongation	50 °C	1 min
1	Inactivation	85 °C	5 min
1	Storage	4 °C	infinity

SDS v2.4.1 Relative Quantification software was used for storing the data obtained from real-time PCR reaction and data analysis. The Ct values for each miRNA on array for biological triplicates were first normalized to the mean Ct value of endogenous control (RNU44) from all three replicates in order to obtain ΔCt value. The fold changes in miRNA expression profiles after radiation were analysed according to $2^{-\Delta\Delta Ct}$ method (Section 3.4.5) for each biological replicate, where ΔΔCt was calculated by normalization to the Ct value of sham-irradiated cells. The final fold changes are presented as mean values of three biological replicates. Fold changes less/equal to 0.90 were considered as downregulated, the ones higher/equal then 1.10 as upregulated miRNAs and the rest as not changed ones.

3.6 Protein immunobloting (Western Blot analysis)

3.6.1 Protein extraction

MCF-10A cells were plated in T75 flasks at a concentration of 2 x 10^6 cells 24 hours prior to irradiation. At 4 and 24 hours after irradiation, the cells were trypsinized and cell pellets for the protein extraction were collected. The pellets were washed twice with PBS before being lysed with 60 µl of cell lysis buffer - T-PER™ Tissue Protein Extraction Reagent with Protease Inhibitor Cocktail and PhosSTOP (Phosphatase Inhibitor Cocktail). Cell lysis was done on ice for 1 hour, afterwards the mixture was centrifuged at 16 000 rpm for 10 min at 4 °C and supernatant was transferred to a new eppendorf tube. These protein extracts were stored at -20°C.

3.6.2 Measurement of protein concentration

Concentration of protein samples was measured using the colorimetric Bradford protein assay with BSA standards. The BSA standards used for the standard curve were: 0.25, 0.5, 1 and 1.4 mg/ml in lysis buffer and the lysis buffer was used as the blank. For each concentration of BSA standards and each protein sample 5 µl was pipetted in triplicates in 96 well flat bottom transparent plate and it was followed by adding 150 µl of Bradford reagent. The plate was covered in aluminium foil (for light protection) and gently mixed for 10 min to develop the colorimetric reaction. The absorbance at 595 nm was measured with a TECAN microplate reader. Protein concentrations of samples were first corrected for the background signal and the concentrations were calculated using the standard curve linear regression equation.

3.7 SDS gel electrophoresis

3.7.1 Preparation of samples for loading

15 µg of each protein sample was mixed with 4X Laemlli buffer in ratio 4:1 (respectively) and heated for 5 min at 95 °C. The volume between samples was set to the equal with lysis buffer. Prior to loading on gel the samples were kept on ice. Proteins were separated using NuPAGE® Novex® 4-12% Bis-Tris Protein Gels, 1.5 mm.

3.7.2 Electrophoretic separation of proteins

NuPAGE® Novex® 4-12% Bis-Tris Protein gels were put in the chamber for the gel electrophoresis that was filled with NuPAGE® MES SDS Running Buffer (1X). On each gel, beside samples, 5 µl of protein molecular weight marker (Precision Plus Protein™ Standard Marker Dual Color) was used. Electrophoresis was run first at 80V for 30 min in order to load the proteins in the stacking part of the gels, after which the voltage was increased to 150V for the next 1 hour for the separation of proteins.

3.7.3 Transfer of separated proteins

The transfer of the electrophoretically separated proteins to nitrocellulose membrane was done by wet electroblotting. Gels were taken out of their cassettes and rinsed for 15 min while gently shaking in the transfer Towbin buffer. A presoaked nitrocellulose membrane was placed on the gel and this was placed in between two presoaked blotting papers and sponges (ensuring that air bubbles were not present). This gel sandwich was loaded into a support cassette and placed in the transfer chamber filled with transfer buffer that contained a magnet stirrer. The transfer chamber was placed in a box filled with ice on a magnet stirrer plate. Transfer was done at 100V for 2 hours. The efficiency of the transfer to the membrane was visualized using Ponceaus-S-Red staining, which was documented by scanning the gels. The Ponceaus-S-Red stain was removed by washing the membrane 3 times for 10 min in TBS-T buffer. Before the detection of selected proteins, the membrane was blocked for 1 hour at room temperature using 8% w/v powdered milk dissolved in TBS-T buffer, after which the membrane was rinsed 3 times in TBS-T.

3.7.4 Antibody detection of target protein

Before incubation with the primary antibody the membrane was cut to contain the region with the protein of interest. Antibodies were diluted in either 3% BSA or in 3% milk in TBS-T. The dilutions used for each antibody are shown in section 2.6. Membranes were incubated with the appropriate primary antibody overnight at 4 °C with continuous shaking, followed by 3 times 5 min washing in TBS-T while shaking. The relevant HRP conjugated secondary antibody was applied and the incubation was performed for 1

hour at room temperature. Excess secondary antibody was removed by washing the membrane 3 times with TBS-T while shaking.

3.7.5 Detection of immunoblot signals

For the detection of immunoblot signals ECL™ Select Western Blotting Detection Reagent was used. The ECL solution was prepared according to the manufacture's protocol by mixing the luminol and peroxide solution (ratio 1:1). The membranes were incubated in 2-3 ml of ECL solution for 5 min at room temperature. The luminescent signal was detected right after the ECL incubation and documented with the Alpha Innotech Chemi Imager system.

3.7.6 Stripping and re-probing

In order to re-probe the nitrocellulose membranes they were stripped using Restore™ PLUS Western Blot Stripping Buffer. Incubation of membrane with stripping buffer was done for at least 20 min at room temperature followed by 3 times 5 min washing with TBS-T while shaking. Antibody detection and development was done as described in 3.6.5.

3.7.7 Quantification of the proteins

Quantification of the detected proteins was performed by TotalLab (TL 100) image analysis software. In each case the value of detected protein was normalized to levels of the endogenous control GAPDH.

3.8 *In silico* mir-21 target predictions

For the purpose of discovering the potential targets of miR-21 four different databases, providing information about miRNA *in silico* target predictions based on complementarity of miRNA sequence to mRNA (3'UTR) of targets, were used – *miRDB*, *Target Scan*, *DIANA* and *microRNA.org* software. Most of miRNA target prediction tools are based on four features of the miRNA:mRNA target interaction - seed match (Watson-Crick match between a miRNA and its target in the seed sequence (2-8 nucleotides)), conservation (maintenance of a sequence across species), free energy (a measure of the stability of a biological system) and site accessibility (measure of the ease with which a miRNA locate and hybridize with an mRNA target) [204]. The

differences in number of predicted targets are the result of different subsets of features softwares are based on. In this prediction we have included both miR-21-5p and miR-21-3p.

3.9 Proteomics

3.9.1 Isotope-Coded Protein Labelling (ICPL)

ICPL presents a method based on stable isotope labelling of the free amino groups of proteins using amine specific reagents. It was based on a reaction of N-nicotinoyloxy-succinimide with the ε-amino group of lysine. By using different isotope tags the ICPL method allows high-throughput comparative profiling of proteins in different samples. In order to check the changes on proteome level of combined radiation and miR-21 knockdown in MCF-10A cells we have used ICPL™ Triplex-Kit (Serva) that enabled the simultaneous quantitative analysis of three independent proteome samples (Figure 9).

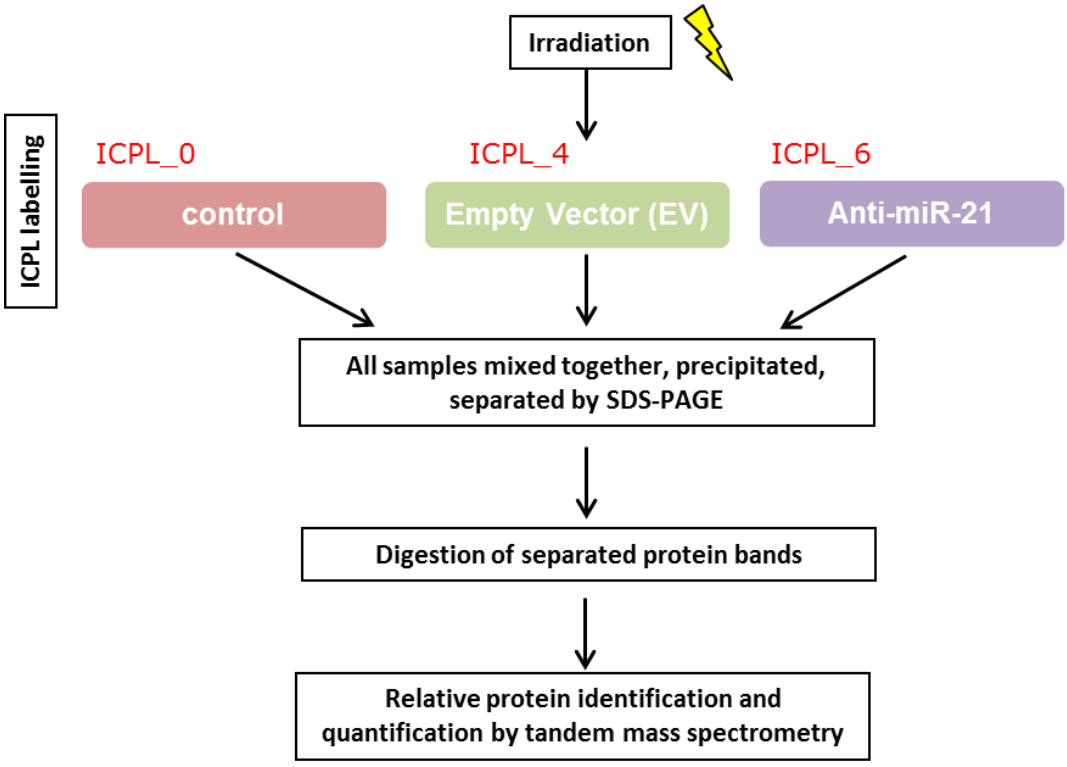

Figure 9. Schematic presentation of ICPL labelling. ICPL_0, ICPL_4 and ICPL_6 present 3 different N-nicotinoyloxysuccinimide labels with the mass differences of 0, 4 and 6 Da introduced by different compositions of $^{12}C/^{13}C$ and hydrogen/deuterium isotopes.

3.9.2 Isolation of proteins

For the protein isolation cell pellets of control and lentiviral treated MCF-10A cells (EV and anti-miR-21) were collected 4 and 24 hours after irradiation (0.25 and 2.5 Gy) and sham-irradiated cells. Cell pellets were centrifuged at 2000 rpm for 5 min, and washed twice with 1 ml of PBS. Cell pellets were resuspended in 20 µl of 6 M guanidine hydrochloride (SERVA) with phosphatase and protease inhibitor cocktails (Roche) and vortexed and incubated at 25 °C for 20 min. Samples were afterwards sonicated 4 times for 30 s and again vortexed and incubated for 15 min at 25 °C. As the lest step of lysis, the samples were centrifuged at 14 000 x g for 4 min at 4 °C and the supernatants containing proteins were collected. Concentration of each protein sample was measured using Bradford assay (Section 3.6.2).

3.9.3 ICPL labelling

A triplex set of labels (light - ICPL_0; medium - ICPL_4 and heavy - ICPL_6) was used. Light label (ICPL_0) was used for labelling of control cells (sham-irradiated or irradiated ones), medium label (ICPL_4) for EV treated cells (sham-irradiated or irradiated ones) and heavy label (ICPL_6) for anti-miR-21 treated (sham-irradiated or irradiated ones) MCF-10A cells.

3.9.4 Separation of ICPL labelled proteins by SDS gel electrophoresis

50 µg of labeled protein from each sample in final volume of 20 µl were all mixed together, precipitated and dissolved in Laemmli sample buffer. Afterwards the proteins were separated by 12% SDS gel electrophoresis before staining by Coomassie blue with 20% ethanol overnight at 4 °C. The excess of the Coomassie was removed by washing the gel in miliQ water while shaking for at least 2 hours. Three biological replicates were used for set of samples.

3.9.5 Mass spectrometric analysis

The Commassie blue stained protein lanes were cut in 5 different slices and each slice was then subjected to in-gel digestion with trypsin after which the ratios of digested peptides in different proteome states were calculated and analysed by tandem mass spectrometry. The digested peptides were concentrated on a nanotrap LC column (300

mm inner diameter 65 mm, packed with Acclaim PepMap100 C18, 5 mm, 100 A˚ ; LC Packings) before being separated by reversed phase chromatography (PepMap, 25 cm, 75 mm ID, 2 mm/100 A˚ pore size, LC Packings) operated on a nano-HPLC (Ultimate 3000 RSLC, Dionex) with a nonlinear 170 min gradient using 2% CAN/0.1% FA (A) and 70% CAN/ 0.1% FA (B) at a flow rate of 300 nl/min. The gradient settings were as follows: 0–140 min: 5–50% B, 141–145 min: 50–95% B, 146–150 min: stay at 95% B and subsequently equilibrate for 20 min to starting conditions as previously published [205].

The MS/MS spectra were searched against the ENSEMBL Human database (Version: 2.4) using the MASCOT search engine (version 2.3.02). Data processing for protein identification and quantification of ICPL-labeled proteins was performed with Proteome Discoverer version 1.3.0.339 (Thermo Scientific).

Proteins were identified by a minimum of two unique peptides detected in at least two out of the three biological replicates. Proteins whose variability between anti-miR-21 and EV treated samples of MCF-10A cells (ICPL_6/ICPL_4 ratio) was less than 30% were considered for further evaluation. The individual proteins with measured ratios of these two labels greater/equal than 1.30-fold or less/equal than 0.77 were considered to be significantly differentially expressed. The biological significance of this fold change cut off is in agreement with previously published data [205-208].

3.9.6 Bioinformatic analysis

The signaling networks and protein-protein interactions that could have been influenced by miR-21 knockdown and exposure to radiation were analysed using Ingenuity Pathway Analysis (IPA) software and STRING protein database. Network analysis was performed for significant differentially regulated proteins. The IPA examines proteins in an uploaded dataset according to curated data on biological function and compares their direction of change to what is expected from the literature stored in the Ingenuity® Knowledge Base. IPA scores were used to estimate the significance of the network predictions. The score for each network was a numerical value to approximate the degree of relevance and size of a network to the molecules in the given dataset. Score ≥ 2 indicated a confidence of 99%. Using pathway libraries that are derived from

scientific literature describing known associations between proteins, IPA also provided information about canonical signaling events. Ratios of number of proteins detected in the proteomic analysis and number of total proteins belonging to a certain pathway were presented as top canonical lists.

The match of observed change and particular predicted activation state of a biological function is made and expressed as activation z-score. Z-score is used to predict activation or inhibition of potential regulators by assessing consistency of the pattern match between changes detected in samples and pattern provided by the network. According to the statistical significance of this match z-score can determine the most likely regulators [209].

3.10 Statistical analysis

All graphical data are presented as mean ± SEM (Standard Error of Mean). Statistical data evaluation among compared groups was performed using two-tailed Student t-test. Statistical significance was considered for following p-values: *p ≤ 0.05, **p ≤ 0.01, ***p ≤0.001.

4 RESULTS

4.1 Array analyses of miRNA expression changes in MCF-10A cells after irradiation

In order to investigate the effects of low and medium doses of ionizing radiation on miRNA expression profiles in non-transformed mammary epithelial cells (MCF-10A) we performed TaqMan® Low Density Arrays. The cells were exposed to 0.25 Gy and 2.5 Gy dose and changes were analysed 4 and 24 hours after radiation. Sham-irradiated MCF-10A cells were used as controls and data represent biological triplicates. Table 16 summarizes the average number of detected and not detected miRNAs of three biological replicates for each sample.

Table 16: Average number of detected miRNA assays

	0 Gy 4 h	0.25 Gy 4 h	2.5 Gy 4 h	0 Gy 24 h	0.25 Gy 24h	2.5 Gy 24 h
detected	158	154	184	206	149	146
not detected	226	230	200	178	235	238

The selection of miRNAs was done according to the fold changes (section 3.5.1). Only miRNAs that expressed the same trends of change in at least 2 out of three biological replicates were taken into further consideration. In Figure 10 each pie chart presents the number of upregulated, downregulated and not changed miRNAs (compared to levels of miRNAs expression in sham-irradiated MCF-10A cells).

For further investigation only significantly changed miRNAs, whose p-values (calculated as described in section 3.10) were less/equal then 0.05, were selected.

The final list of miRNAs was narrowed to 4 upregulated and 76 downregulated ones after 0.25 Gy and to 9 upregulated and 71 downregulated miRNAs after 2.5 Gy 4 hours after radiation treatment. At 24 hour time point, list was downsized to 33 upregulated and 32 downregulated after 0.25 Gy and to 32 upregulated and 20 downregulated miRNAs after 2.5 Gy (Table 17).

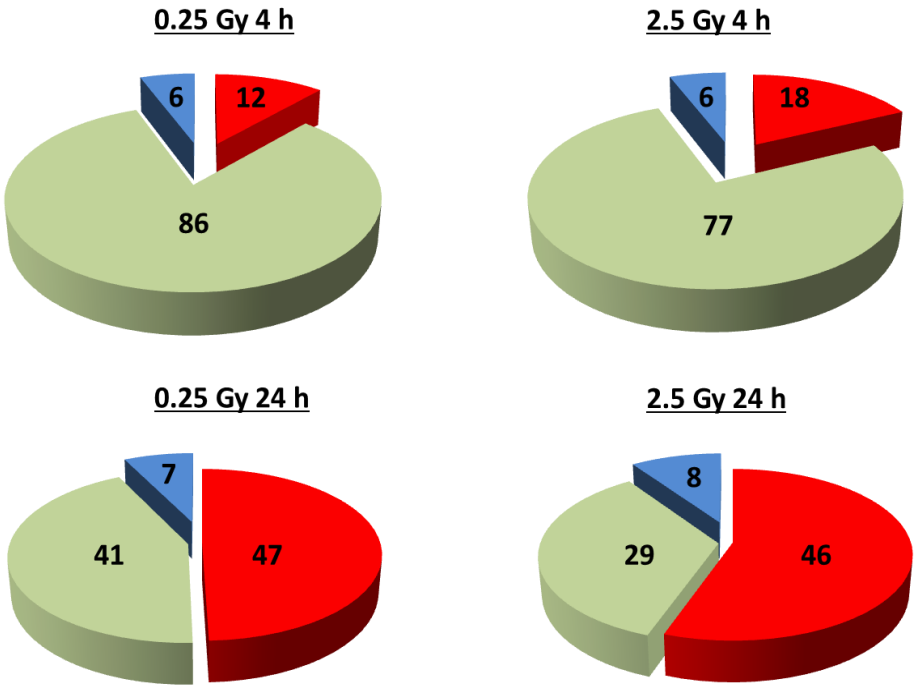

Figure 10. Number of changed miRNAs 4 and 24 hours after radiation treatment. Expression profiles of miRNAs in radiation exposed cells are compared to the sham-irradiated MCF-10A cells. The number of upregulated (red), downregulated (green) or not changed (blue) miRNAs in three biological replicates are shown in each section.

Table 17. Number of significantly deregulated miRNAs 4 and 24 hours after radiation treatments.

	0.25 Gy 4 h	2.5 Gy 4 h	0.25 Gy 24 h	2.5 Gy 24 h
Upregulated	4	9	33	32
Downregulated	76	71	32	20

Lists of significantly upregulated and downregulated miRNAs in MCF-10A cells 4 hours after exposure to 0.25 Gy and 2.5 Gy dose of radiation and their fold changes, in comparison to sham-irradiated cells, are presented in Figure 11 and Figure 12. The changes in miRNA expression profiles 24 hours after 0.25 Gy and 2.5 Gy are displayed in Figure 13 and Figure 14, respectively.

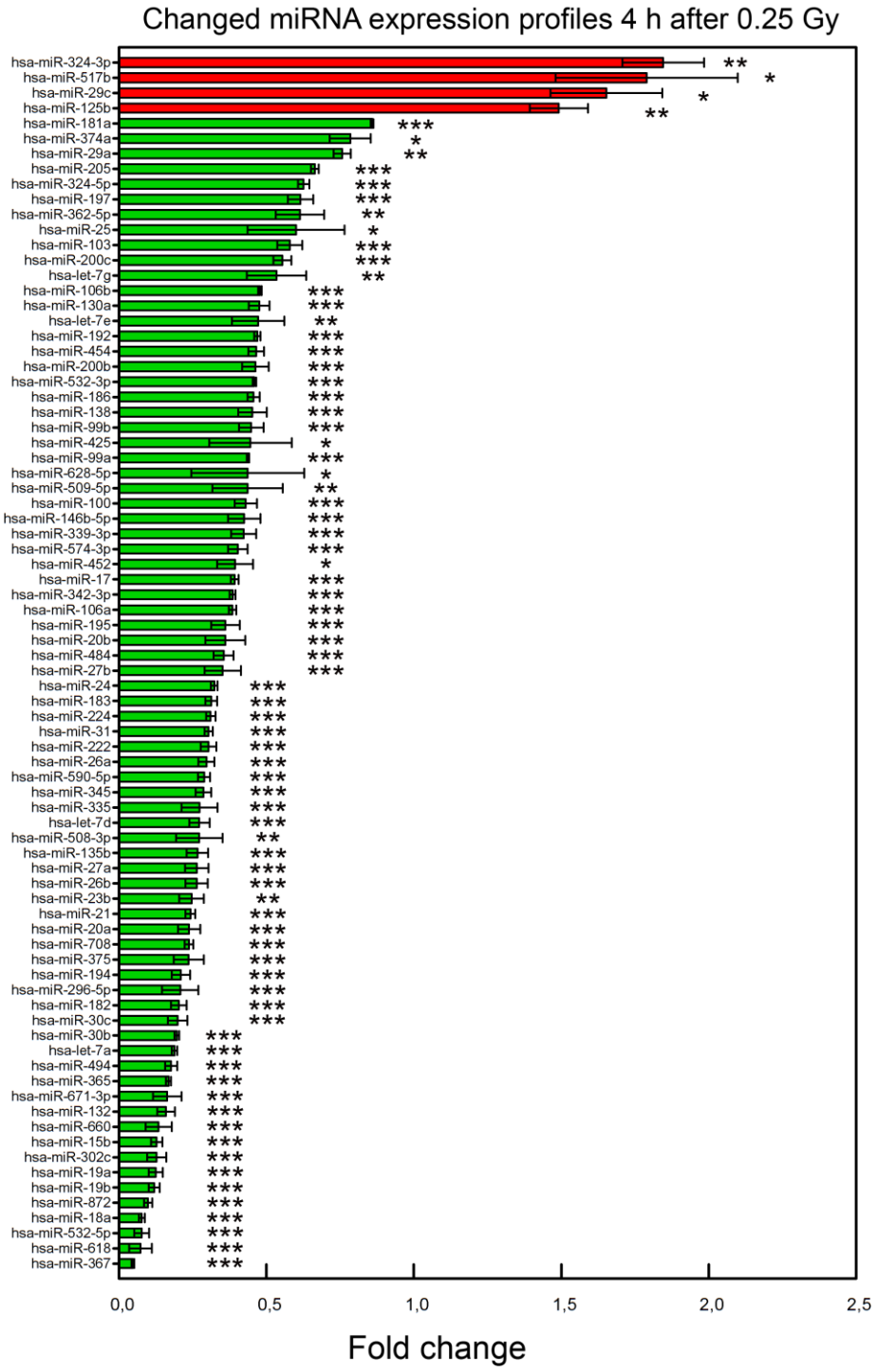

Figure 11. Fold changes of significantly changed miRNAs 4 hours after 0.25 Gy. List of significantly changed miRNA expression profiles compared to control (sham-irradiated) cells 4 hours after exposure to 0.25 Gy dose of radiation. The upregulated miRNAs (red) and the downregulated miRNAs (green) are shown. Data represent mean values ± SEM (n=3). The Student's t-test was used for statistical analysis. *p ≤ 0.05, **p ≤ 0.01, ***p ≤ 0.001

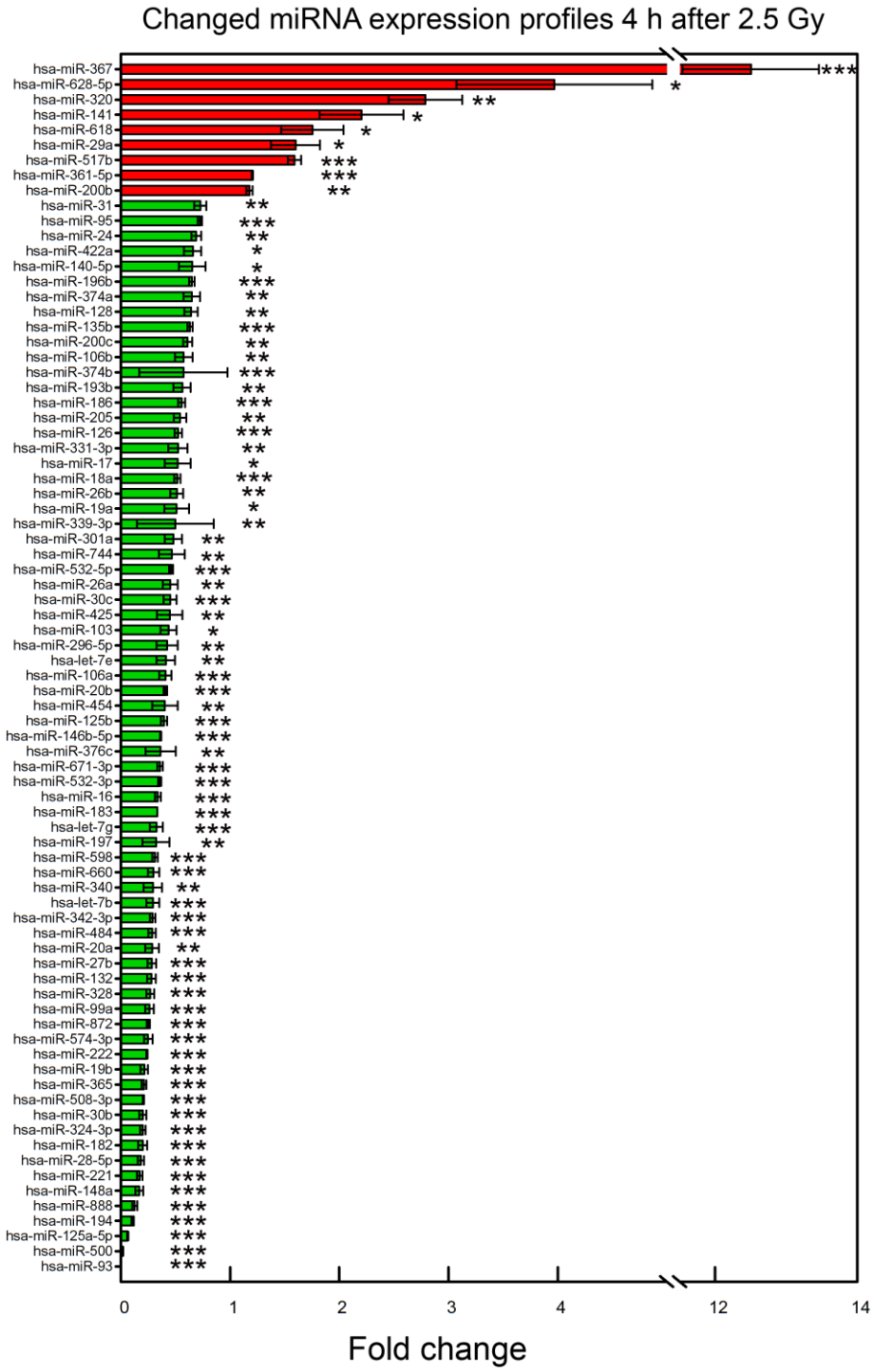

Figure 12. Fold changes of significantly changed miRNAs 4 hours after 2.5 Gy. List of significantly changed miRNA expression profiles compared to control (sham-irradiated) cells 4 hours after exposure to 2.5 Gy dose of radiation. The upregulated miRNAs (red) and the downregulated miRNAs (green) are shown. Data represent mean values ± SEM (n=3). The Student's t-test was used for statistical analysis. *p ≤ 0.05, **p ≤ 0.01, ***p ≤ 0.001

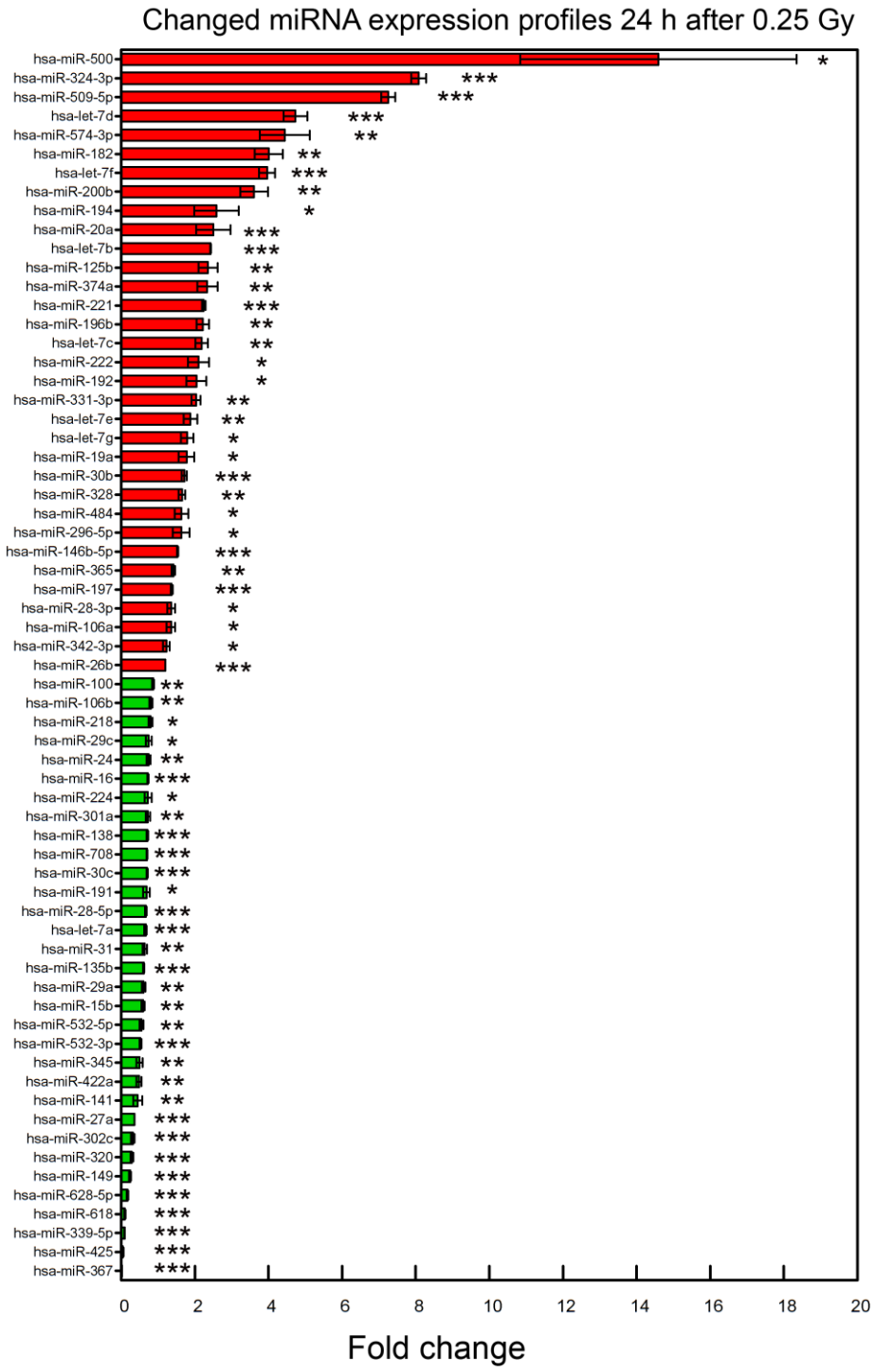

Figure 13. Fold changes of significantly changed miRNAs 24 hours after 0.25 Gy. List of significantly changed miRNA expression profiles compared to control (sham-irradiated) cells 24 hours after exposure to 0.25 Gy dose of radiation. The upregulated miRNAs (red) and the downregulated miRNAs (green) are shown. Data represent mean values ± SEM (n=3). The Student's t-test was used for statistical analysis. *p ≤ 0.05, **p ≤ 0.01, ***p ≤ 0.001

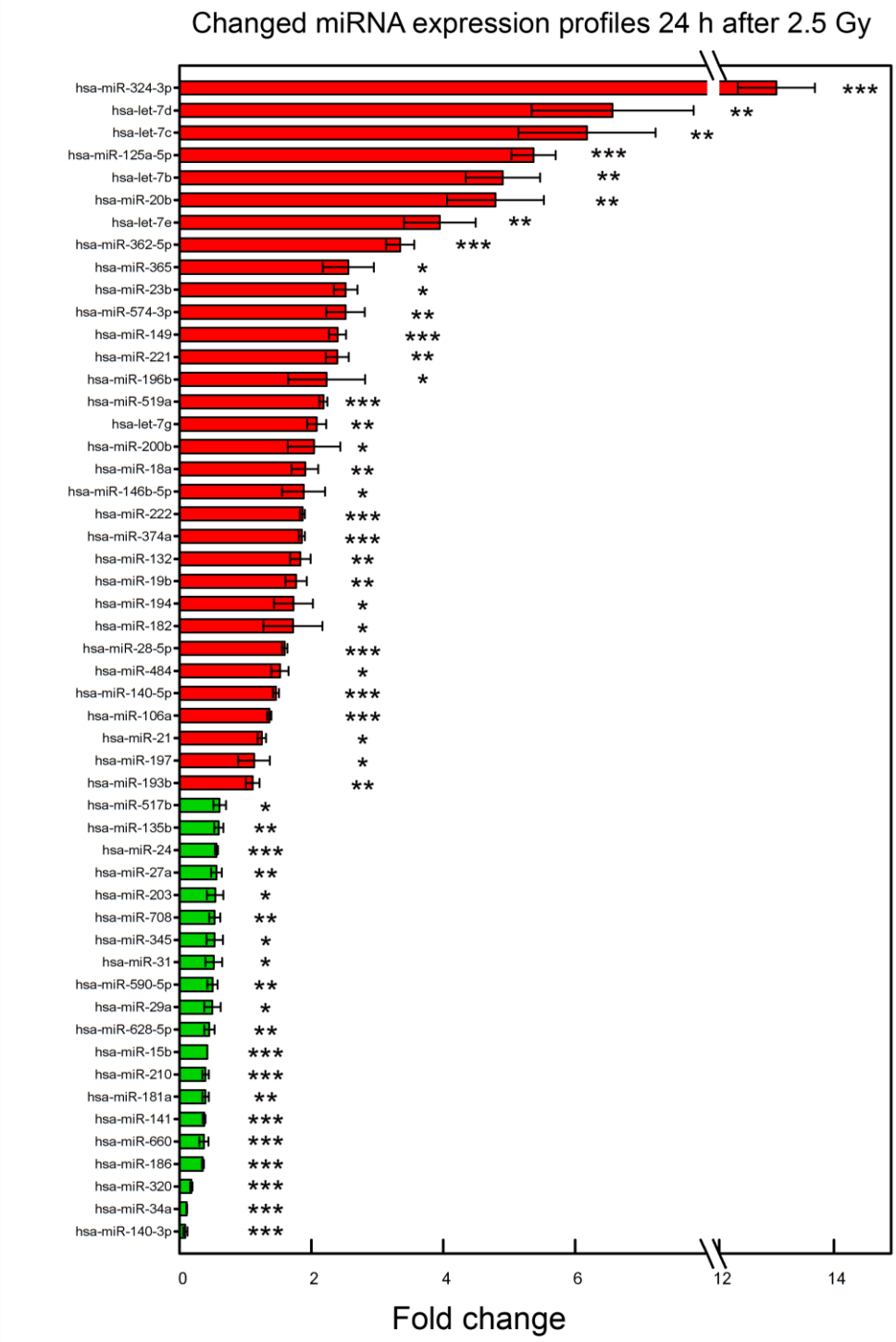

Figure 14. Fold changes of significantly changed miRNAs 4 hours after 2.5 Gy. List of significantly changed miRNA expression profiles compared to control (sham-irradiated) cells 24 hours after exposure to 2.5 Gy dose of radiation. The upregulated miRNAs (red) and the downregulated miRNAs (green) are shown. Data represent mean values ± SEM (n=3). The Student's t-test was used for statistical analysis. *p ≤ 0.05, **p ≤ 0.01, ***p ≤ 0.001

4.2 Selection of miRNAs and verification of changes by single assays

For further validation of the data from TaqMan® Low Density Arrays, 8 radiation regulated miRNAs were chosen due to their role in breast cancer. Validation is performed by single qRT-PCR assays in non-transformed mammary epithelial cells (MCF-10A). These 8 miRNAs are hsa-miR-21, hsa-miR-221, hsa-miR-222, hsa-miR-125-5p, hsa-miR-335, hsa-miR-335*, hsa-miR-494, hsa-miR-891. In addition miRNA - hsa-miR-1226, not present on the array, was added for the selection. The changes in miRNAs expression were followed 4 and 24 hours after irradiation (Figure 15).

The single assays results verified some of the changes obtained with TaqMan® Low Density Arrays in MCF-10A cells (in 4 out of 7 performed single assays (labeled with red) the expression of miRNA showed same changes as detected in Low Density Arrays) (Table 18).

In order to validate the changes in miRNA expression, we examined miRNA levels of miR-21, miR-221 and miR-1226 at different time points (Figure 16). After 0.25 Gy, miR-21 was upregulated after 48 hours. MiR-221 changes were mostly not changed and the pick of miR-1226 expression is noticed after 12 hours. Dose of 2.5 Gy of radiation made more fluctuations in miRNA expression, where all three miRNAs showed that significant changes are seen at later time points (30 hours) after exposure to radiation.

The MDA-MB-361 breast cancer cell line was selected for the investigation of changes in miRNA expression profiles of nine pre-selected miRNAs after radiation exposure (Figure 17). Similar trend in changes of miRNA expression profiles between MCF-10A and MDA-MB-361 cells was detected for miR-222, miR-335, miR-335*, miR-125a-5p, miR-494 and miR-1226. Mir-222 and miR-1226 expressed similar changes between the two cell lines 4 hours after 0.25 Gy while miR-335, miR-125a-5p and miR-494 showed similarities in expression 4 and 24 hours after 2.5 Gy dose. Overview of miRNA expression changes in MCF-10A and MDA-MB-361 cells is presented in Table 19, showing that changes of miRNAs to radiation are different between non-tumorigenic epithelial and breast cancer cells.

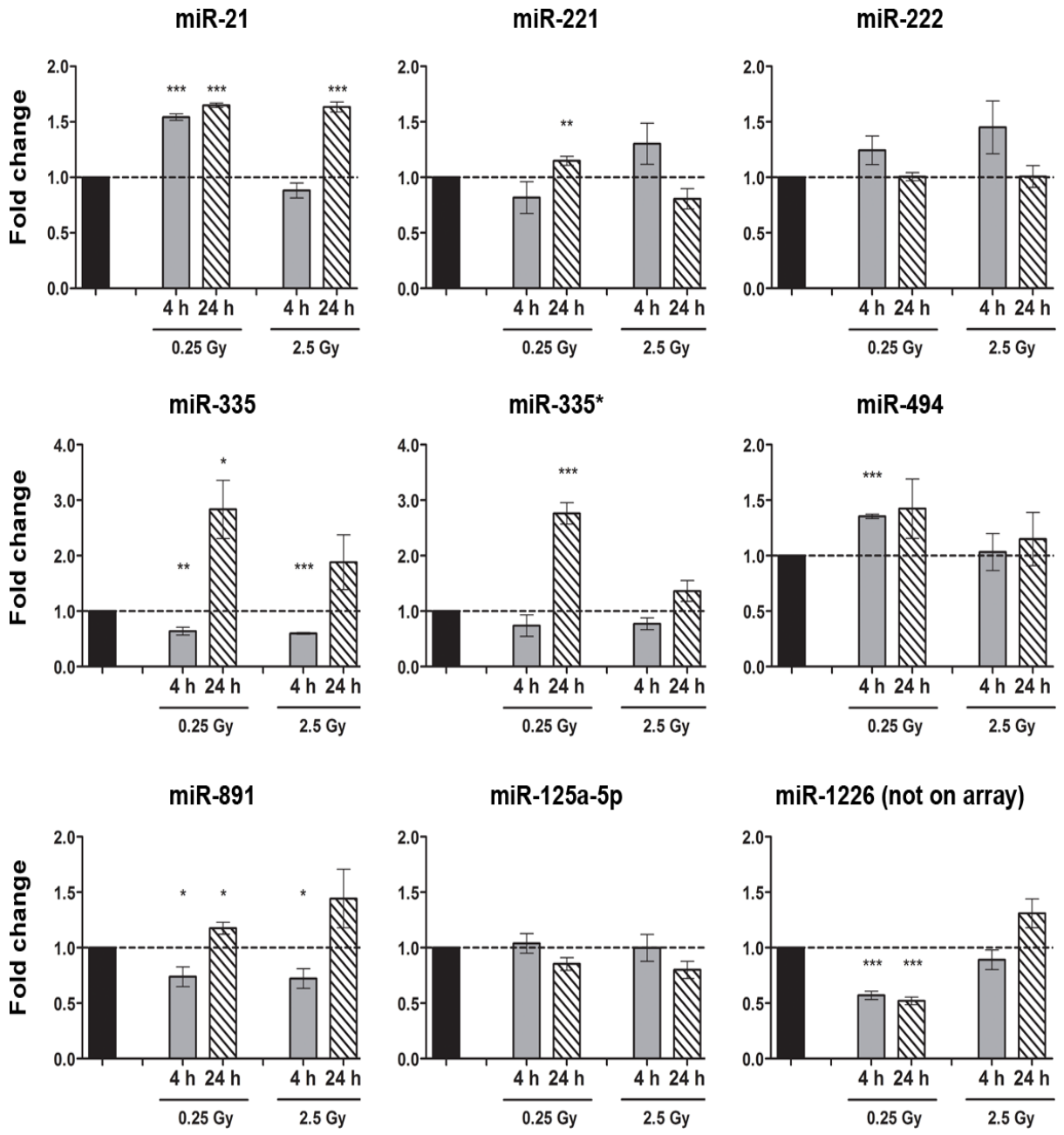

Figure 15. Expression of 9 miRNAs in MCF-10A cells. The expression of 9 miRNAs in MCF-10A cells detected with single assays 4, 24 and 48 hours after exposure to 0.25 Gy and 2.5 Gy dose of radiation. The fold changes are calculated compared to control (sham-irradiated cells) set to 1. Data represent mean values ± SEM (n=3). The Student's t-test was used for statistical analysis. *p ≤ 0.05, **p ≤ 0.01, ***p ≤ 0.001

Table 18: Comparison of Low density array and TaqMan single assay analyses in MCF-10A. The detected changes of 7 listed miRNAs from Low density array analysis and TaqMan single assays (down – downregulated, up – upregulated, nc – not changed compared to sham-irradiated cells, x – not detected, * significant change in miRNA expression according to p-value; red –single assays that confirmed changes detected with Low density arrays)

	0.25 Gy 4 h	2.5 Gy 4 h	0.25 Gy 24 h	2.5 Gy 24 h	0.25 Gy 4 h	2.5 Gy 4 h	0.25 Gy 24 h	2.5 Gy 24 h
miRNA	**Low density array**				**TaqMan single assays**			
miR-21	Down *	Down *	nc	Up *	Up*	nc	Up*	Up*
miR-221	Down *	Down *	Up *	Up *	Down	Up	Up*	Down
miR-222	Down *	Down *	Up *	Up *	Up	nc	nc	nc
miR-335	Down *	Down	Up	Down	Down*	Down*	Up*	Up
miR-125a-	Down	Down *	Up	Up *	nc	nc	Down	Down
miR-494	Down *	Up *	Up	x	Up*	nc	Up	nc
miR-891	x	x	x	x	Down*	Up*	Down*	Up

Table 19: Changes of 9 miRNAs in MCF-10A and MDA-MB-361 obtained with TaqMan single assays. Down – downregulated, up – upregulated, nc – not changed compared to sham-irradiated cells , * significant change in miRNA expression according to p-value; red – cases where the miRNAs are showing the same trend of changes in both cell lines.

	0.25 Gy 4 h	2.5 Gy 4 h	0.25 Gy 24 h	2.5 Gy 24 h	0.25 Gy 4 h	2.5 Gy 4 h	0.25 Gy 24 h	2.5 Gy 24 h
miRNA	**MCF-10A**				**MDA-MB-361**			
miR-21	Up*	Up*	nc	Up	Down*	Down	Down*	nc
miR-221	Down	Up*	Up	Down	Up*	nc	nc	Up
miR-222	Up	nc	Up	nc	Up	Down*	Down*	nc
miR-335	Down*	Up*	Down*	Up	nc	Up*	Up*	Up*
miR-335*	Down	Up*	Down	Up	Down*	nc	Up*	Up*
miR-125a	nc	Down	nc	Down	Up*	Down*	nc	Down
miR-494	Up*	Up	nc	nc	nc	Up*	nc	Up
miR-891	Down*	Up*	Down*	Up	Up	nc	Up	nc
miR-1226	Down*	Down*	nc	Up	Down*	nc	Down*	Up

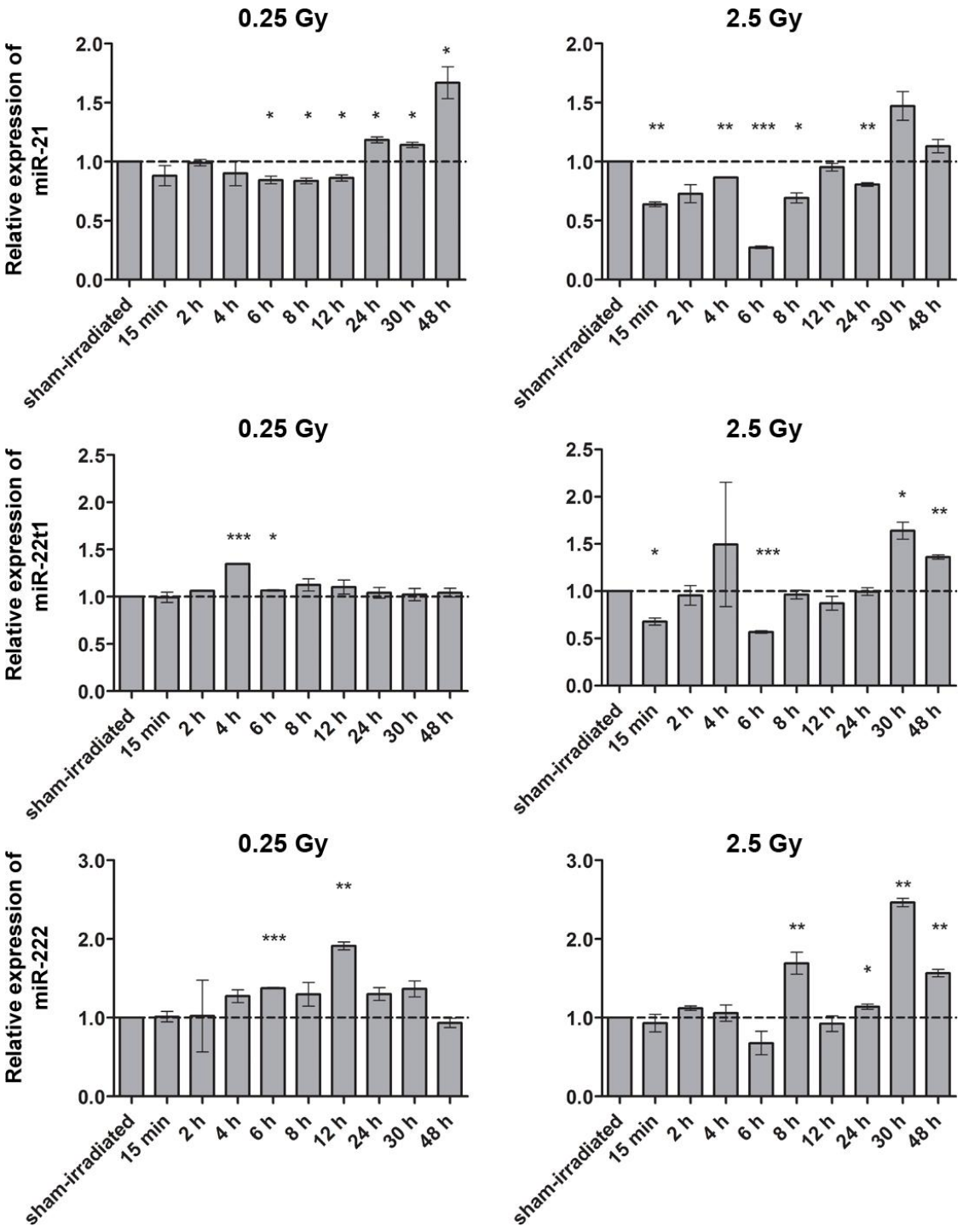

Figure 16. Timeline expression of 3 miRNAs in MCF-10A cells. Timeline of miR-21 (up), miR-221 (middle) and miR-1226 (down) expression in MCF-10A cells following 0.25 Gy and 2.5 Gy doses of radiation. Normalization is done to the value of sham-irradiated cells. Data represent mean values ± SEM (n=3). The Student's t-test was used for statistical analysis. *p ≤ 0.05, **p ≤ 0.01, ***p ≤ 0.001

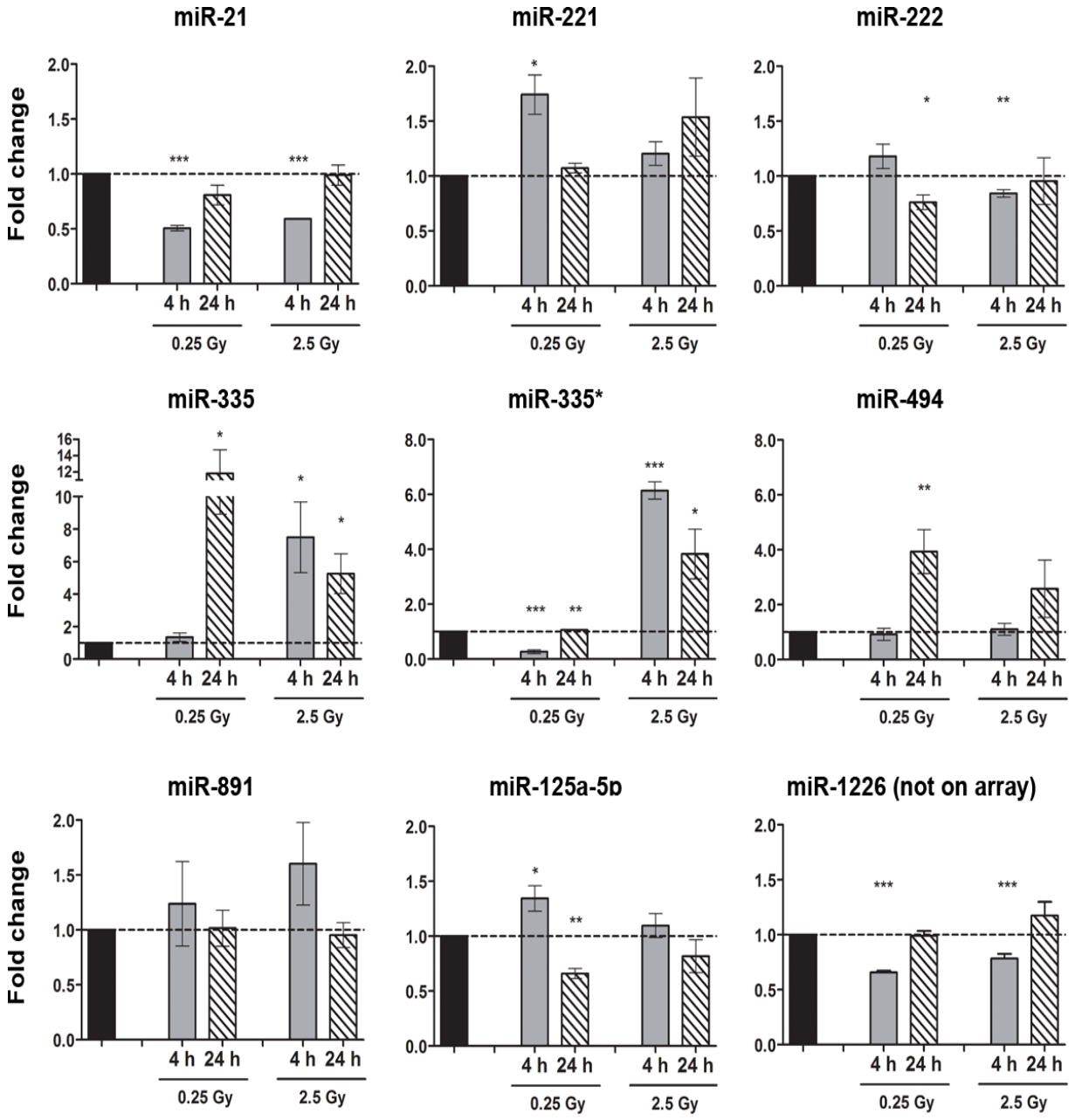

Figure 17. Expression of 9 miRNAs in MDA-MB-361 cells. The expression of 9 miRNAs in MDA-MB-361 cells detected with single assays 4, 24 and 48 hours after exposure to 0.25 and 2.5 Gy dose of radiation. The fold changes are calculated compared to control (sham-irradiated cells) which value is set to 1. Data represent mean values ± SEM (n=3). The Student's t-test was used for statistical analysis. *p ≤ 0.05, **p ≤ 0.01, ***p ≤ 0.001

According to the miRNA expression analyses it was not possible to detect highly significant regulation of any individual miRNA. Therefore, we decided to proceed with analysis of miR-21 as one of the important miRNAs for cellular development. This miRNA was upregulated in irradiated MCF-10A cells and downregulated in irradiated cancer cell line MDA-MB-361, indicating miR-21 as a potential biomarker.

4.3 Cellular response of MCF-10A and MDA-MB-361 after combined treatment with anti-miR-21 and radiation

The endogenous levels of miR-21 in non-irradiated MCF-10A and MDA-MB-361 cells were determined. In MDA-MB-361 miR-21 levels were 3.99 ± 0.01 fold higher than in MCF-10A cells (set to 1) (Figure 18). This result correlates with previous observations indicating that miR-21 is highly expressed in tumour cells.

4.3.1 FACS analysis of GFP expressing cells proved the successful lentiviral transduction of MCF-10A and MDA-MB-361 cells

The effectiveness of lentiviral transduction was determined using cytofluorimetric analysis (FACS) to detect GFP expression in the cells. The lentivirus activity was also check in HEK293T cells as control cells.

MCF-10A cells show 86.34% and 92.76% transduction efficiency with EV and anti-miR-21, respectively while MDA-MB-361 cells show 98.40% (EV) and 99.37% (anti-miR-21). In HEK293T cells 94.82% (EV) and 94.64% (anti-miR-21) GFP positive expressing cells were detected with the same virus concentration used (Figure 20).

4.3.2 Knockdown of miR-21 using lentiviral approach

In order to investigate the effects of miR-21 knockdown in both MCF-10A and MDA-MB-361 cell lines, the cells were transduced with anti-miR-21 lentivirus as previously described (Section 3.2.3). The miR-21 knockdown efficiency was analysed 72 hours after lentiviral transduction with anti-miR-21 (Figure 19) and before using the cells in further experiments. The fold change of miR-21 expression was decreased to 0.27 ± 0.06 in MCF-10A and to 0.34 ± 0.01 in MDA-MB-361 cells when compared to control (EV) (set to 1).

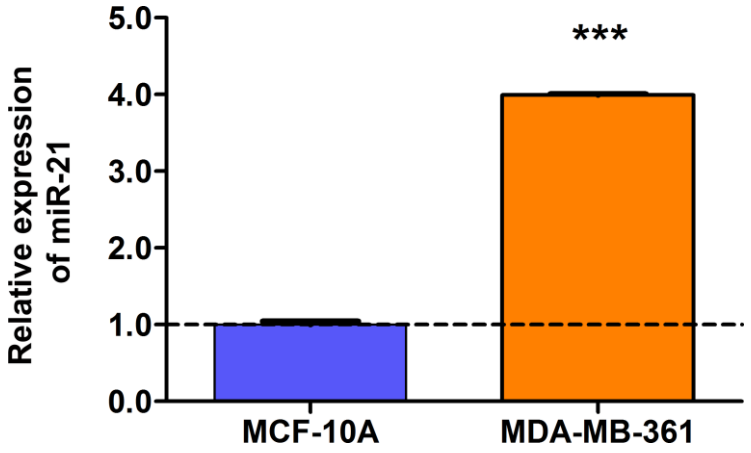

Figure 18. Endogenous expression of miR-21 in MCF-10A and MDA-MB-361 cells. Relative expression of endogenous miR-21 presented as fold change after normalization to RNU44 and to non-transformed mammary epithelial cells MCF-10A (set as 1). Data represent means ± SEM (n=3). The Student's t-test was used for statistical analysis. ***p ≤ 0.001

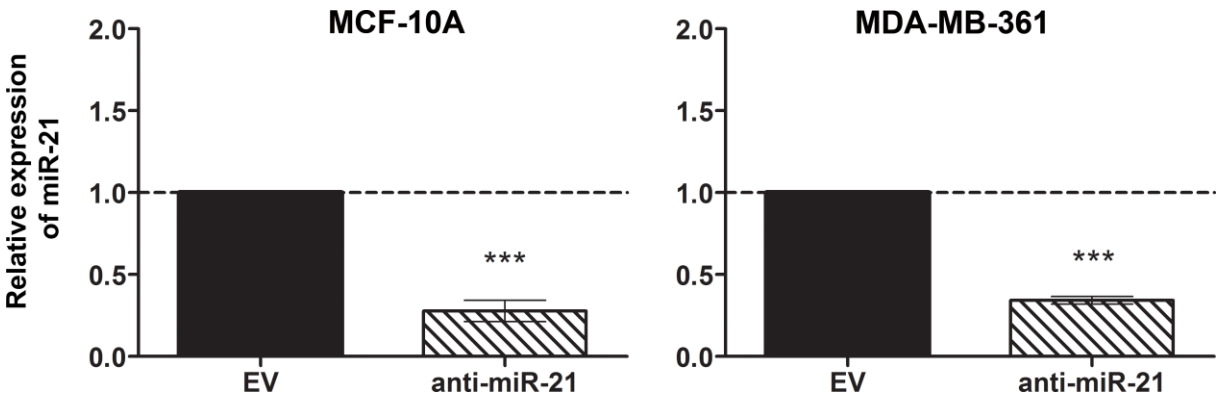

Figure 19. MiR-21 expression levels of miR-21 after anti-miR-21 treatment. MiR-21 expression levels 72 hour after lentiviral transduction with anti-miR-21 in MCF-10A (left) and MDA-MB-361 cells (right) compared to the levels in cells transduced with EV (set to 1). Data represent means ± SEM (n=3). The Student's t-test was used for statistical analysis. ***p ≤ 0.001

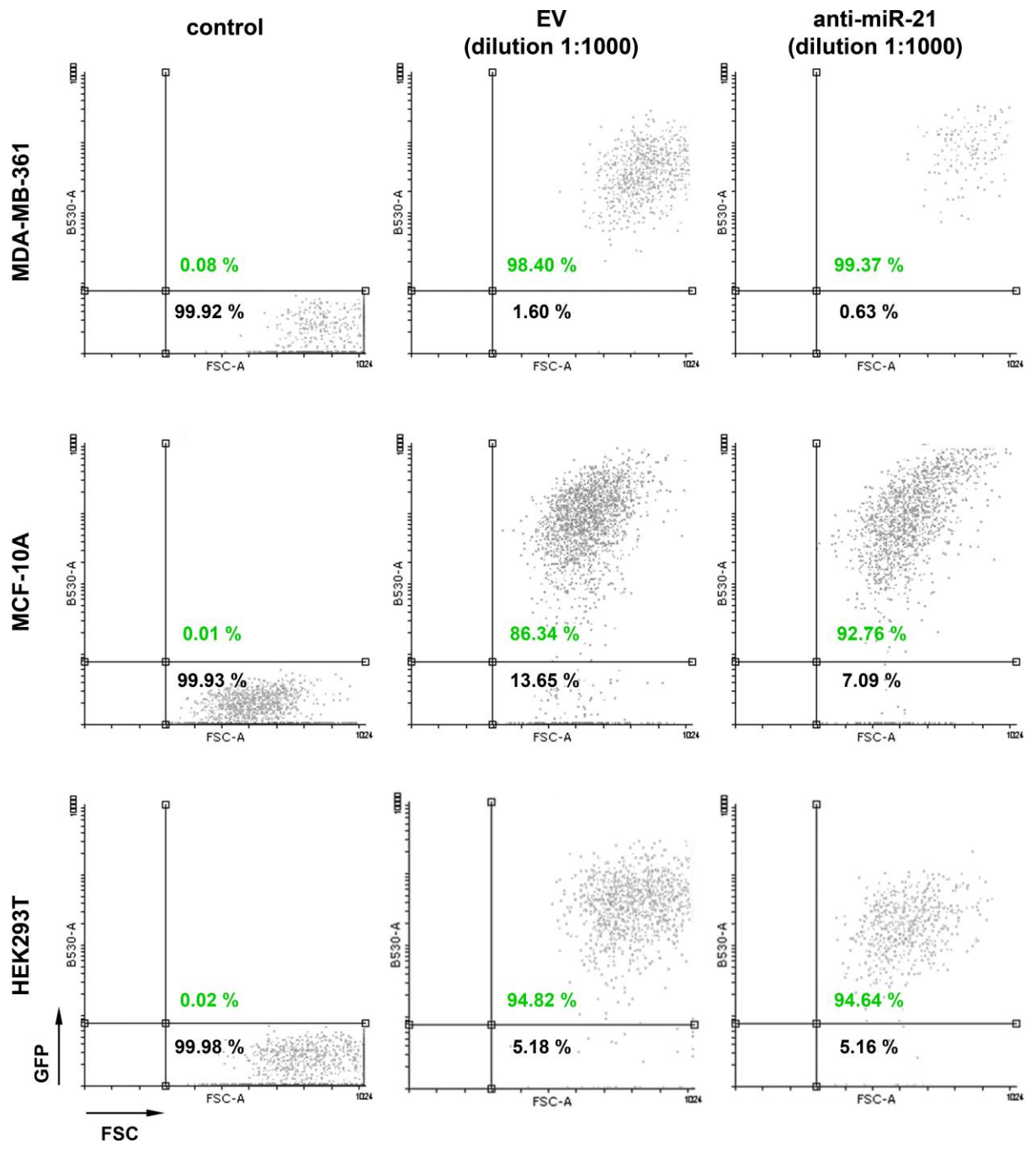

Figure 20. FACS analyses of GFP expressing cells after lentiviral transduction. The FACS analyses of GFP expressing MDA-MB-361 (up), MCF-10A (middle), and HEK293T (down) cells after lentiviral transduction. The cells were treated with the EV or anti-miR-21 lentivirus in dilution 1:1000 and the analysis was done 72 hours after transduction.

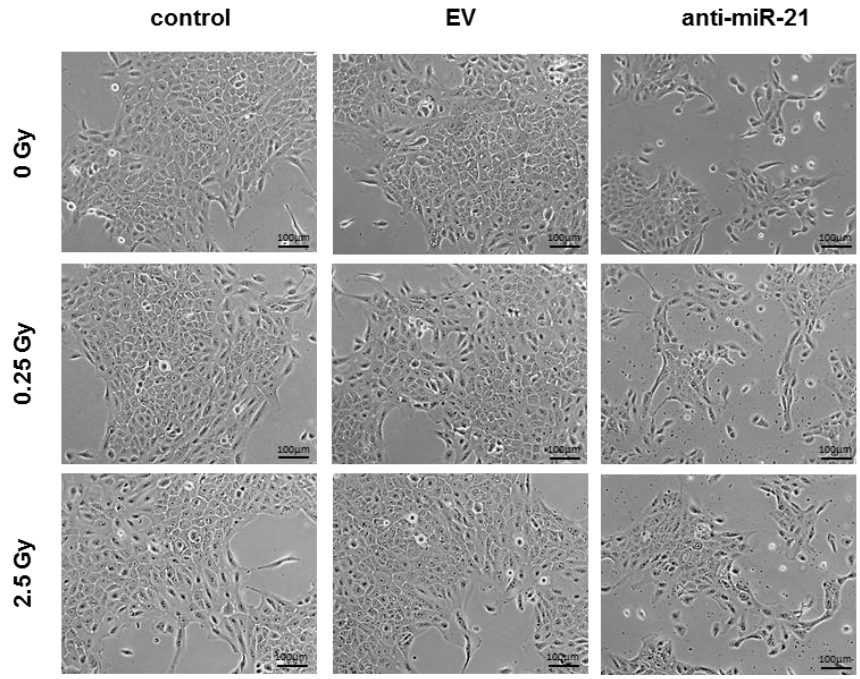

Figure 21. Morphology of MCF-10A cells after radiation treatment. Morphology of MCF-10A control cells (without lentiviral transduction) and cells transduced with EV and anti-miR-21, 24 hours after 0.25 Gy and 2.5 Gy dose of radiation (bright field detection). Scale bar=100μm.

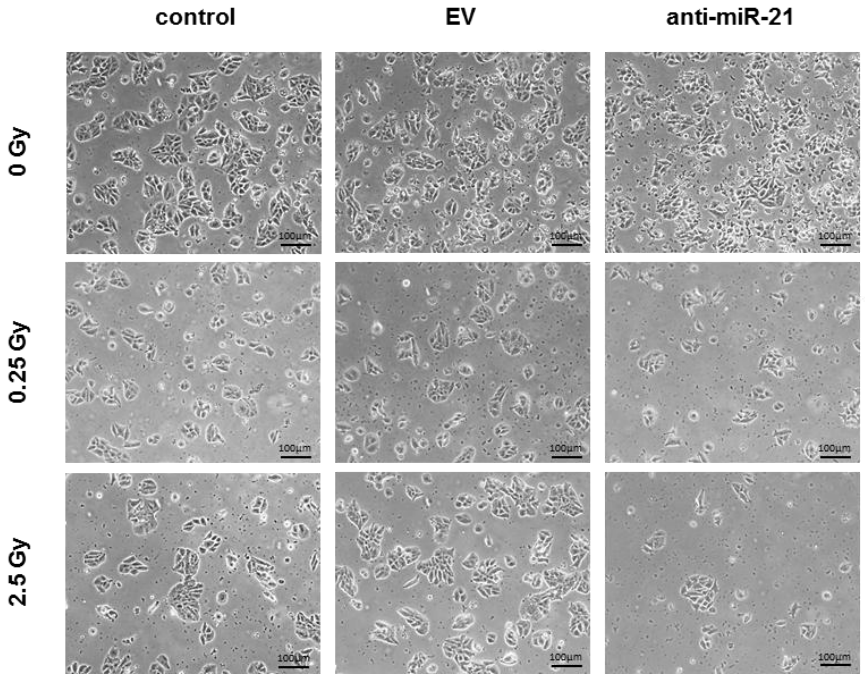

Figure 22. Morphology of MDA-MB-361 cells after radiation treatment. Morphology of MDA-MB-361 control cells (without lentiviral transduction) and cells transduced with EV and anti-miR-21, 24 hours after 0.25 Gy and 2.5 Gy dose of radiation (bright field detection). Scale bar=100μm.

The morphology of MCF-10A and MDA-MB-361 cells after combined treatment with anti-miR-21 and radiation was monitored 24 hours post-radiation. No changes in morphology of between control cells, EV treated and anti-miR-21 treated MCF-10A cells were noticed. Proliferation of cells after the knockdown of miR-21 was affected, where fewer cells were noticed compared to EV treated and control cells. Radiation did not have any effect on the morphology of cells or their proliferation rate (Figure 21).

Unlike MCF-10A, the radiation did affect the proliferation ability of control and EV treated MDA-MB-361 cells according to less cells detected 24 hours after radiation. Radiation in combination with miR-21 knockdown had stronger effect on proliferation of MDA-MB-361 cells (Figure 22).

4.3.3 Colony formation of MCF-10A and MDA-MB-361 cells after knockdown of miR-21

No significant difference was detected in colony formation between MCF-10A cells (expressing low levels of miR-21) treated with EV or anti-miR-21 seven days after radiation treatment. MDA-MB-361 cells, expressing high endogenous miR-21 levels, had difficulties to form colonies after treatment with anti-miR-21, even without radiation (Figure 23). MiR-21 knockdown further diminish clonogenic ability of MDA-MB-361 cells.

The clonogenic ability of MCF-10A cells is diminished equally in EV and anti-miR-21 treated cells when radiation dose used was higher than 4 Gy. Dose of 8 Gy was enough to strongly reduce colony formation characteristic.

EV treated MDA-MB-361 cells also showed that with the exposure to 4 Gy of higher dose of radiation diminish their clonogenic ability. Unlike EV, breast cancer cells showed that knockdown of miR-21 alone is enough to significantly decrease their clonogenic ability. With dose of radiation higher than 2 Gy, ability to form colonies was further decreased as the number of formed colonies was significantly reduced (number of detected colonies were less than 5). These findings are based on the results from 4 biological replicates (Figure 24).

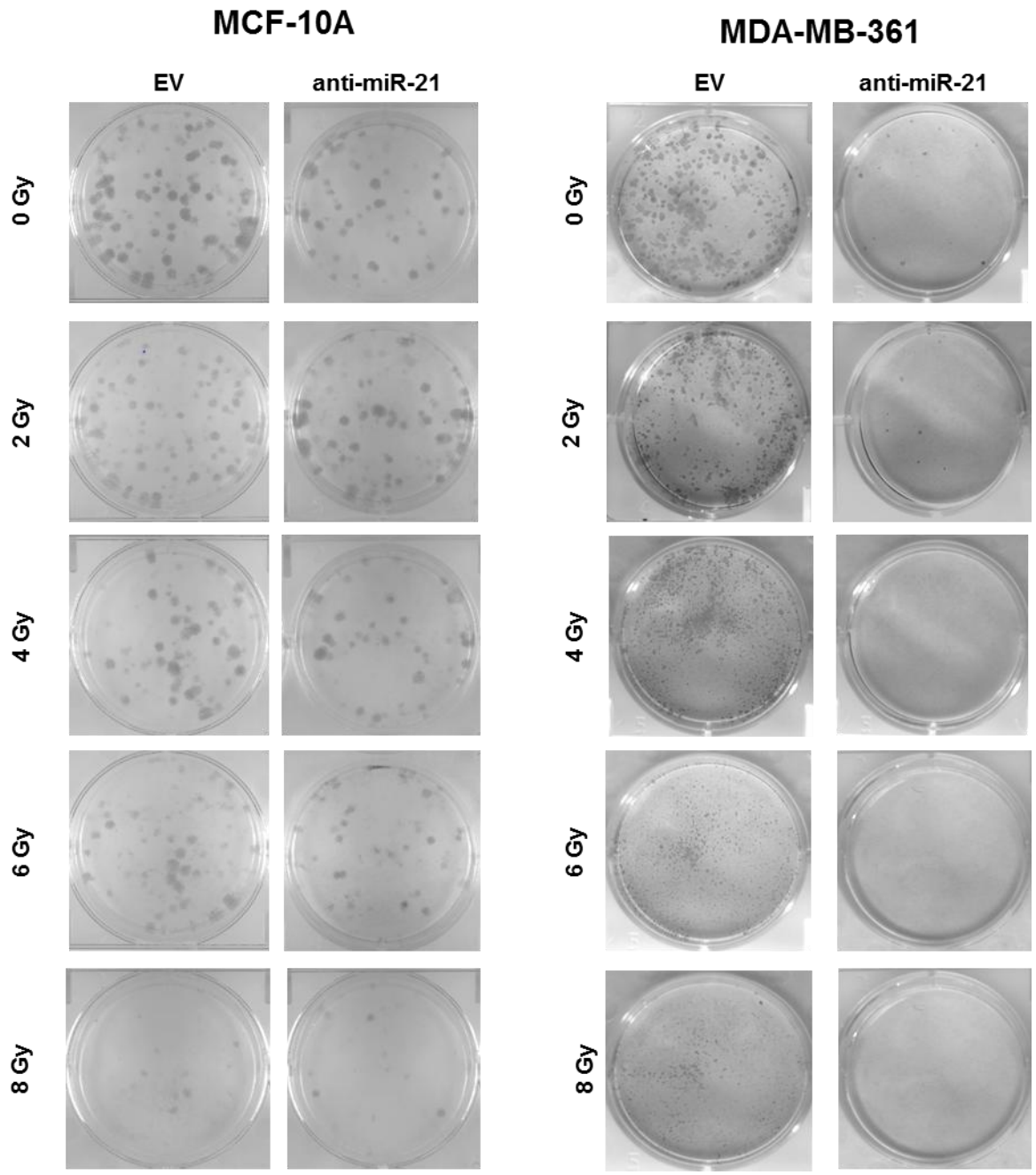

Figure 23. Clonogenic survival assays of MCF-10A and MDA-MB-361 cells.MDA-Clonogenic survival assay of EV and anti-miR-21 treated MCF-10A (left) and MDA-MB-361 (right) cells after exposure to 0, 2, 4, 6 and 8 Gy dose of irradiation.

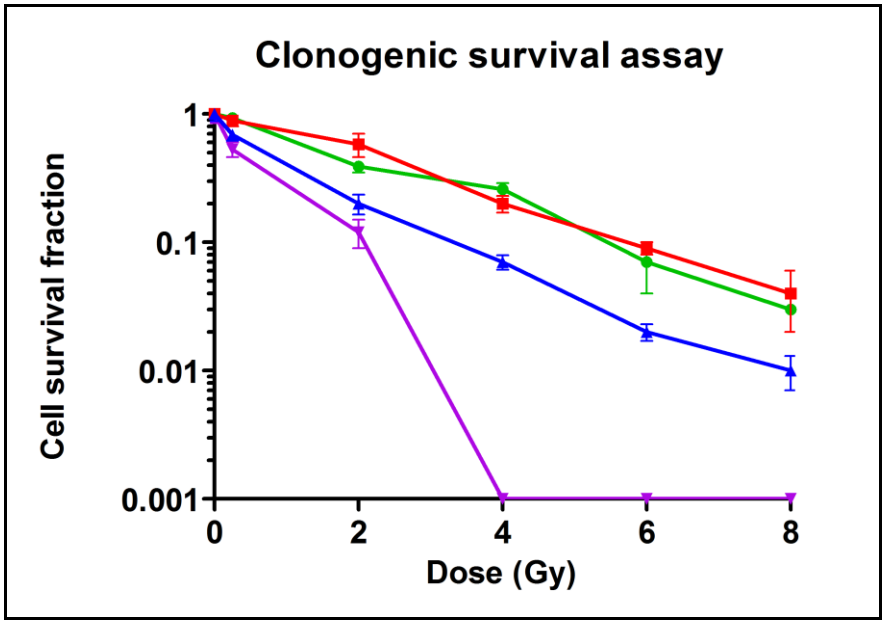

Figure 24. Clonogenic survival fractions of MCF-10A and MDA-MB-361 cells. Clonogenic survival fraction of EV (green) and anti-miR-21 treated MCF-10A (red) and EV (blue) and anti-miR-21 treated MDA-MB-361 cells (purple) after treatment with 0, 2, 4, 6 and 8 Gy dose of irradiation. Data obtained from 4 independent experiments and graphically presented. Data represent means ± SEM (n=4).

4.3.4 MiR-21 downregulation in combination with radiation leads to increase of apoptosis and reduction of the G2 cell fraction in MDA-MB-361 but not in MCF-10A cells

MCF-10A (Figure 25) and MDA-MB-361 (Figure 26) cells were analysed for cell cycle changes 24 hours after 0.25 Gy and 2.5 Gy irradiation after being transduced with EV or anti-miR-21 as well as for the non lentivirally transduced cells (labelled as control cells). The analysis was done in three biological replicates and the percentage of cells in each cell cycle phase is presented for MCF-10A (Table 20) and MDA-MB-361 (Table 21). Significant changes in cell cycle of MCF-10A cells after radiation were detected only in S phase while the changes of MDA-MB-361 cells were noticed in all phases after miR-21 knockdown.

The relative number of cells in each cell cycle is compared between EV and anti-miR-21 treated cells as well as between EV and control cells (normalized to the EV 0 Gy). No significant differences in cell cycle analysis were detected between control cells and EV

treated cells in both MCF-10A and MDA-MB-361 cell line, confirming that lentiviral transduction did not influence the cell cycle phases.

Differences in cell cycle distributions of MCF-10A cells are presented in Figure 27. MiR-21 knockdown did not significantly change the population of MCF-10A cells in subG1 phase compared to the EV sham-irradiated cells and radiation did not have any effect on the cell population in this phase. Number of MCF-10A cells in S phase after knockdown of miR-21 was reduced to 0.78 ± 0.10 in sham-irradiated cells. Radiation dose of 2.5 Gy further reduced this cell population to 0.70 ± 0.03 in EV treated and to 0.46 ± 0.06 in anti-miR-21 treated cells. The anti-miR-21 slightly reduced the number of MCF-10A cells in G2 phase with no further reduction when combined with radiation.

In Figure 28 the differences in cell cycle distributions of MDA-MB-361 cells are presented. SubG1 cell population number was significantly increased after miR-21 knockdown in sham-irradiated cells (3.45 ± 0.39) and after exposure to 0.25 Gy (3.83 ± 0.19) and 2.5 Gy irradiation (3.59 ± 0.07). MDA-MB-361 cells expressed prominent reduction in number of cells in S and G2 phase following miR-21 knockdown. In S phase, number of cells is reduced to 0.18 ± 0.12 in sham-irradiated cells and radiation further reduced the number to 0.05 ± 0.004 after 0.25 Gy and to 0.12 ± 0.02 after 2.5 Gy. Anti-miR-21 treatment led to reduction of MDA-MB-361 cell population in G2 phase to 0.46 ± 0.09 in sham-irradiated cells and exposure to 0.25 Gy (0.41 ± 0.09) and 2.5 Gy (0.41 ± 0.04) did not further decrease the cell number.

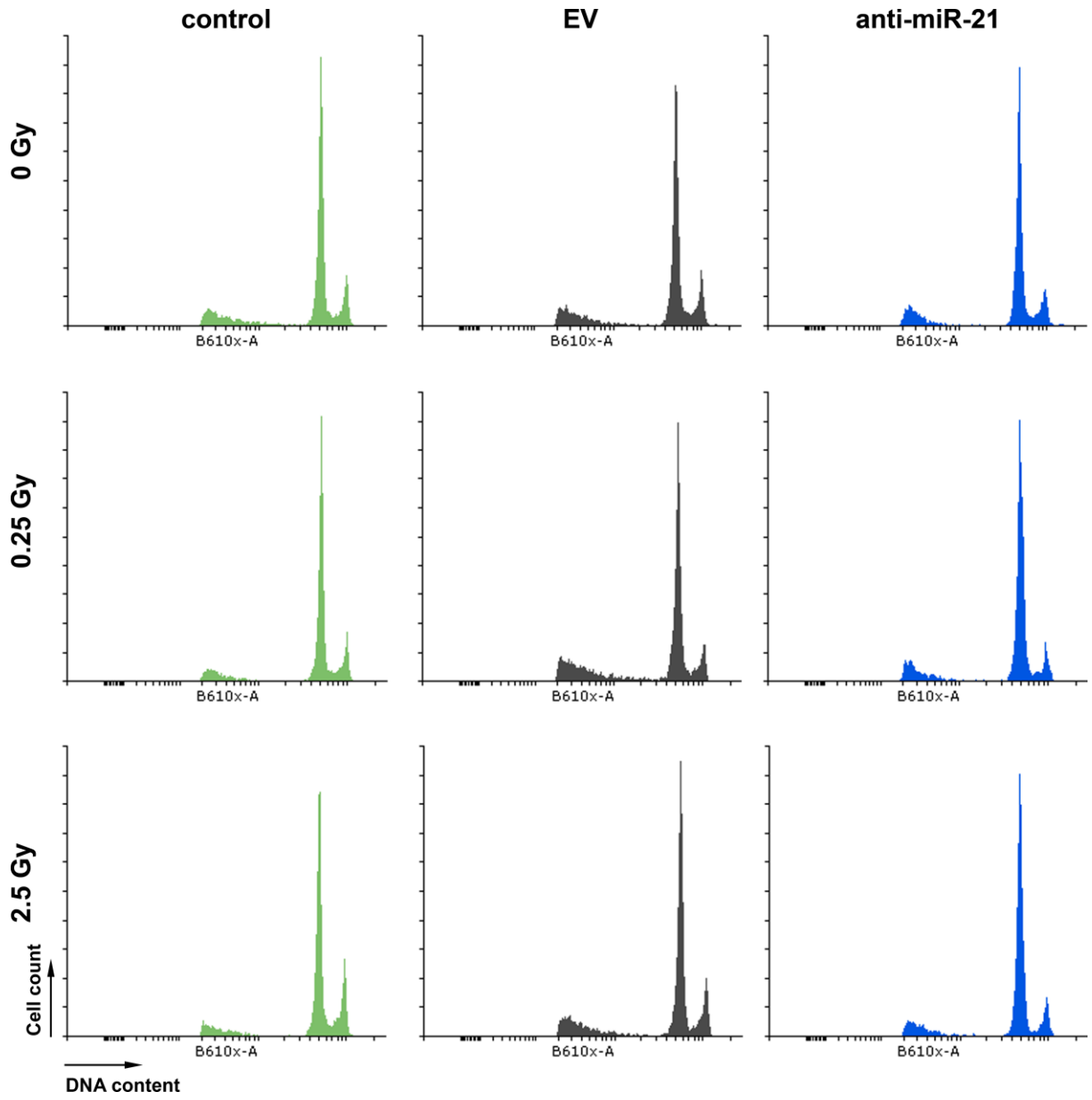

Figure 25. Overview of MCF-10A cells cell cycle analysis. The cell cycle overview of control (green), EV (black) and anti-miR-21 (blue) treated sham-irradiated MCF-10A cells and 24 hours after exposure to low (0.25 Gy) and medium dose (2.5 Gy) of radiation.

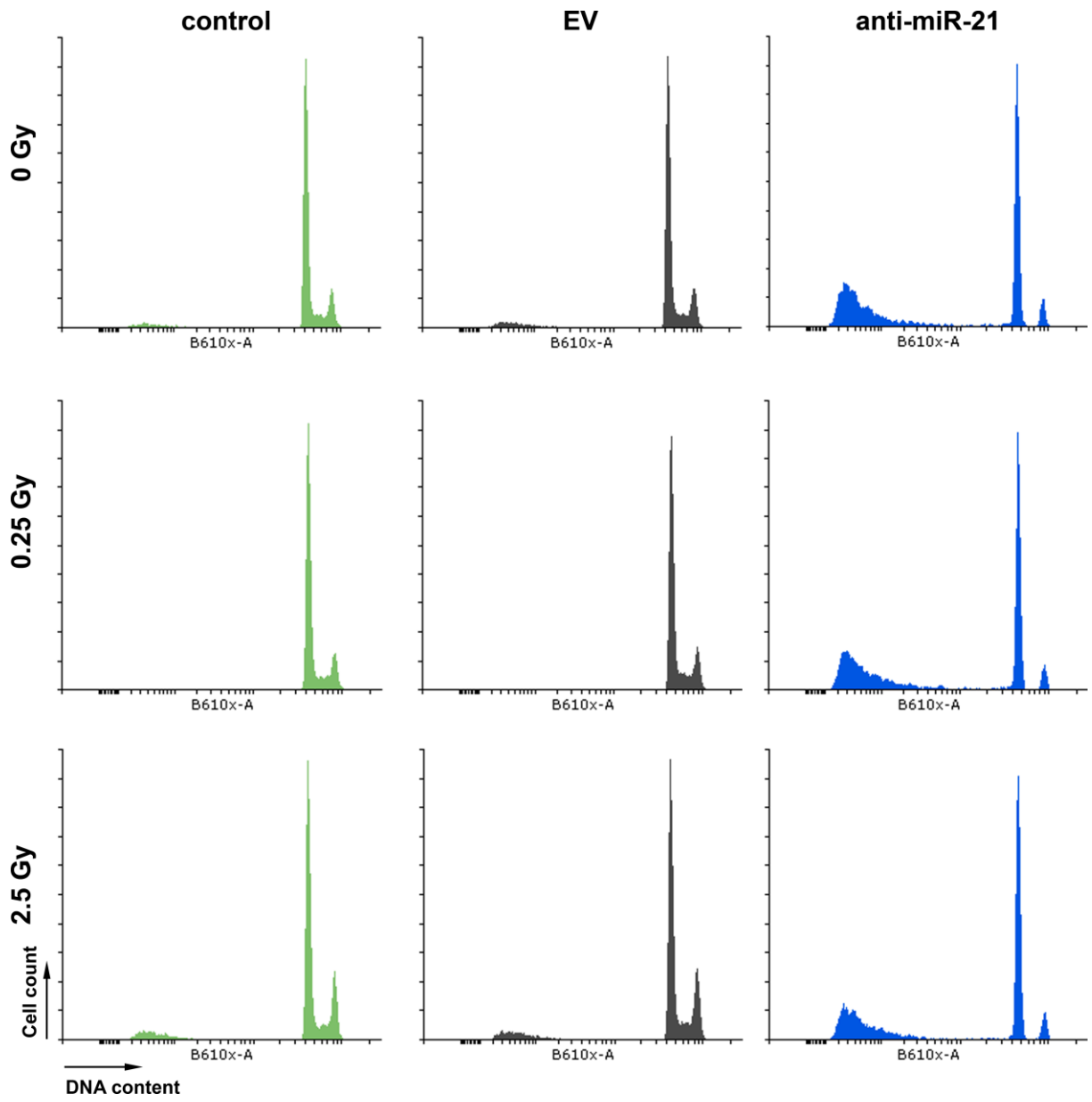

Figure 26. Overview of MDA-MB-361 cells cycle analysis. The cell cycle overview of control (green), EV (black) and anti-miR-21 (blue) treated sham-irradiated MDA-MB-361 cells and 24 hours after exposure to low (0.25 Gy) and medium dose (2.5 Gy) of radiation.

Table 20: The percentage of MCF-10A cells in each phase of cell cycle. Data represent mean values ± SEM (n=3).

MCF-10A	0 Gy			0.25 Gy			2.5 Gy		
	Control	EV	anti-miR-21	Control	EV	anti-miR-21	Control	EV	anti-miR-21
subG1	28.4 ± 10.5	29.6 ± 7.1	39.1 ± 10.7	31.3 ± 7.1	31.3 ± 7.1	35.1 ± 9.2	33.4 ± 9.7	29.5 ± 6.4	32.0 ± 10.5
G1	55.5 ± 6.7	55.6 ± 5.6	49.9 ± 9.3	55.2 ± 5.1	54.9 ± 5.2	55.3 ± 9.3	51.8 ± 6.6	56.0 ± 4.6	56.5 ± 10
S	3.6 ± 0.6	4.0 ± 0.8	3.1 ± 0.8	3.8 ± 0.8	3.9 ± 0.8	2.4 ± 0.1	2.8 ± 0.8	2.8 ± 0.6	1.7 ± 0.2
G2	12.5 ± 3.5	10.8 ± 0.9	7.8 ± 1.2	9.8 ± 1.4	9.9 ± 1.1	7.2 ± 0.6	12.0 ± 2.5	11.7 ± 1.2	9.7 ± 0.3

Table 21: The percentage of MDA-MB-361 cells in each phase of cell cycle. Data represent mean values ± SEM (n=3).

MDA-MB-361	0 Gy			0.25 Gy			2.5 Gy		
	Control	EV	anti-miR-21	Control	EV	anti-miR-21	Control	EV	anti-miR-21
subG1	19.9 ± 10.1	18.4 ± 3.7	74.3 ± 6.4	17.5 ± 7.5	24.4 ± 3.7	75.7 ± 5.1	21.4 ± 7.4	25.3 ± 4.9	75.2 ± 8.9
G1	73.5 ± 4.9	70.1 ± 0.3	37.4 ± 6.4	72.0 ± 2.8	66.9 ± 0.4	30.6 ± 14.4	64.4 ± 1.5	61.9 ± 0.5	33.2 ± 17.2
S	3.7 ± 2.0	3.6 ± 2.0	0.4 ± 0.06	4.8 ± 2.2	4.2 ± 2.6	0.2 ± 0.08	4.1 ± 2.0	3.9 ± 2.4	0.4 ± 0.14
G2	7.8 ± 3.2	7.3 ± 1.6	3.8 ± 0.5	8.6 ± 2.5	4.9 ± 1.1	3.3 ± 0.5	11.5 ± 3.8	7.5 ± 1.7	3.3 ± 0.7

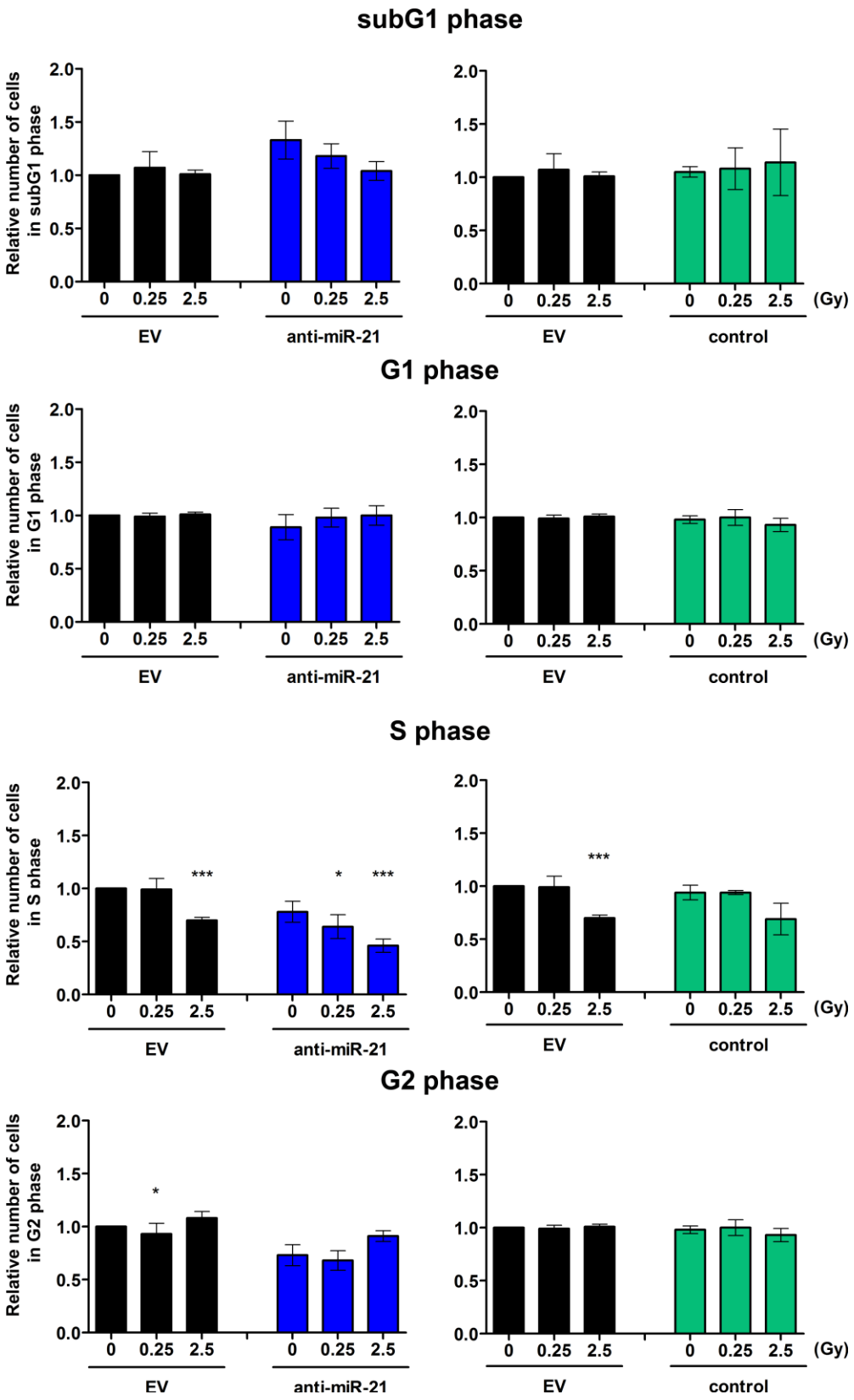
subG1 phase
Relative number of cells in subG1 phase
G1 phase
Relative number of cells in G1 phase
S phase
Relative number of cells in S phase
G2 phase
Relative number of cells in G2 phase
2.0
1.5
1.0
0.5
0.0
0
0.25
2.5
(Gy)
EV
anti-miR-21
control
*
***

Figure 27. Representation of each phase of cell cycle in MCF-10A cells. Relative number of cells in different phases of cell cycle of MCF-10A cells (24 hours after exposure to radiation). All values are normalized to the sample of EV 0 Gy. Data represent mean values ± SEM (n=3). Black – EV treated cells, blue – anti-miR-21 treated cells, green – control cells. *$p \leq 0.05$, ***$p \leq 0.001$

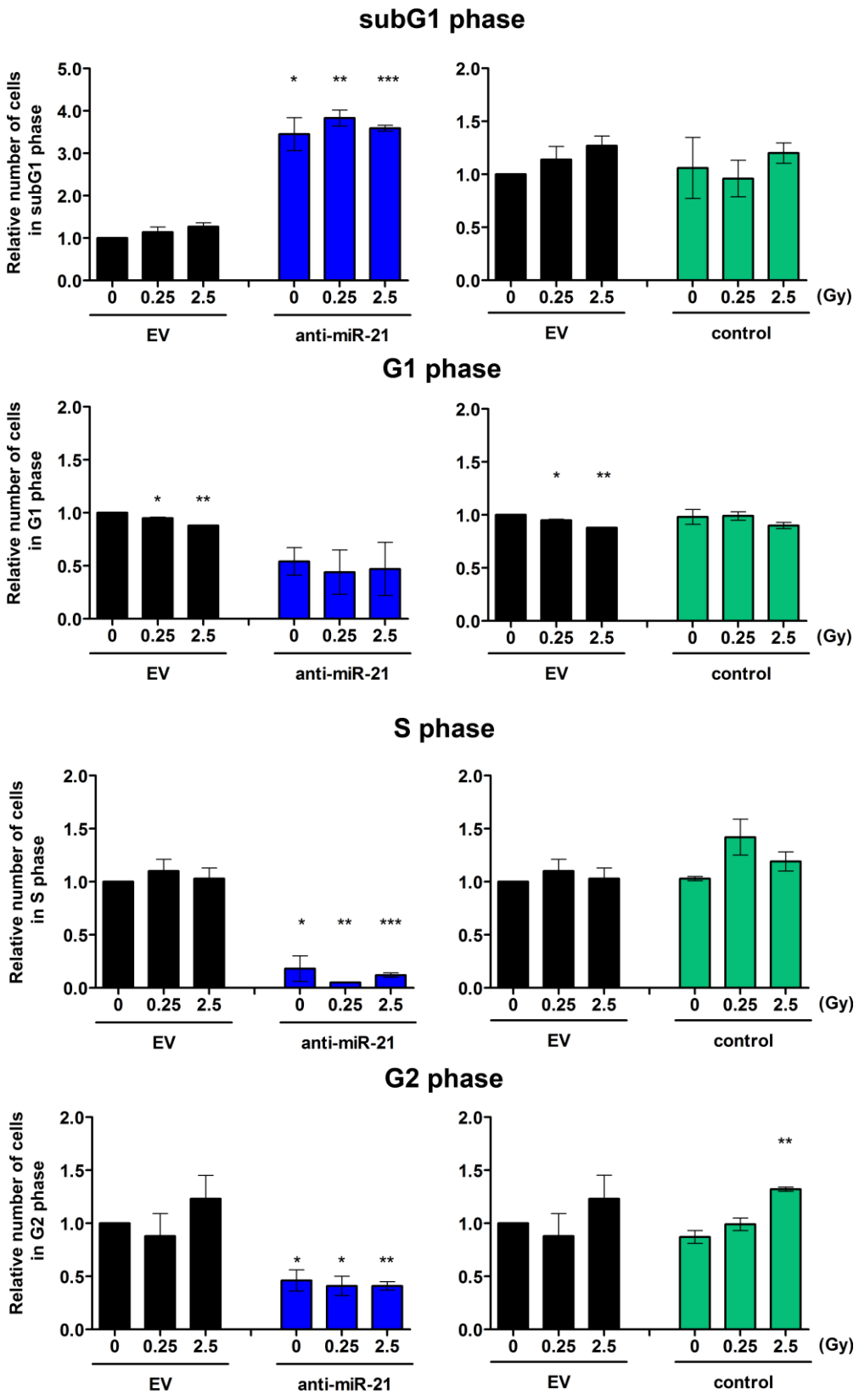
subG1 phase
Relative number of cells in subG1 phase
5.0
4.0
3.0
2.0
1.0
0.0
*
**
***
0
0.25
2.5
EV
anti-miR-21
control
(Gy)
G1 phase
Relative number of cells in G1 phase
S phase
Relative number of cells in S phase
G2 phase
Relative number of cells in G2 phase

Figure 28. Representation of each phase of cell cycle in MDA-MB-361 cells. Relative number of cells in different phases of cell cycle of MDA-MB-361 cells (24 hours after exposure to radiation). All values are normalized to the sample of EV 0 Gy. Data represent mean values ± SEM (n=3). Black – EV treated cells, blue – anti-miR-21 treated cells, green – control cells. *$p \leq 0.05$, ***$p \leq 0.001$

4.3.5 Cell viability of MCF-10A cells is less affected by anti-miR-21 compared to MDA-MB-361 cells

The cell viability was measured using two different assays, CellTiter-Glo® assay and WST-1 assay) as described (Sections 3.3.2.1 and 3.3.2.2) that measure metabolic activity of the cells. Luciferase based assay showed that knockdown of miR-21, without radiation, reduces the cell viability of MCF-10A cells to 1.29 ± 0.09 relative light units (RLU) compared to EV cells (2.26 ± 0.08 RLU) 24 hours after treatment (Figure 29).

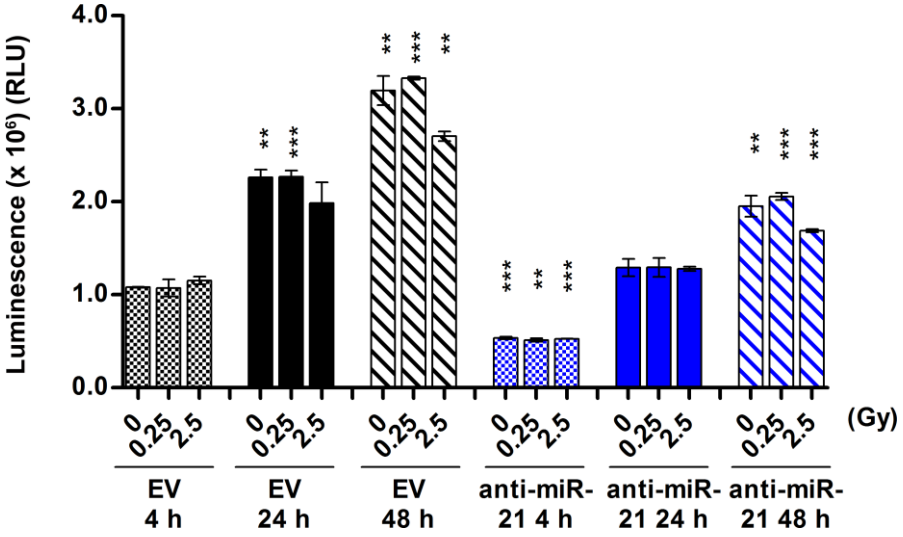

Figure 29. CellTiter-Glo® viability assay of EV and anti-miR-21 MCF-10A cells. The cell viability of MCF-10A cells quantified luminescence (relative light units - RLU) of EV (black) and anti-miR-21 (blue) treated cells measured with CellTiter-Glo® assay. Viability of the cells was measured 4 hours (checker boxes), 24 hours (solid color boxes) and 48 hours (downward diagonal boxes) after exposure to 0.25 Gy and 2.5 Gy dose of radiation. Luminescence was quantified and corrected with blank. Data represent mean values ± SEM (n=3). **p ≤ 0.01, ***p ≤ 0.001

Treatment with radiation (0.25 Gy and 2.5 Gy) did not significantly change the viable cell fraction after 24 hours. Viable cell fraction of MCF-10A showed after 48 hours additional increase compared to cell viability detected 24 hours after treatment in both EV and anti-miR-21 treated cells. The dose of 2.5 Gy slightly reduced the number of viable MCF-10A cells treated with EV (2.70 ± 0.05 RLU) and anti-miR-21 (1.69 ± 0.02 RLU) after 48 hours, in comparison to sham irradiated (3.19 ± 0.16 RLU and 1.95 ± 0.11 RLU, respectively) and cells exposed to 0.25 Gy (3.33 ± 0.02 RLU and 2.05 ± 0.04 RLU,

respectively). No differences in cell viability between control and EV treated cells were detected (Figure 30).

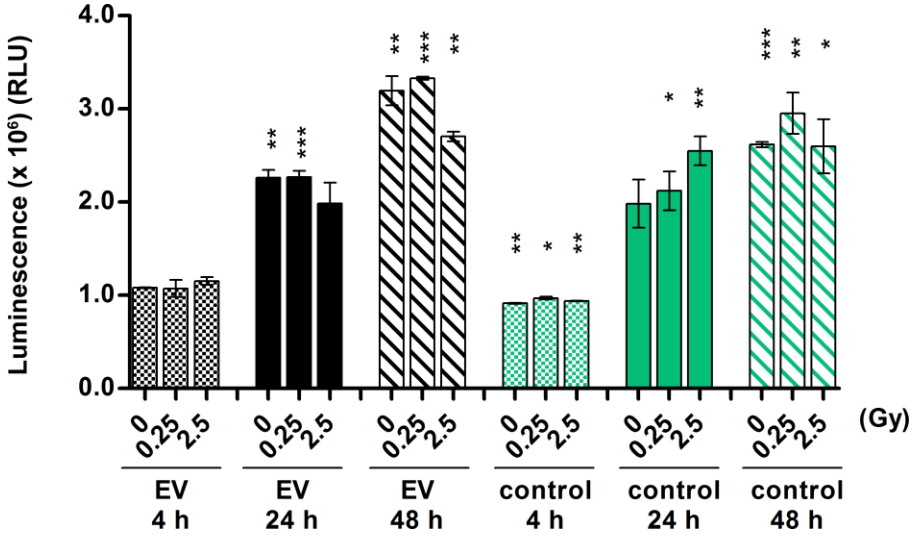

Figure 30. CellTiter-Glo® viability assay of EV and control MCF-10A cells. The cell viability of MCF-10A cells quantified luminescence (relative light units - RLU) of EV (black) and control (green) cells measured with CellTiter-Glo® assay. Viability of the cells was measured 4 hours (checker boxes), 24 hours (solid color boxes) and 48 hours (downward diagonal boxes) after exposure to 0.25 Gy and 2.5 Gy dose of radiation. Luminescence was quantified and corrected with blank. Data represent mean values ± SEM (n=3). *p ≤ 0.05 **p ≤ 0.01, ***p ≤ 0.001

MDA-MB-361 EV treated cells showed significant increase in viable cell fraction 24 hours (0.83 ± 0.01 RLU) and 48 hours (0.95 ± 0.02 RLU) after treatment compared to 4 hour time point (0.47 ± 0.01), without additional influence of radiation. Cells treated with anti-miR-21 did not show changes in cell viability after 24 hours (0.45 ± 0.02 RLU) and 48 hours (0.42 ± 0.02) compared to 4 hour time point (0.37 ± 0.01 RLU). Treatment of MDA-MB-361 cells with anti-miR-21 led to the reduction of cell viability - to 0.46 ± 0.02 RLU compared to EV cells (0.84 ± 0.01 RLU) 24 hours after treatment. The dose of 2.5 Gy did slightly decrease proliferation capacity of MDA-MB-361 cells to 0.37 ± 0.01 RLU after 48 hours (Figure 31). Low dose irradiation (0.25 Gy) in both cell lines did not show significant differences when compared to sham-irradiated cells.

No differences in cell viability between control and EV treated MDA-MB-361 cells were detected (Figure 32). The increase in luminescence, from 4 to 48 hour time point after radiation of anti-miR-21 treated MCF-10A cells, indicates that cells retain the ability to

proliferate. Decrease in luminescence of anti-miR-21 treated MDA-MB-361 cells, compared to EV cells, suggest that this treatment affects their proliferation ability.

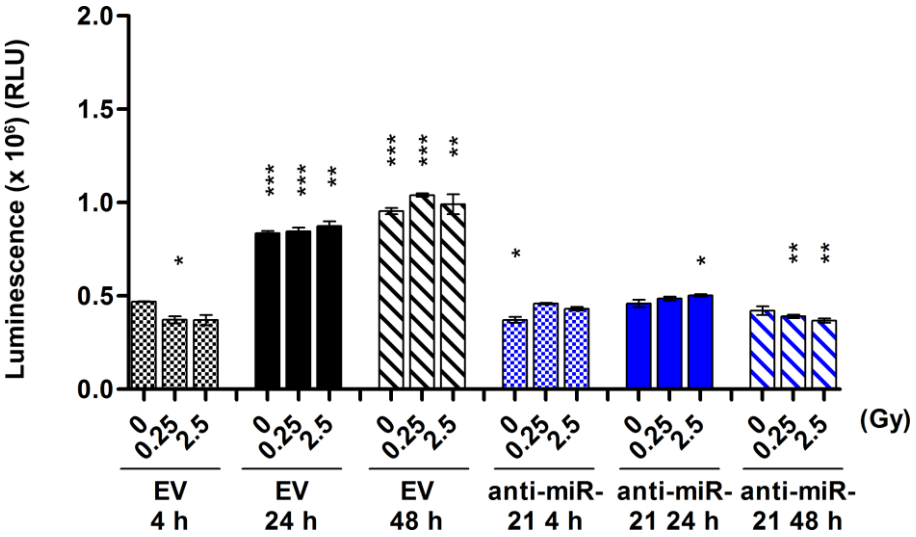

Figure 31. CellTiter-Glo® viability assay of EV and anti-miR-21 MDA-MB-361 cells. The cell viability of MDA-MB-361 cells quantified luminescence (relative light units - RLU) of EV (black) and anti-miR-21(blue) treated cells measured with CellTiter-Glo® assay. Viability of the cells was measured 4 hours (checker boxes), 24 hours (solid color boxes) and 48 hours (downward diagonal boxes) after exposure to 0.25 Gy and 2.5 Gy dose of radiation. Luminescence was quantified and corrected with blank. Data represent mean values ± SEM (n=3). **p ≤ 0.01, ***p ≤ 0.001

Next we have performed colorimetric based cell viability analysis using WST-1 assay measuring the absorbance units (AU). It confirmed that number of viable EV treated MCF-10A cells after 24 hours (0.31 ± 0.01 AU) and 48 hours (0.58 ± 0.03 AU) is increased compared to 4 hour time point (0.06 ± 0.00 AU). Reduction of viable cells after miR-21 knockdown without radiation to 0.14 ± 0.01 AU compared to EV treated cells at 24 hour time point was also confirmed. After 48 hours the number of viable cells was further increased (0.32 ± 0.03 AU). The dose of 2.5 Gy reduced the number of viable MCF-10A cells treated with EV and anti-miR-21 after 24 and 48 hours in comparison to sham-irradiated cells. With this assay contribution of 0.25 Gy dose on lower cellular viability of EV and anti-miR-21 MCF-10A cells 48 hours after radiation was detected (Figure 33).

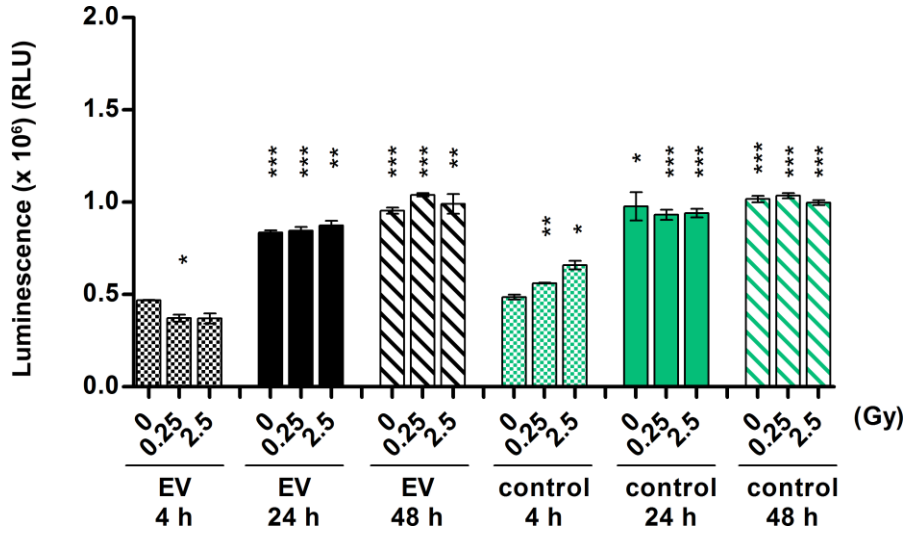

Figure 32. CellTiter-Glo® viability assay of EV and control MDA-MB-361 cells. The cell viability of MDA-MB-361 cells quantified luminescence (relative light units - RLU) of EV (black) and control (green) cells measured with CellTiter-Glo® assay. Viability of the cells was measured 4 hours (checker boxes), 24 hours (solid color boxes) and 48 hours (downward diagonal boxes) after exposure to 0.25 Gy and 2.5 Gy dose of radiation. Luminescence was quantified and corrected with blank. Data represent mean values ± SEM (n=3). *p ≤ 0.05 **p ≤ 0.01, ***p ≤ 0.001

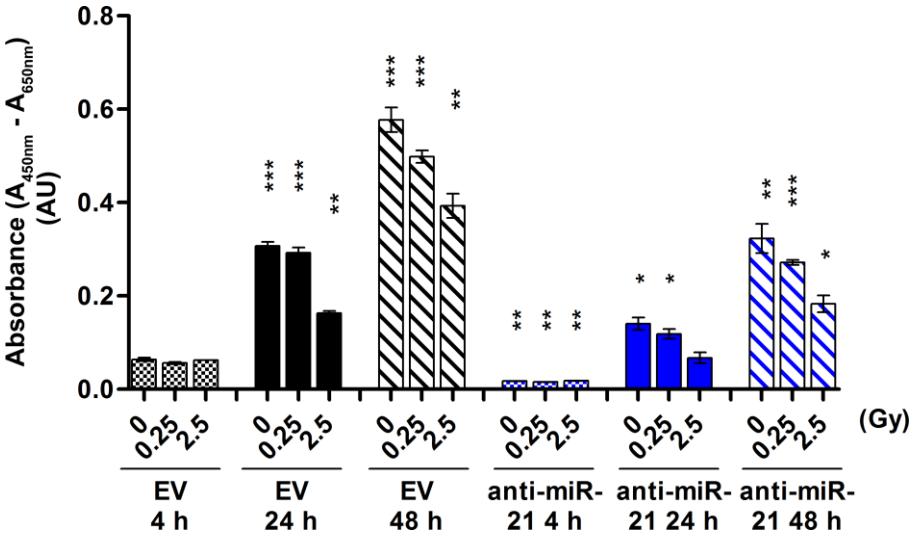

Figure 33. WST-1 viability assay of EV and anti-miR-21 MCF-10A cells. The cell viability of MCF-10A cells quantified absorbance (absorbance units (AU)) of EV (black) and anti-miR-21 (blue) treated cells measured with WST-1 assay. Absorbance was measured 4 hours (checker boxes), 24 hours (solid color boxes) and 48 hours (downward diagonal boxes) after exposure to 0.25 Gy and 2.5 Gy dose of radiation. Relative absorbance is quantified as difference between measurement (450 nm) and reference wavelength (650 nm) at each analysed time point. Data represent mean values ± SEM (n=3). *p ≤ 0.05, **p ≤ 0.01, ***p ≤ 0.001

WST-1 assay also showed the ability of MCF-10A cells to proliferate after treatment with miR-21 knockdown and radiation. No differences in cell viability between control and EV treated MCF-10A cells were detected (Figure 34)

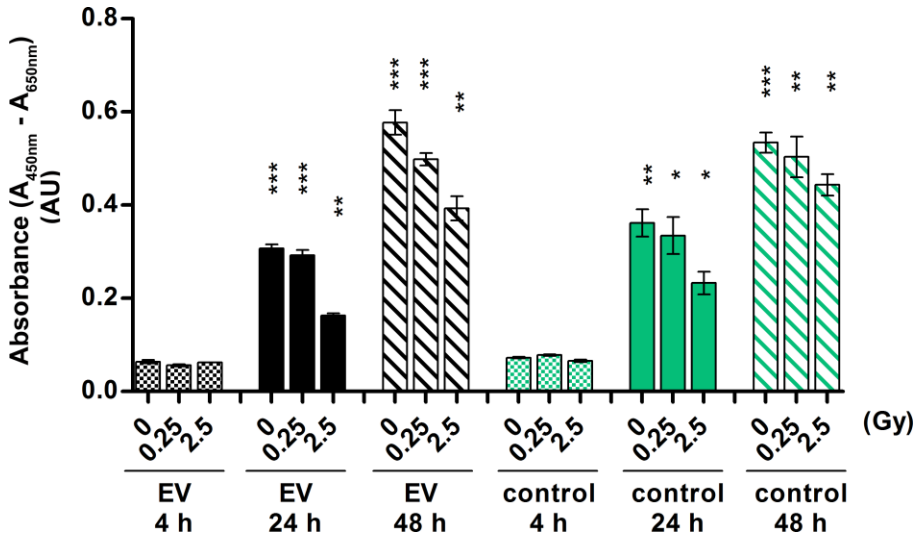

Figure 34. WST-1 viability assay of EV and control MCF-10A cells. The cell viability of MCF-10A cells quantified absorbance (absorbance units (AU)) of EV (black) and control (green) treated cells measured with WST-1 assay. Absorbance was measured 4 hours (checker boxes), 24 hours (solid color boxes) and 48 hours (downward diagonal boxes) after exposure to 0.25 Gy and 2.5 Gy dose of radiation. Relative absorbance is quantified as difference between measurement (450 nm) and reference wavelength (650 nm) at each analysed time point. Data represent mean values ± SEM (n=3). *p ≤ 0.05, **p ≤ 0.01, ***p ≤ 0.001

Sham-irradiated MDA-MB-361 EV treated cells showed significant increase in cell viability after 24 (0.54 ± 0.01 AU) and 48 hours (0.65 ± 0.02 AU) compared to 4 hour time point (0.18 ± 0.01 AU), without additional influence of radiation. Cells treated with anti-miR-21 did not show significant changes in cells viability after 24 hours (0.20 ± 0.03 AU) and 48 hours (0.13 ± 0.01 AU) compared to 4 hour time point (0.11 ± 0.01 AU). The reduction of MDA-MB-361 cell viability after treatment with anti-miR-21 was also detected compared to EV cells 24 hours after treatment (Figure 35). Doses of 0.25 Gy and 2.5 Gy did not have additional effect on the number of viable anti-miR-21 treated cells. No differences in cell viability between control and EV treated MDA-MB-361 cells were detected (Figure 36).

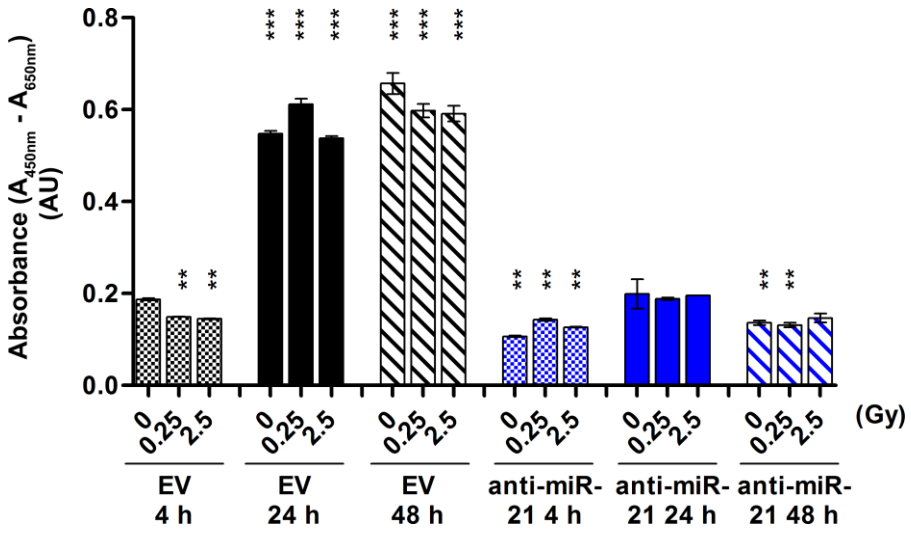

Figure 35. WST-1 viability assay of EV and anti-miR-21 MDA-MB-361 cells. The cell viability of MDA-MB-361 cells quantified absorbance (absorbance units (AU)) of EV (black) and anti-miR-21 (blue) treated cells. Absorbance was measured 4 hours (checker boxes), 24 hours (solid color boxes) and 48 hours (downward diagonal boxes) after exposure to 0.25 Gy and 2.5 Gy dose of radiation. Relative absorbance is quantified as difference between measurement (450 nm) and reference wavelength (650 nm) at each analysed time point. Data represent mean values ± SEM (n=3). *p ≤ 0.05, **p ≤ 0.01, ***p ≤ 0.001

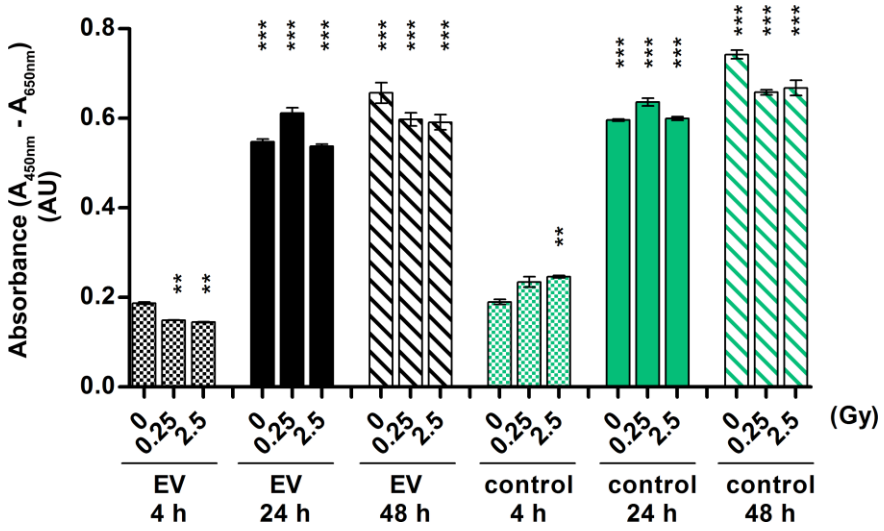

Figure 36. WST-1 viability assay of EV and control MDA-MB-361 cells. The cell viability of MDA-MB-361 cells quantified absorbance (absorbance units (AU)) of EV (black) and control (green) treated cells measured with WST-1 assay. Absorbance was measured 4 hours (checker boxes), 24 hours (solid color boxes) and 48 hours (downward diagonal boxes) after exposure to 0.25 Gy and 2.5 Gy dose of radiation. Relative absorbance is quantified as difference between measurement (450 nm) and reference wavelength (650 nm) at each analysed time point. Data represent mean values ± SEM (n=3). *p ≤ 0.05, **p ≤ 0.01, ***p ≤ 0.001

4.3.6 Anti-miR-21 is responsible for low attachment ability of MDA-MB-361 compared to MCF-10A cells

Along with the cell viability assays, cell attachment and detachment was also analysed. The number of detached MCF-10A cells in supernatant between EV and anti-mir-21 cells was not changed 24 hours after exposure to 0.25 Gy and 2.5 Gy. The number of detached anti-miR-21 treated cells was increased 1.49 ± 0.06 (0 Gy), 1.65 ± 0.08 (0.25 Gy) and 1.83 ± 0.21 (2.5 Gy) folds 48 hours post-irradiation compared to EV sham-irradiated cells (24 hours) set as 1. The radiation contributed to the increase of detached anti-miR-21 cells (Figure 37).

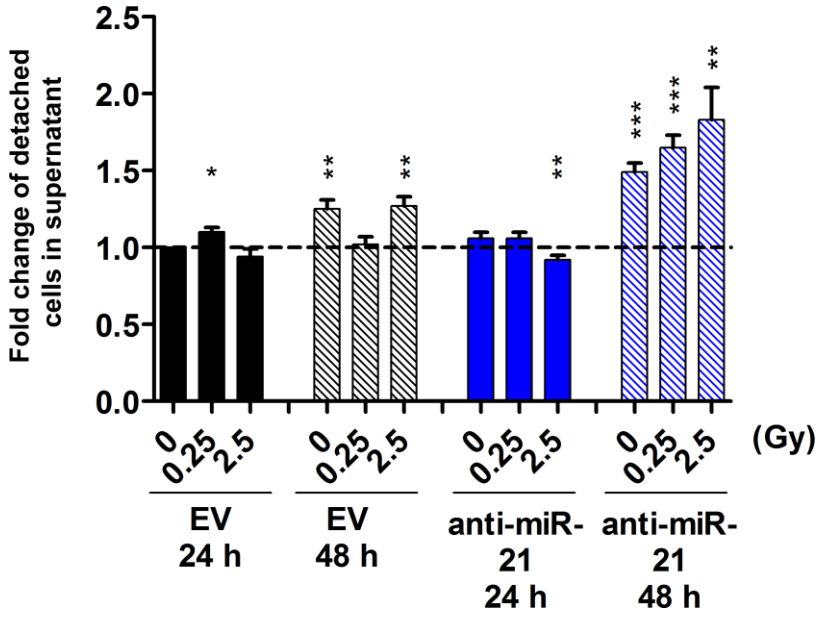

Figure 37. Detached EV and anti-miR-21 MCF-10A cells detected in supernatant. Fold change of EV (black) and anti-miR-21 (blue) treated MCF-10A cells detected in supernatant 24 hours (solid color boxes) and 48 hours (downward diagonal boxes) after radiation. All values were normalized to the value of EV 0 Gy 24 hour sample. Data represent mean values ± SEM (n=3).*p ≤ 0.05, **p ≤ 0.01, ***p ≤ 0.001

The EV treated cells showed more detached cells in supernatant compared to control cells 24 and 48 hours after radiation. Radiation caused increase in number of detached control cells (Figure 38).

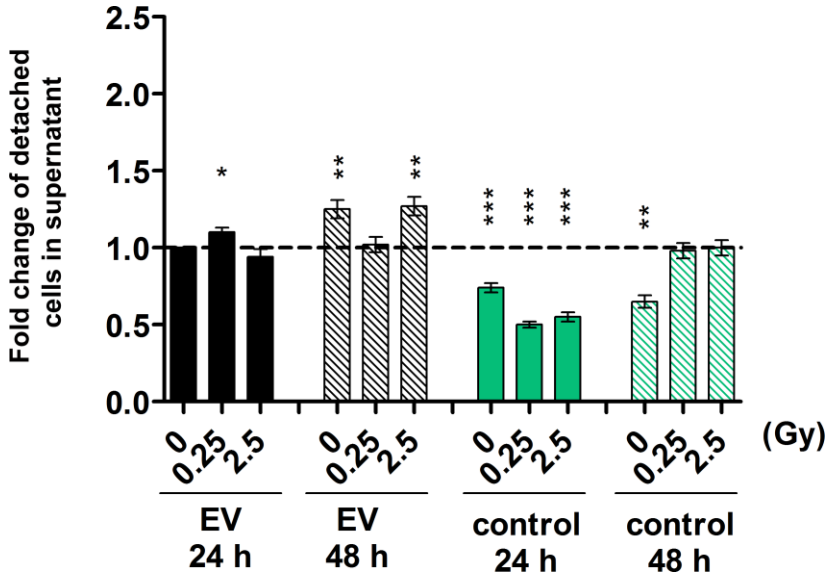

Figure 38. Detached EV and control MCF-10A cells detected in supernatant. Fold change of EV (black) and control (green) treated MCF-10A cells detected in supernatant 24 hours (solid color boxes) and 48 hours (downward diagonal boxes) after radiation. All values were normalized to the value of EV 0 Gy 24 hour sample. Data represent mean values ± SEM (n=3).*p ≤ 0.05, **p ≤ 0.01, ***p ≤ 0.001

In parallel, the analysis of attached cell number 48 hours after exposure to radiation was performed. In MCF-10A cells miR-21 knockdown did not significantly changed the number of attached sham-irradiated cells (0.91 ± 0.10 fold). Dose of 0.25 Gy influenced slightly the decrease of anti-miR-21 treated cells (0.75 ± 0.08 fold) but not EV cells. The medium dose of 2.5 Gy decreased the ability of MCF-10A cells to attach in both EV and anti-miR-21 cells to 0.81 ± 0.10 and 0.54 ± 0.04 folds, respectively (Figure 39, left). Number of attached control cells is higher compared to EV cells in sham-irradiated and cells exposed to 0.25 Gy, while after 2.5 Gy dose the difference was not detected (Figure 39, right).

The increased number of detached anti-miR-21 MCF-10A cells 48 hours after radiation, correlates with the decrease in attached cells at the same time point and same correlation is detected for control cells.

Sham-irradiated MDA-MB-361 anti-miR-21 treated cells expressed significant increase of 5.04 ± 1.12 fold and 8.58 ± 0.66 fold, at 24 and 48 hour time points (respectively) compared to number of EV treated cells at 24 hour (set to 1). Exposure to radiation (both doses) did not further influence the cells to detach (Figure 40).

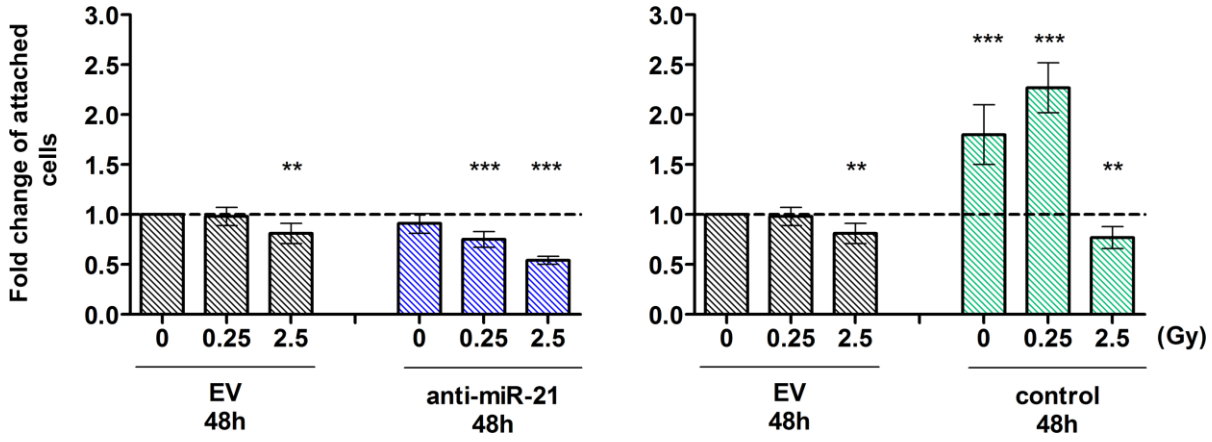

Figure 39. Fold change of attached MCF-10A cells. Fold change of attached EV (black), anti-miR-21 (blue) treated and control (green) MCF-10A cells measured 48 hours after the radiation treatment. All values were normalized to the value of EV 0 Gy 48 hour sample. Data represent mean values ± SEM (n=3). **p ≤ 0.01, ***p ≤ 0.001

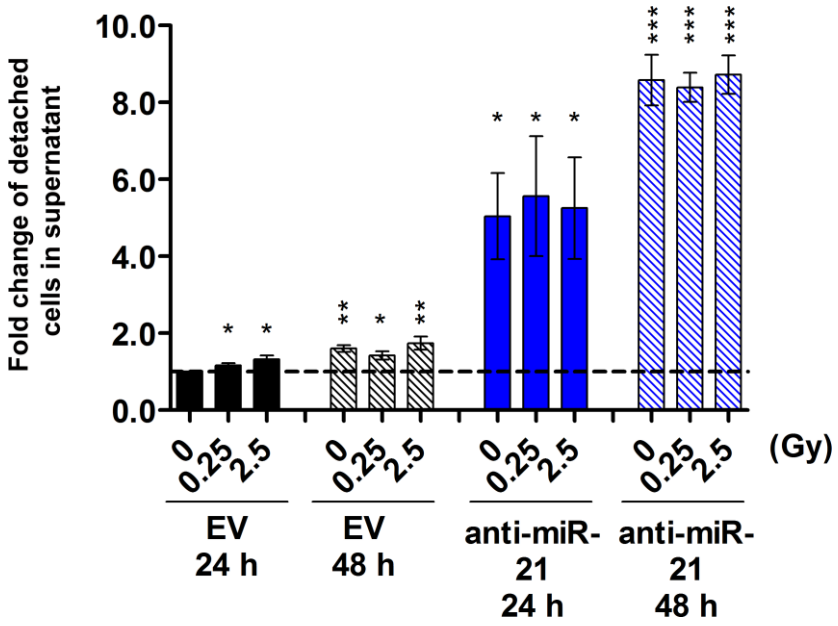

Figure 40. Detached EV and anti-miR-21 MDA-MB-361 cells in supernatant. Fold change of EV (black) and anti-miR-21 (blue) treated MDA-MB-361 cells detected in supernatant 24 hours (solid color boxes) and 48 hours (downward diagonal boxes) after radiation. All values were normalized to the value of EV 0 Gy 24 hour sample. Data represent mean values ± SEM (n=3).*p ≤ 0.05, **p ≤ 0.01, ***p ≤ 0.001

No significant differences between control and EV treated MDA-MB-361 cells were detected (Figure 41).

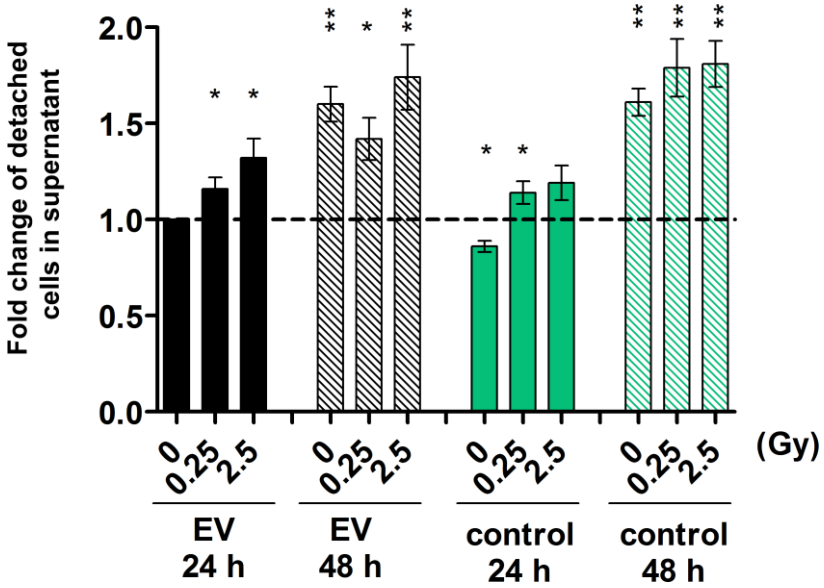

Figure 41. Detached EV and control MDA-MB-361 cells in supernatant. Fold change of EV (black) and control (green) treated MDA-MB-361 cells detected in supernatant 24 hours (solid color boxes) and 48 hours (downward diagonal boxes) after radiation. All values were normalized to the value of EV 0 Gy 24 hour sample. Data represent mean values ± SEM (n=3).*p ≤ 0.05, **p ≤ 0.01, ***p ≤ 0.001

Attachment ability of MDA-MB-361 anti-miR-21 treated cells was significantly reduced to 0.42 ± 0.05 fold in sham-irradiated cells, 0.39 ± 0.04 fold after 0.25 Gy and 0.27 ± 0.03 fold after 2.5 Gy, compared to sham-irradiated EV treated cells (set to 1). The dose of 2.5 Gy had effect on both EV and anti-miR-21 treated MDA-MB-361 cells, decreasing their attachment ability (Figure 42, left). The ability of control MDA-MB-361 cells to attach was slightly better compared to EV treated cells (Figure 42, right).

The increased number of detached anti-miR-21 MDA-MB-361 cells 48 hours after radiation, correlates with the decrease of attached cells at the same time point. Number of attached and detached MDA-MB-361 cells was in mutual correlation.

The effect of miR-21 knockdown on decreased cellular attachment and increased detachment ability was in general stronger in breast cancer cell line (MDA-MB-361) than in non-cancer cells (MCF-10A).

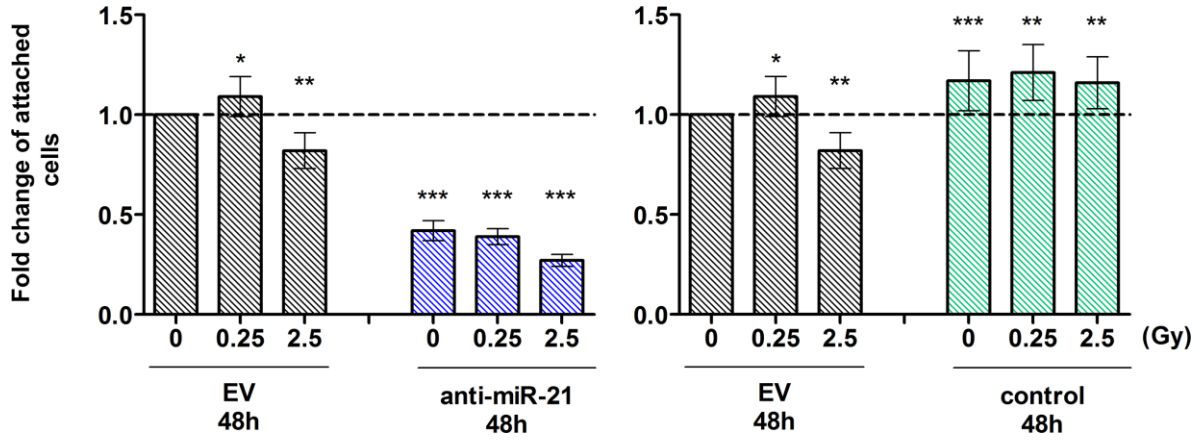

Figure 42. Fold change of attached MDA-MB-361 cells. Fold change of attached EV (black), anti-miR-21 (blue) treated and control (green) MDA-MB-361 cells measured 48 hours after the radiation treatment. All values were normalized to the value of EV 0 Gy 48 hour sample. Data represent mean values ± SEM (n=3). **p ≤ 0.01, ***p ≤ 0.001

4.3.7 3D-microtissue growth analysis

Both MCF-10A and MDA-MB-361 cells were able to form 3D-microtissues. The growth rate of 3D microtissues is followed for 13 days.

EV and anti-miR-21 MCF-10A treated cells showed that the growth is affected by the dose of 2.5 Gy. This effect was detected at day 6 of cultivation for EV and at day 9 for anti-miR-21 cells. No difference in the growth rate between microtissues previously transduced with EV and anti-miR-21 was shown (Figure 43, up).

The growth of MDA-MB-361 3D-microtissues was affected by the dose of 2.5 Gy at day 9 of cultivation for both EV and anti-miR-21 treated cells. MiR-21 knockdown led to formation of tissues which detected area was smaller compared to EV treated cells (Figure 43, down).

The day 9 of cultivation of 3D microtissues was in both cell lines the day when the changes were detected so we decided on this time point to be most suitable for analysing the changes after radiation treatment.

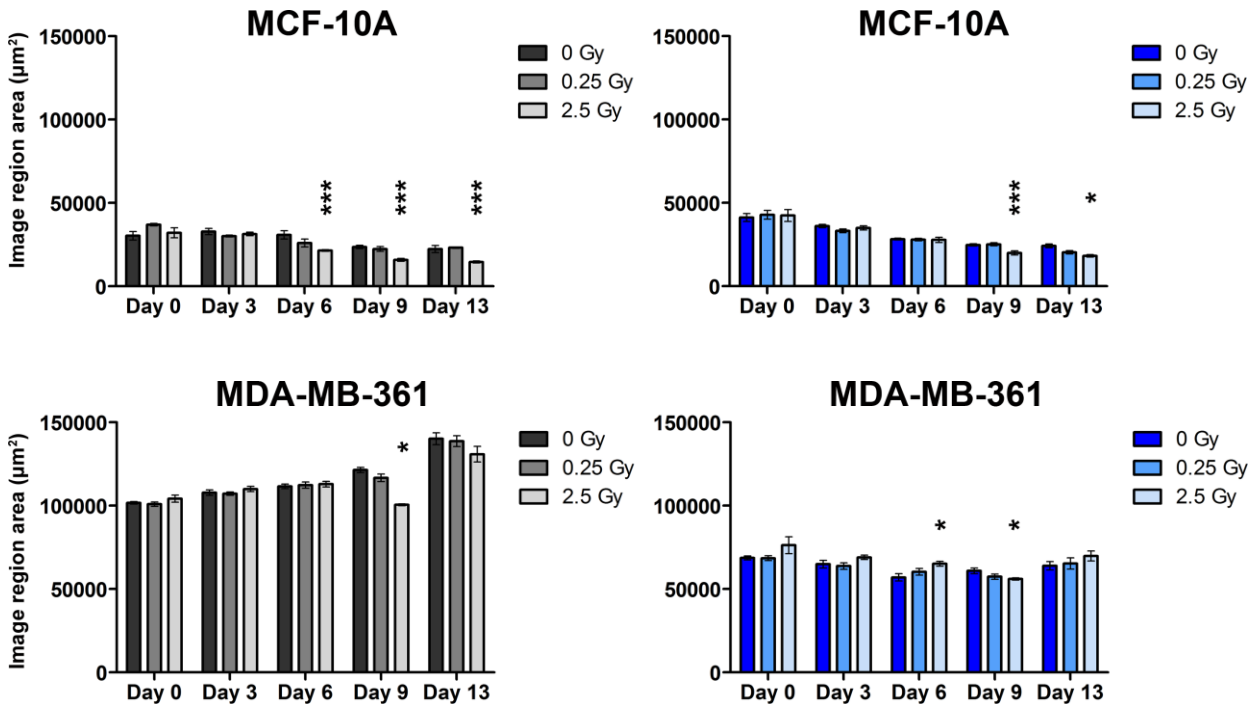

Figure 43. Growth of MCF-10A 3D microtissues over 13 days. The growth of MCF-10A (up) and MDA-MB-361 (down) 3D microtissues during 13 days of cultivation time and after exposure to low (0.25 Gy) and medium dose (2.5 Gy) of radiation at day 0. Black – sham-irradiated cells treated with EV, dark grey - cells treated with EV exposed to 0.25 Gy, light grey - cells treated with EV exposed to 2.5 Gy; dark blue – sham-irradiated cells treated with anti-miR-21, blue - cells treated with anti-miR-21 exposed to 0.25 Gy, light blue - cells treated with anti-miR-21 exposed to 2.5 Gy. Data represent mean values ± SEM (n=3). *p ≤ 0.05, ***p ≤ 0.001

MCF-10A cells treated with anti-miR-21 do not show growth delay compared to EV cells In both cases, the smaller microtissue size was detected after the radiation of 2.5 Gy dose (Figure 44). The size of EV 3D microtissues was reduced from 23568 ± 2734 µm^2 in sham-irradiated cells to 15796 ± 2294 µm^2 while the size of anti-miR-21 3D microtissues was diminished from 24733 ± 1829 µm^2 to 19909 ± 2818 µm^2.

Growth delay was detected between 3D microtissues of sham-irradiated MDA-MB-361 EV (121407 ± 4130 µm^2) and anti-mir-21 treated cells (60896 ± 4828 µm^2). Radiation dose of 2.5 Gy led to smaller size of EV microtissue (100536 ± 1486 µm^2), while radiation did not have further impact on the size of anti-miR-21 microtissues (Figure 45).

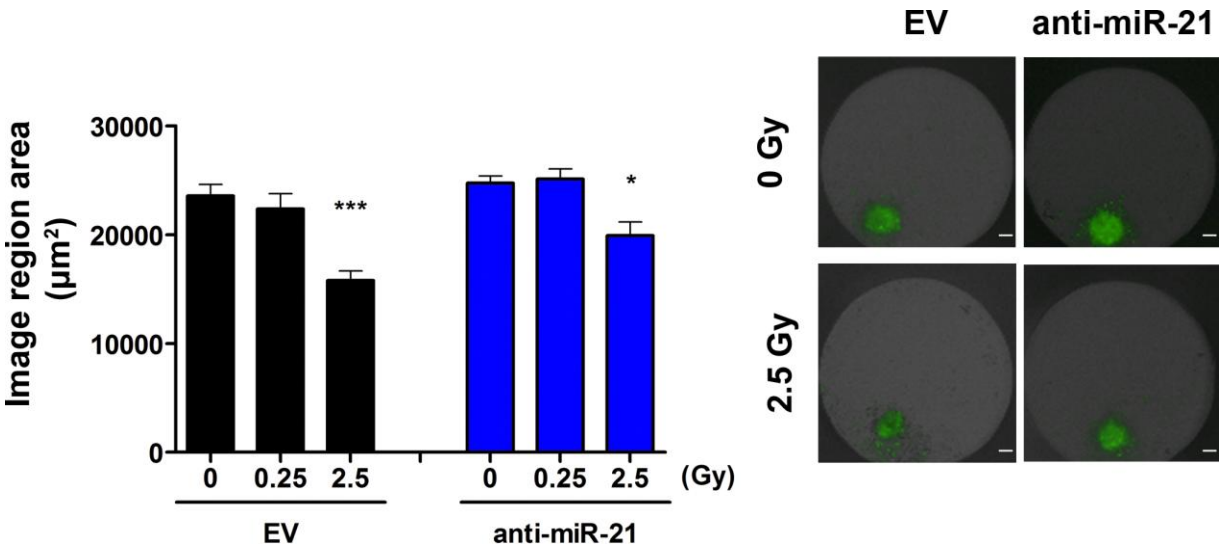

Figure 44. MCF-10A EV and anti-miR-21 3D microtissues comparison. Presented is comparison of 3D microtissues at the cultivation day 9. Black – cells treated with EV, blue – cells treated with anti-miR-21. Scale bar – 100 µm. Data represent mean values ± SEM (n=3). *p ≤ 0.05, ***p ≤ 0.001

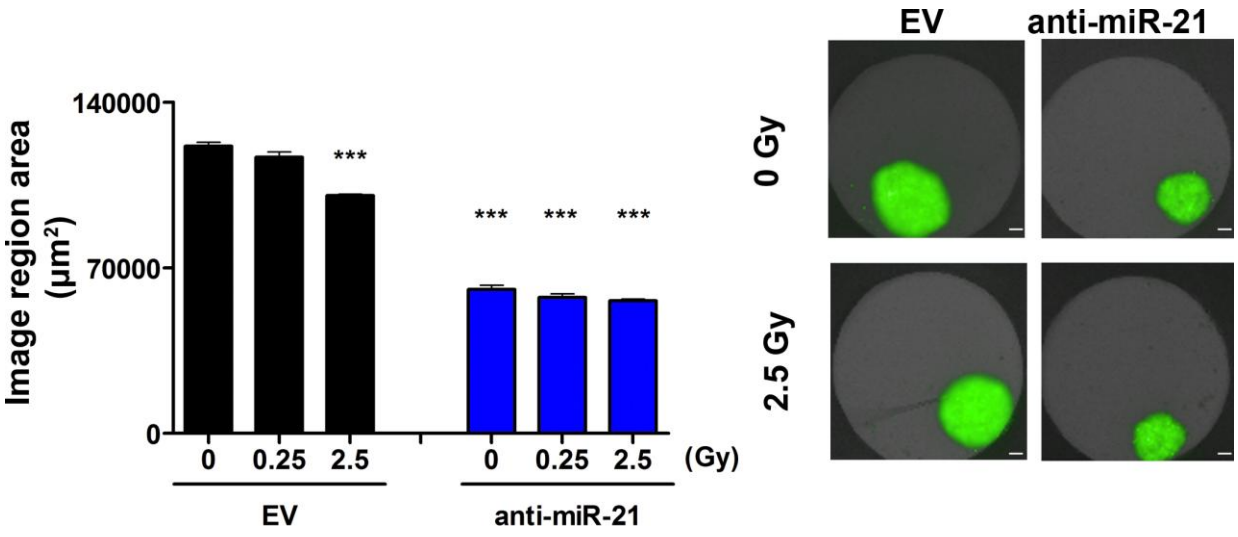

Figure 45. MDA-MB-361 EV and anti-miR-21 3D microtissues comparison. Presented is comparison of 3D microtissues at the cultivation day 9. Black – cells treated with EV, blue – cells treated with anti-miR-21. Scale bar – 100 µm. Data represent mean values ± SEM (n=3). *p ≤ 0.05, ***p ≤ 0.001

Combined anti-miR-21 and radiation treatment effect is evident for the tumour cells (MDA-MB-361) using 3D microtissue analysis what is in correlation with results obtained in 2D cell culture and colony formation assay, where the difference in cellular response to combined treatment between MCF-10A and MDA-MB-361 cells was identified.

4.4 MiR-21 target predictions

In order to discover how miR-21 knockdown could influence cell response to radiation, it was of great importance to investigate potential targets of this miRNA. Using 4 different *in silico* analyses (see Section 3.8) we have included both miR-21-5p (sense strand) and miR-21-3p (antisense strand). Each of the software used showed a different number of predicted targets as shown in Table 20. It is important to mention that *microRNA.org* showed significantly higher number of predicted targets compared to other 3 databases used.

Table 20. Number of predicted miR-21 targets for miR-21-5p and miR-21-3p according to 4 databases used.

	miR-21-5p	miR-21-3p
DIANA TOOLS (MicroT-CDS)	521	607
miRDB	240	485
TargetScan Human 7.1	382	3673
microRNA.org	5203	6209

In order to predict possible signaling pathways influenced by miR-21, the top 50 targets from each database (excluding *microRNA.org*) were taken into consideration (Figure 46). In the case of miR-21-5p, 10 common targets were predicted to be regulated among three databases used while for miR-21-3p only one common target was found.

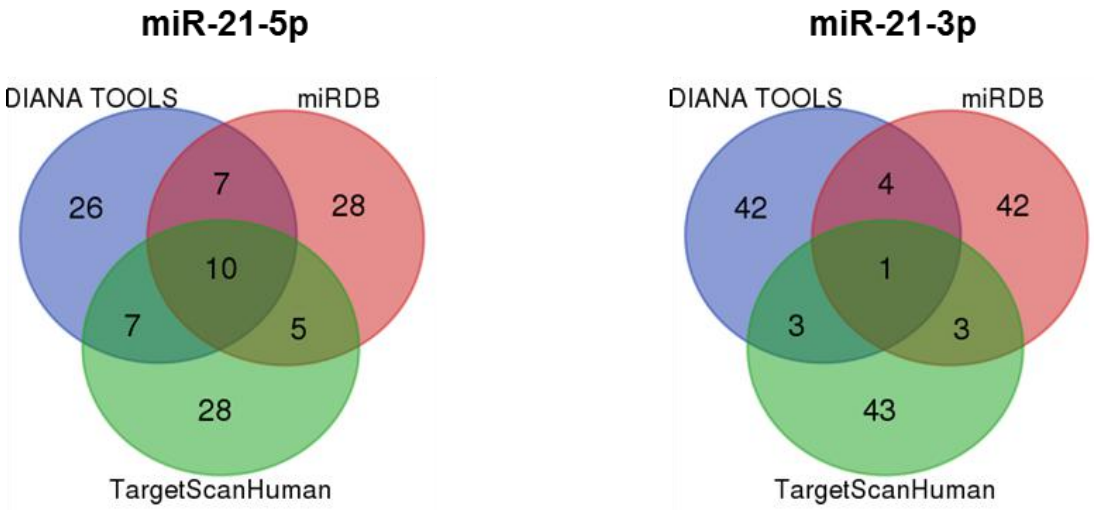

Figure 46. Mutual targets of miR-21 between 3 databases. Venn diagrams present common targets for miR-21-5p (left) and miR-21-3p (right) detected in 3 databases according to the top 50 predicted targets.

In the lists of potential targets the members of MAPK signaling pathway were detected as potential targets of miR-21-5p and miR-21-3p. MiR-21-5p was predicted to bind to the 3' UTR sequence of MAP3K1 and MAP2K3, whereas the predictions suggest that miR-21-3p binds to more members of this pathway such as MAP3K1, MAP2K3, MAP2K4 and MAP2K6 (Figure 47). MAP2K3, MAP2K4 and MAP2K6 are kinases responsible for the activation of ERK and JNK members of MAPK cascade (Figure 2).

MAP3K1 have appeared in all datasets as a potential target of not only miR-21-5p but also miR-21-3p (Figure 47). It is a member of the mitogen-activated protein kinase kinase kinase (MAP3K) family of serine/threonine kinases and present a part of important signal transduction cascades such as ERK, JNK kinase pathways and the NF-kB pathway. MAP3K1 is responsible for the activation of ERK and JNK kinase pathways by phosphorylation of different MAP2Ks. In this way this kinase can regulate different cellular functions like cell survival, apoptosis, and cell motility/migration in normal and tumors cell lines.

TargetScan	Representative transcript	CWCS score*
miR-21-5p		
MAP3K1	ENST00000399503.3	-0,29
MAP2K3	ENST00000342679.4	-0,30
miR-21-3p		
MAP3K1	ENST00000399503.3	-0,24
MAP2K3	ENST00000342679.4	-0,25
MAP2K4	ENST00000415385.3	-0,19
MAP2K6	ENST00000590474.1	-0,04

*Cumulative weighted context ++ score

miRDB	Target rank	Target score
miR-21-5p		
MAP3K1	26	93
MAP2K3	187	57
miR-21-3p		
MAP3K1	2	99
MAP2K3	334	61
MAP2K4	281	65
MAP2K6	-	-

DIANA TOOLS	Ensembl Gene Id	miTG score*
miR-21-5p		
MAP3K1	ENSG00000095015	0.789949
MAP2K3	-	-
miR-21-3p		
MAP3K1	ENSG00000095015	0.909822
MAP2K3	ENSG00000034152	0.864376
MAP2K4	ENSG00000065559	0.895038
MAP2K6	-	-

*The prediction score. Higher miTG score – higher is the probability of targeting

Figure 47. Predictions of miR-21 targeting MAPK family members. *In silico* predictions of miR-21-5p and miR-21-3p targeting the members of MAPK signaling pathway according to *TargetScan Human 7.1*, *miRDB.org* and *DIANA TOOLS*.

For the alignment of miR-21 and MAP3K1, the resource of microRNA target predictions and expression profiles - *microRNA.org* was used. Target predictions are based on the miRanda algorithm that includes current and updated knowledge of targets and miRNAs [210]. This analysis showed that miR-21 has in total 3 binding sites in 3'UTR sequence of MAP3K1, one for miR-21-5p at the position 1418 and two for the miR-21-3p at positions 1972 and 2420. All of these bindings had high miRSVR score (providing indication how strong is a miRNA's regulatory effect). Binding of miR-21-5p had the highest miRSVR score of -1.2518 (Figure 48). This confirms the importance of miR-21 binding to the untranslated region of MAP3K1 and that it could influence its functional regulation.

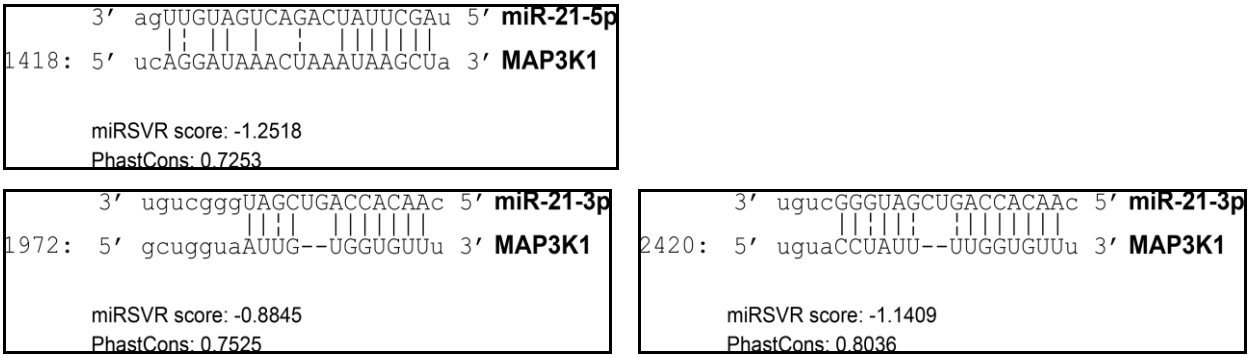

Figure 48. Alignment of miR-21 and MAP3K1. *In silico* alignment of miR-21-5p (up) and miR-21-3p (down) with the 3'UTR sequence of MAP3K1, according to the microRNA.org database. PhastCons score measures the evolutionary conservation of sequence blocks. MirSVR present the support vector regression (SVR) approach and it provides the indication of how strong the regulatory effect of certain miRNA is on particular target.

4.5 Proteomic analysis in MCF-10A after miR-21 knockdown and radiation

4.5.1 MCF-10A cell line proteome after radiation and miR-21 knockdown

In order to detect the changes in MCF-10A cells on the protein levels after miR-21 knockdown and radiation ICPL was performed (Section 3.9.1). Triplex set of labels were used for control cells (ICPL_0), cells treated with EV (ICPL_4) and cells treated with anti-miR-21 (ICPL_6). Prior to labelling, these cells were exposed to two different doses of radiation (0.25 Gy or 2.5 Gy) or sham-irradiated. This was done in biological triplicates. We wanted to track the changes 4 hours and 24 hours after irradiation. Relative protein identification and quantification was performed and further selection was done according to the previously explained settings (section 3.9.5). Our focus was on the comparison between anti-miR-21 and EV treated MCF-10A cells and what changes are caused by radiation. Proteins whose measured ICPL_6/ICPL_4 ratio was greater/equal than 1.30-fold or less/equal than 0.77, were considered to be significantly differentially expressed. The number of significantly deregulated proteins for each treatment is shown in Table 21.

At 4 hour time point in sham-irradiated cells 66 proteins were deregulated out of which 34 were upregulated and 32 downregulated in anti-miR-21 treated MCF-10A cells compared to EV cells. After exposure to the radiation the number of differentially regulated proteins increased to 88 after 0.25 Gy (c) and 125 after 2.5 Gy (93 up- and 32

downregulated). Increase in number of upregulated proteins was detected after exposure to 2.5 Gy. Since the number of differentially regulated proteins was smallest in sham-irradiated cells and was increased with higher dose of radiation we concluded that these proteomic changes could potentially be dose dependent.

Table 21: Number of significantly deregulated proteins in MCF-10A cells treated with anti-miR-21 4 hours after radiation (compared to EV treated cells)

Dose (Gy)	4 hours after irradiation, anti-miR-21	
	Number of significantly upregulated proteins	Number of significantly downregulated proteins
0	34	32
0.25	46	42
2.5	93	32

24 hours after irradiation, the number of significantly deregulated proteins was higher in sham-irradiated cells (comparted to 4 hour time point) where 123 proteins were deregulated out of which 92 were upregulated and 31 downregulated. The number of deregulated proteins detected after 0.25 Gy was 127 (85 up- and 42 downregulated) and 167 (93 up- and 74 downregulated) after 2.5 Gy as shown in Table 22. More deregulated proteins were detected 24 hours after radiation treatment, with the highest number detected after exposure to 2.5 Gy.

Table 22: Number of significantly deregulated proteins in MCF-10A cells treated with anti-miR-21 24 hours after radiation (compared to EV treated cells)

Dose (Gy)	24 hours after irradiation, anti-miR-21	
	Number of significantly upregulated proteins	Number of significantly downregulated proteins
0	92	31
0.25	85	42
2.5	93	74

A number of common deregulated proteins were detected between all three treatments.

Seven proteins (4 upregulated and 3 downregulated) were shared between treatments 4 hours after irradiation (Table 23), including upregulated ANP32A, HNRNPA2B1 and HNRNPC proteins, with role in pre-mRNA processing and stability and trafficking of mRNAs, and downregulated HSPA1A protein that stabilizes and mediate the folding of newly translated polypeptides. PANTHER Classification System and STRING database were used to classify proteins (as well their genes) and predict protein–protein interactions of proteins common for all three radiation treatments. The interaction network of common proteins detected 4 hours after radiation showed that there were no known interactions between these proteins (Figure 49).

Table 23: List of common significantly deregulated proteins detected 4 hours after exposure to 0, 0.25 and 2.5 Gy dose of radiation.

Common significantly deregulated proteins 4 h post irradiation		0 Gy	0.25 Gy	2.5 Gy
		Fold change		
SCRIB	scribbled homolog (Drosophila)	2,4	1,7	1,9
HNRNPA2B1	heterogeneous nuclear ribonucleoprotein A2/B1	1,3	1,3	1,6
ANP32A	acidic (leucine-rich) nuclear phosphoprotein 32 family	1,5	1,5	1,5
HNRNPC	heterogeneous nuclear ribonucleoprotein C (C1/C2)	1,4	1,4	1,6
G3BP2	GTPase activating protein (SH3 domain) binding protein 2	0,6	0,7	0,8
HSPA1A	heat shock 70kDa protein 1A	0,7	0,7	0,7
AHNAK	AHNAK nucleoprotein	0,5	0,6	0,7

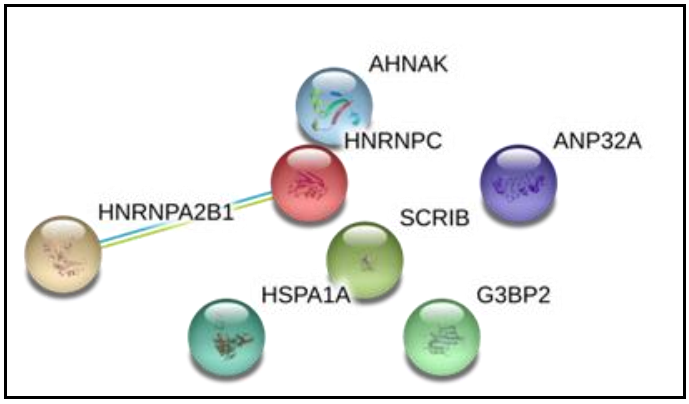

Figure 49. STRING prediction of protein interactions 4 hours after radiation. Predicted protein–protein interaction network (using STRING database) of common proteins detected in MCF-10A cells 4 hours after radiation for all three treatments.

The number of common proteins between all three treatments 24 hours after irradiation was nineteen (13 upregulated and 6 downregulated) listed in Table 24. This list contain proteins involved in nucleic acid binding, such as H3 histone (H3FB), GTPase activating protein (G3BP1), histone cluster 1 and 2 (HIST1H3B and HIST2H3D) and ribosomal protein (RPLP0) which were all upregulated in anti-miR-21 treated cells. Histone clusters and ribosomal protein were more upregulated after 0.25 Gy in comparison to sham-irradiated and cells exposed to 2.5 Gy. Proteins such as reticulocalbin 2 (RCN2), acidic (leucine-rich) nuclear phosphoprotein (ANP32E) are responsible for protein binding and were downregulated after all three treatments (Figure 50).

Table 24: List of common significantly deregulated proteins detected 4 hours after exposure to 0, 0.25 and 2.5 Gy dose of radiation.

Common significantly deregulated proteins 24 h post irradiation		0 Gy	0.25 Gy	2.5 Gy
		Fold change		
HIST1H3B	histone cluster 1, H3b	2,1	2,8	1,9
GLUD1	glutamate dehydrogenase 1	1,3	1,3	1,3
CKMT1B	creatine kinase, mitochondrial 1B	1,3	1,3	1,2
SFXN1	sideroflexin 1	1,9	2,4	1,7
HIST2H3D	histone cluster 2, H3d	2,0	2,6	1,8
PRDX5	peroxiredoxin 5	2,0	2,6	1,8
PTGES	prostaglandin E synthase	1,4	1,4	1,3
G3BP1	GTPase activating protein (SH3 domain) binding protein 1	1,4	1,4	1,3
HNRNPA2B1	heterogeneous nuclear ribonucleoprotein A2/B1	1,3	2,1	1,4
LMNA	lamin A/C	2,0	2,5	1,8
RPLP0	ribosomal protein, large, P0	1,4	2,1	1,4
H3F3B	H3 histone, family 3B (H3.3B)	2,1	2,5	1,5
GSTP1	glutathione S-transferase pi 1	1,5	2,0	1,9
NDUFA5	NADH dehydrogenase (ubiquinone) 1 alpha subcomplex,	0, 7	0,7	1,3
ANP32E	acidic (leucine-rich) nuclear phosphoprotein 32 family	0,7	0,6	0,7
HSPA1A	heat shock 70kDa protein 1A	0,7	0,7	0,7
AHNAK	AHNAK nucleoprotein	0,7	0,6	0,6
RCN2	reticulocalbin 2, EF-hand calcium binding domain	0,7	0,7	0,7
PAICS	Phosphoribosylaminoimidazole carboxylase,	0,7	0,7	0,7

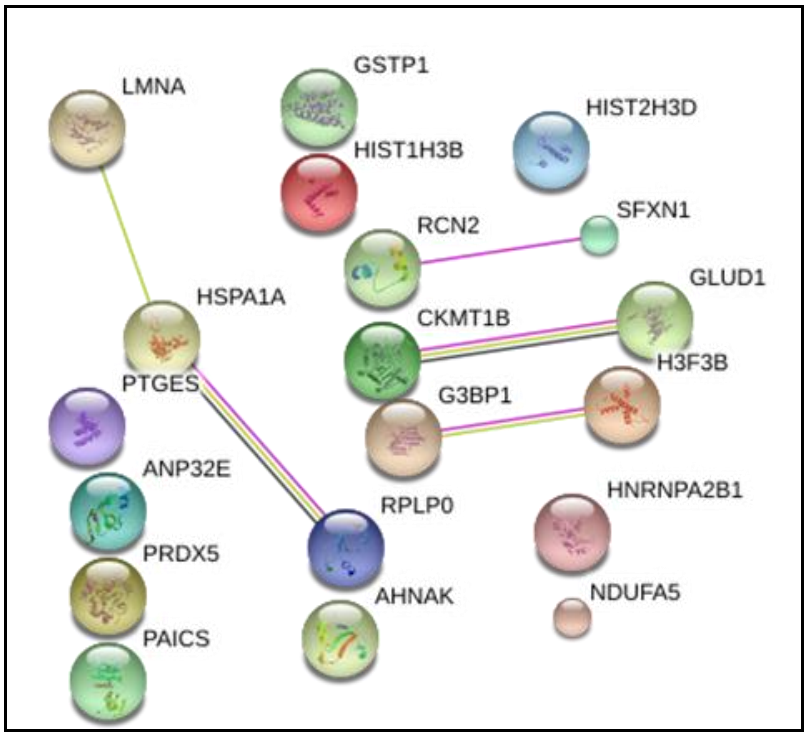

Figure 50. STRING prediction of protein interactions 24 hours after radiation. Predicted protein–protein interaction network (using STRING database) of common proteins detected in MCF-10A cells 24 hours after radiation for all three treatments.

The prediction of pathways influenced by miR-21-knockdown and radiation was analysed using Ingenuity Pathway Analysis (IPA).

Upstream analysis was performed for the 4 hour and 24 hour time points in order to predict upstream regulators (genes) that were possibly influenced by miR-21 knockdown. For this purpose, our datasets from MCF-10A cells treated with different doses of radiation were used. The activation state of *NFE2L2* gene was, according to the predictions, increased 4 hours after both doses of radiation and was increased after 24 hours even without exposure to radiation after anti-miR-21 treatment (Figure 51).

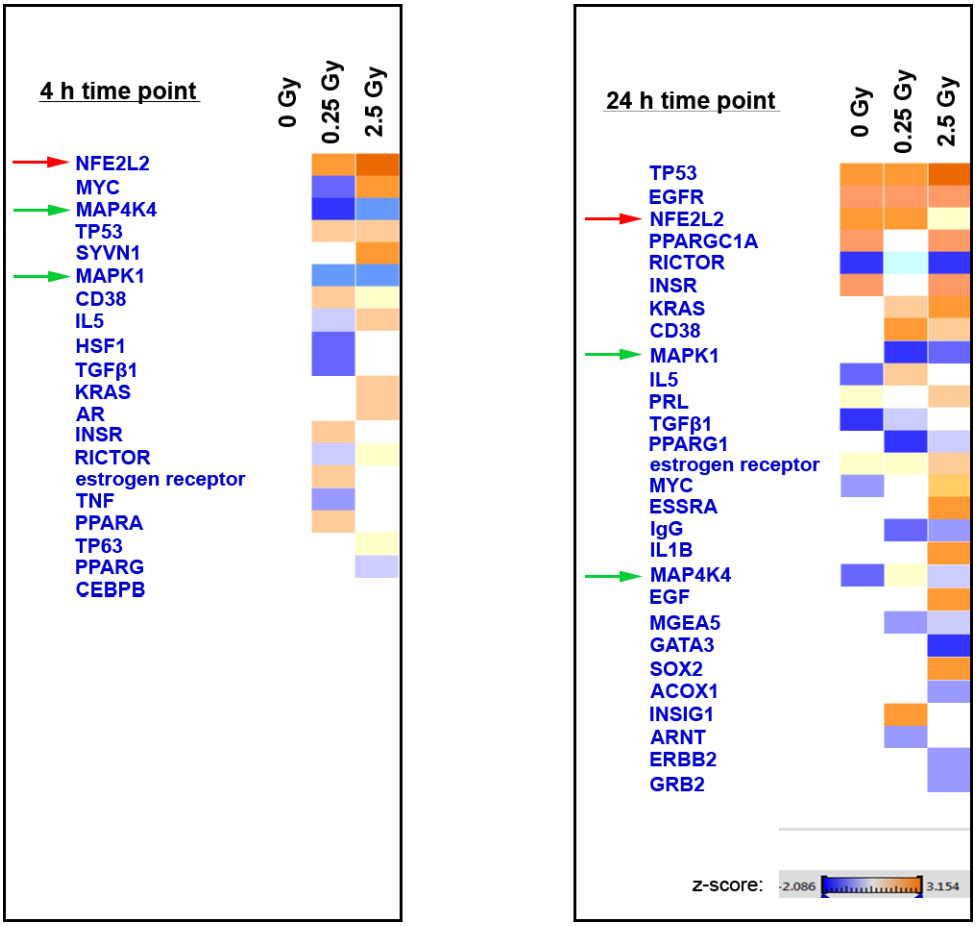

Figure 51. IPA prediction of upstream transcriptional regulators after radiation. List of affected regulators (genes) detected 4 hours (left) or 24 hours (right) after the exposure to low (0.25 Gy) or medium (2.5 Gy) dose of radiation combined with miR-21 knockdown. Blue – expressing the decreased activation state and orange – expressing increased activation state of transcriptional regulators according to the activation z-score (right corner).

Members of the MAPK cascade such as *MAPK1, MYC, MAP4K4* were also detected in the top 30 predictions of both time points and their activation state was decreased at both time points. *NFE2L2* and the MAPK cascade were further selected for the validation.

In IPA analysis we also searched for changed canonical pathways after combined anti-miR-21 and radiation treatment in MCF-10A cells. According to the predictions, integrin signaling pathway was affected at both time points. At 24 hour time point, activation state of ERK/MAPK and PI3K/AKT signaling pathways were predicted to be decreased in our MCF-10A samples after exposure to 2.5 Gy.

The integrin signaling pathway was selected for further validation, since its activation state was decreased after 4 and 24 hours post-irradiation (Figure 52).

Therefore, in parallel with further validation of *NFE2L2* and MAPK cascade, integrin signaling pathway was also included.

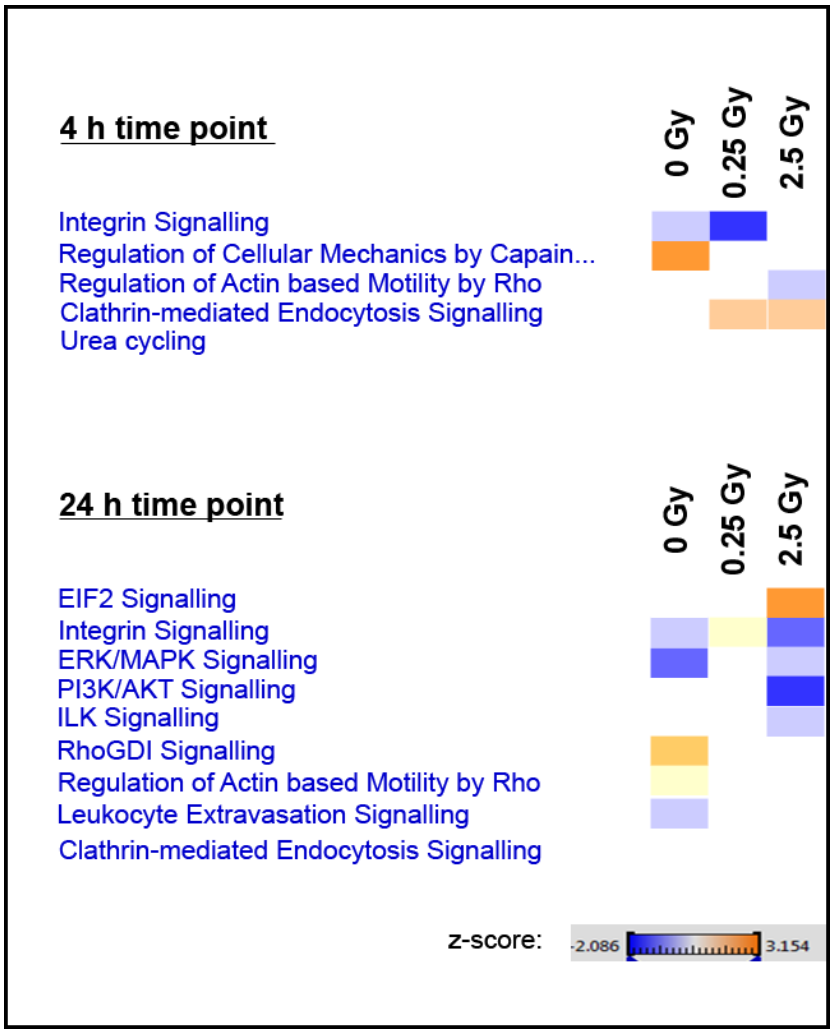

Figure 52. IPA prediction of canonical pathways after radiation. Top 10 canonical pathways detected 4 hours (up) or 24 hours (down) after the exposure to low (0.25 Gy) or medium (2.5 Gy) dose of radiation combined with miR-21 knockdown. Blue – expressing the decreased activation state and orange – expressing increased activation state of transcriptional regulators according to the activation z-score (right corner).

4.5.2 Changes of NFE2L2 and its validation

The NFE2L2 (nuclear factor erythroid 2–related factor 2) also known as Nrf2 is predicted to be activated 4 hours and 24 hours after radiation. Nrf2 activity is mainly regulated by Keap1 protein. Its activity as response to stress signals, results from a disruption of Keap1/Nrf2 association, releasing Nrf2 into the nucleus for its transcriptional activity.

To validate the previous predictions, Nrf2 and its phosphorylated form was examined by immunoblotting preforming Western blot analysis. Due to the difficulties with the detection of total Nrf2 protein expression we obtained the data from two biological replicates.

In sham-irradiated cells treated with anti-miR-21, expression of Nrf2 was upregulated in one and not changed compared to EV treated cells in other replicate. Phospho-Nrf2 (p-Nrf2) was significantly upregulated in sham-irradiated cells of both replicates. Radiation did not have any additional effect to the knockdown of miR-21 on the expression of Nrf2 and phospho-Nrf2 (Figure 53). Changes in its total and phosphorylated form were not detected (Figure 54). The Western blot analyses obtained from replicates could not validate activation of NRF2 suggested by IPA prediction due to contrary results and not enough replicates.

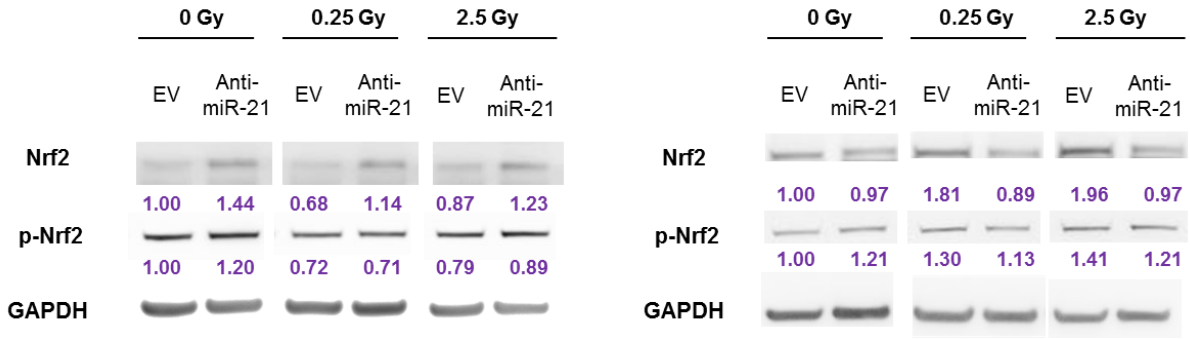

Figure 53. Representative blot of Nrf2 and p-Nrf2 changes 24 hours after radiation. The changes in Nrf2 (68 kDa) and phospho-Nrf2 (90 kDa) proteins in EV and anti-miR-21 MCF-10A cells 24 hours after 0.25 Gy and 2.5 Gy dose of radiation in two biological replicates (n=2). Expressed fold changes are calculated by normalization to the value of EV 0 Gy sample. GAPDH (37 kDa) is used as endogenous control.

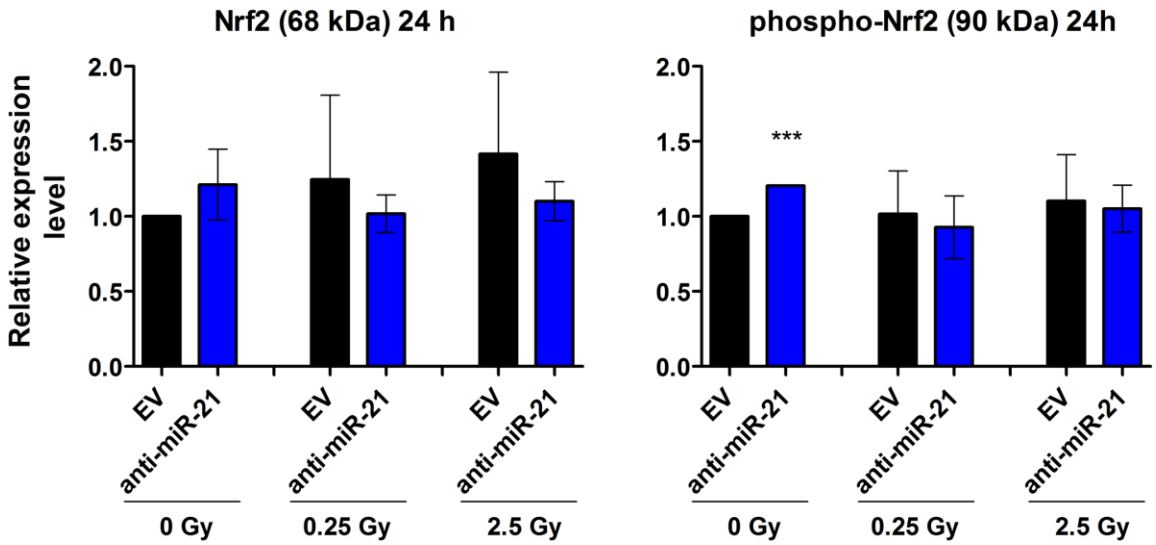

Figure 54. Western blot analysis of Nrf2 and phospho-Nrf2 protein expression 24 hours after radiation in MCF-10A cells. Graph represents quantification of proteins relative to GAPDH. Expressed fold changes are calculated by normalization to the value of EV 0 Gy sample. Mean values and standard error of mean (SEM) are shown (n= 2). The Student's t-test was used for statistical analysis. ***p <0.001

4.5.2.1 Assay for oxidative stress used for validation of Nrf2

NFE2L2 (Nrf2) represent the protein important for regulation of the expression of antioxidant proteins that protect against oxidative damage. In order to detect the changes in Nrf2 pathway the RT^2 Profiler PCR Assay for oxidative stress was performed. The changes in 84 gene`s expression detected 24 hours after radiation are shown in Table 25. Fold changes are calculated by normalizing C_t values to the *GAPDH* (one of five endogenous controls provided).

Table 25: Results of the RT^2 Profiler PCR Assay for oxidative stress in MCF-10A cells

	not changed	upregulated	downregulated	not detected
EV 2.5 Gy	67	4	5	8
anti-miR-21 0 Gy	66	4	7	7
anti-miR-21 2.5	57	4	15	8

The genes having fold change less/equal to 0.5 or greater/equal to 1.5 were considered to be deregulated. Each gene was normalized to the levels of gene expression in EV sham-irradiated cells. The number of downregulated genes raise to fifteen in the anti-

miR-21 treated cells after 2.5 Gy dose of radiation when compared to EV treated cells (five) and sham-irradiated cells treated with anti-miR-21 (seven). Out of the fifteen, selected deregulated, 4 genes (Table 28) were selected to be further validated with the single TaqMan® Gene Expression Assay.

Table 26: The fold changes of selected 4 genes in RT^2 Profiler PCR Assay for oxidative stress in MCF10A cells

Gene	Fold change
HMOX1	0.44
HSPA1A	0.45
TXNRD1	0.19
TXNRD2	0.48

HMOX1, HSPA1A, TXNRD1 and *TXNRD2* are genes whose regulation is dependent on *NRF2* and its activation. The expression of 4 selected genes and *NRF2* is done as previously described (Section 3.4.7) using single TaqMan® Gene Expression Assays.

The expression of these genes was performed in 4 biological replicates. No significant changes in expression profiles were detected for *TXNRD1* and *TXNRD2*. *NRF2* showed the tendency to be upregulated in cells treated with anti-miR-21 24 hours after exposure to 2.5 Gy as well as *HMOX1,* whose trend of upregulation was also detected in cells treated with miR-21 knockdown regardless of radiation. *HSPA1A* did not show any significant changes in its expression between EV and anti-miR-21 treated cells, without any effect of radiation exposure (Figure 55).

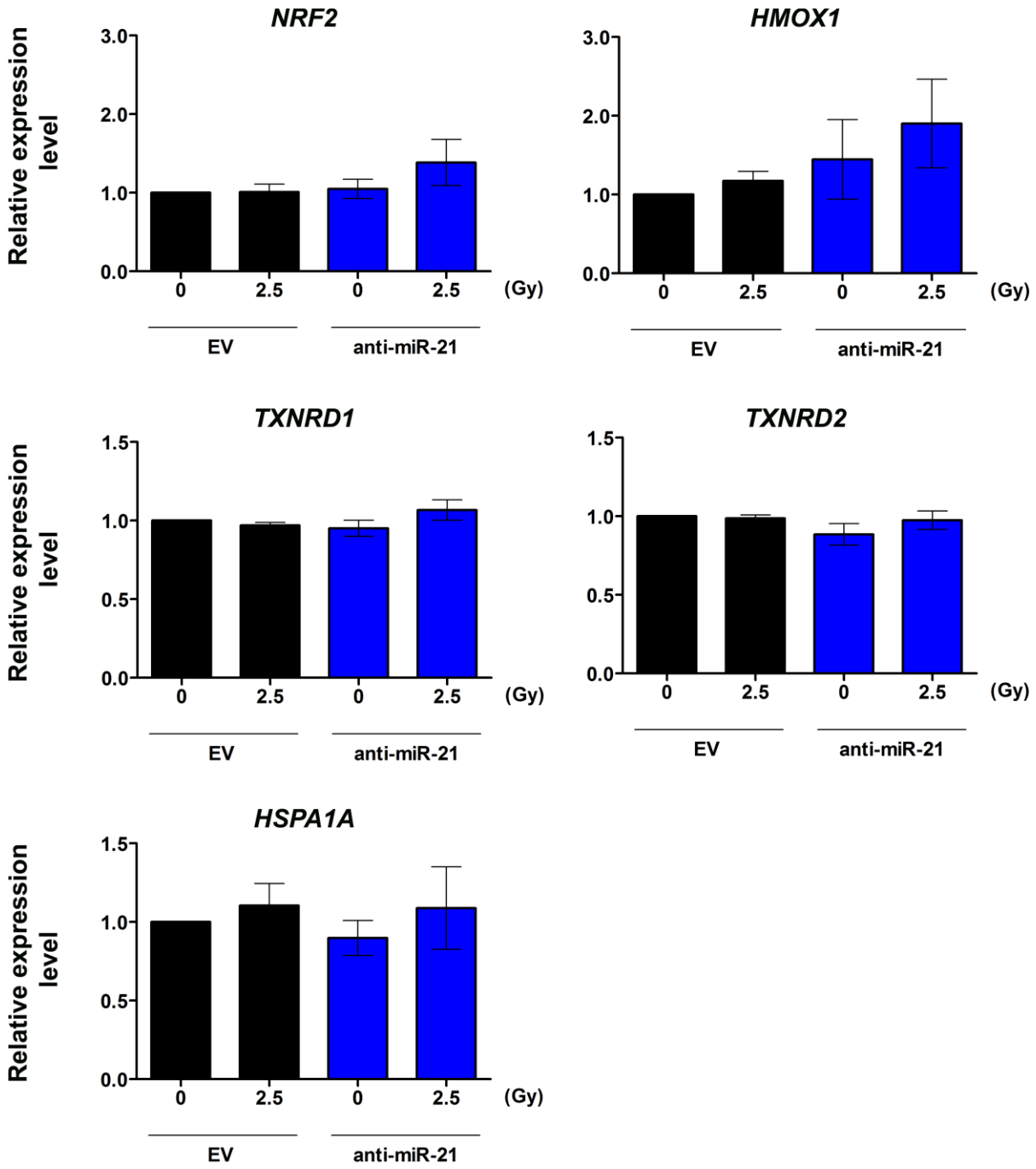

Figure 55. Expression of 5 genes in MCF-10A cells after exposure to 2.5 Gy. Expression of NRF2 and 4 selected genes (*HSPA1A, TXNRD1, TXNRD2* and *HMOX1*) in EV (black) and anti-miR-21 (blue) treated MCF-10A cells 24 hours after exposure to 2.5 Gy dose of radiation. Nrf2 is transcription factor that regulates the expression of other 4 selected genes. Normalization was done to the value of EV 0 Gy sample. Mean values and standard error of mean (SEM) are shown (n= 4). The Student's t-test was used for statistical analysis.

4.5.3 Integrin signaling pathway changes

Integrins represent cell adhesion receptors and are major mediators of cell adhesion to extracellular matrix (ECM) and ECM-induced intracellular signaling. IPA predicted that integrin signaling is less induced with miR-21 knockdown after 0.25 Gy dose at 4 hour time point and in sham-irradiated and cells exposed to 2.5 Gy 24 hours after radiation (compared to EV treated cells). While members of β-integrin family are less induced after miR-21 knockdown irrelevant of exposure to the radiation, the activation state of α-integrin family members after low dose irradiation is increased and after medium dose decreased (Figure 56). These predictions we detected in our samples in case of ITGβ1, ITGβ4 and ITGα3. The fold changes of all detected members of integrin families are presented in Table 27.

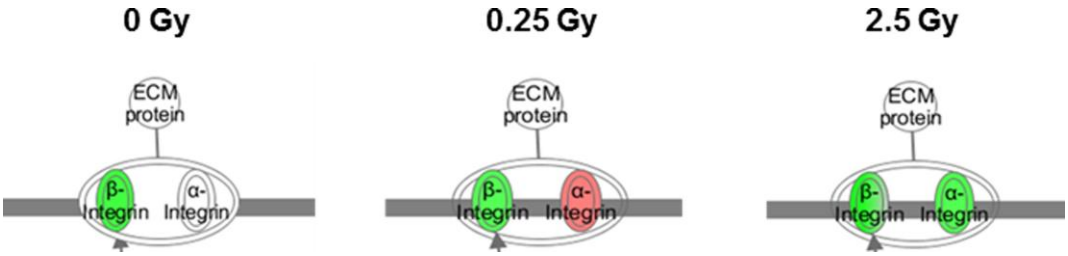

Figure 56. IPA predicted changes of integrin family members. Scheme of changes in α- and β-integrin families in anti-miR-21 treated MCF10A cells 24 hours after irradiation according to the IPA prediction. Green – less induced, red – more induced members of integrin families 24 hours after exposure to radiation.

Table 27. Fold changes of detected members of integrin families with ICPL (comparison of anti-miR-21 and EV (ICPL_6/ICPL_4)) 4 hours and 24 hours after radiation.

Integrins	0 Gy	0.25 Gy	2.5 Gy	0 Gy	0.25 Gy	2.5 Gy
	4 hours time point			24 hours time point		
ITGβ1	0,63	0,74	0,98	1,01	0,80	0,54
ITGβ4	x	0,86	1,33	1,19	0,81	0,71
ITGα6	0,52	1,06	1,81	x	0,78	0,33
ITGα3	0,49	x	1,74	0,75	1,49	0,62
ITGαV	0,68	0,49	0,97	0,61	0,61	0,49

Members of β- integrin family (ITGβ1 and ITGβ4) were both downregulated in anti-miR-21 treated cells 24 hours after radiation and α-integrin members (ITGα6 and ITGα3) showed increase in fold change after 0.25 Gy and downregulation after 2.5 Gy. All these results were in correlation with IPA predictions.

Since the IPA predicted that integrin signaling pathway is less induced after miR-21 knockdown, we decided to validate the downstream targets of the pathway by Western blot.

4.5.3.1 Validation of Integrin signaling pathway changes by Western blots

In order to validate these predictions and the changes in integrin signaling pathway obtained with IPA, downstream targets of α- and β-integrin family members were selected for the Western blot analyses as previously described (section 3.7). The selected targets were – FAK (focal adhesion kinase), MAP kinases ERK1/2 (extracellular signal-regulated kinase 1/2), JNK1/2 (c-Jun N-terminal kinase 1/2) and their phosphorylated forms. Members of the MAPK pathways showed potential of being targets of miR-21 according to previously performed *in silico* analysis. GAPDH was used as endogenous control in all Western blot experiments.

According to the proposed model of integrin signaling pathway [211], FAK is the direct target of integrins and is proposed to be dependent on their changes. In sham-irradiated cells, FAK and phospho-FAK (p-FAK) protein expression was not significantly changed between EV and anti-miR-21 treated MCF-10A cells. Radiation treatment did not change the expression of FAK and phospho-FAK at 4 hour time point, between EV and anti-miR-21 treated cells, except that FAK was reduced in anti-miR-21 treated cells after exposure to 0.25 Gy. On the other hand, after 24 hours the band intensity of both proteins, after miR-21 knockdown, had tendency to be diminished comparing to EV but it was not statistically significant (Figure 57).

This was done for 4 biological replicates and quantification of data is presented in Figure 58. No significant changes in total FAK protein expression were detected with Western blot analyses between EV and anti-miR-21 treated MCF-10A cells 4 and 24 hours after radiation treatment.

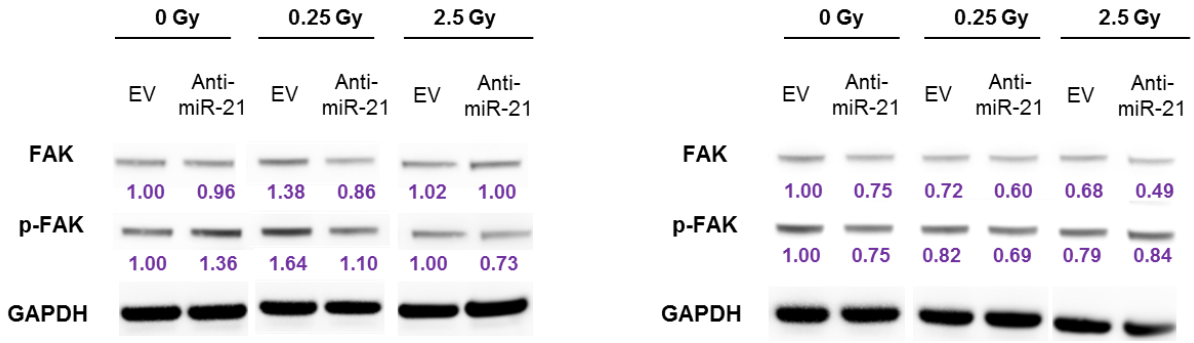

Figure 57. Representative blots of FAK and p-FAK protein changes after radiation. Representative blots of FAK (125 kDa) and p-FAK (125 kDa) changes in EV and anti-miR-21 treated MCF-10A cells after 0.25 Gy and 2.5 Gy dose of radiation 4 hours (left) and 24 hours (right) after radiation. Numbers represent fold changes calculated by normalization of each band value to the value of EV 0 Gy sample for each time point. GAPDH (37 kDa) is used as endogenous control.

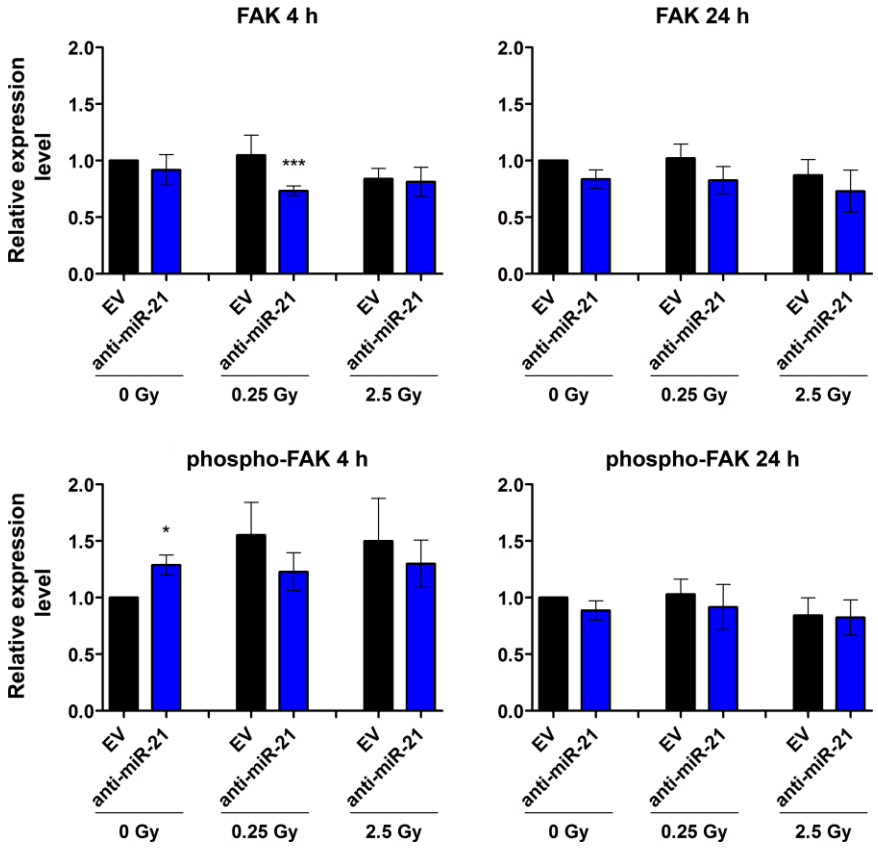

Figure 58. Western blot analysis of FAK and phospho-FAK 4 hours and 24 hours after radiation in MCF-10A cells. Quantification for FAK (upper row) and phospho-FAK (lower row) 4 hours (left) and 24 hours (right) after radiation, relative to GAPDH. Expressed fold changes are calculated by normalization to the value of EV 0 Gy sample. Mean values and standard error of mean (SEM) are shown (n=4). The Student's t-test was used for statistical analysis. *p <0.05, ***p <0.001

Expression of phospho-FAK was slightly increased at 4 hour time point compared to EV treated cells and decreased but not significantly after 24 hours which is in correlation with previously showed results in Figure 57.

Further members of downstream signaling pathway of integrins and FAK were analysed.

Representative Western blot of changes in ERK1/2 and phospho-ERK1/2 protein expression after radiation exposure is presented in Figure 59. The expression of total ERK1 showed that 4 hours after radiation it was either downregulated (in sham-irradiated and cells exposed to 0.25 Gy) or not changed after 2.5 Gy in anti-miR-21 treated cells, compared to EV cells. After 24 hours only change noticed was in anti-miR-21 treated cells after exposure to 2.5 Gy where it was upregulated. ERK2 expression was not changed at 4 hour time point, while after 24 hours its expression showed tendency to be diminished in anti-miR-21 treated cells in sham-irradiated and ones exposed to 0.25 Gy and 2.5 Gy dose of radiation.

Phospho-ERK2 (p-ERK2) expression was significantly downregulated in anti-miR-21 treated cells 4 hours after 0.25 Gy and 2.5 Gy, compared to EV treated MCF-10A cells. The changes in p-ERK1 were following the changes seen in p-ERK2.

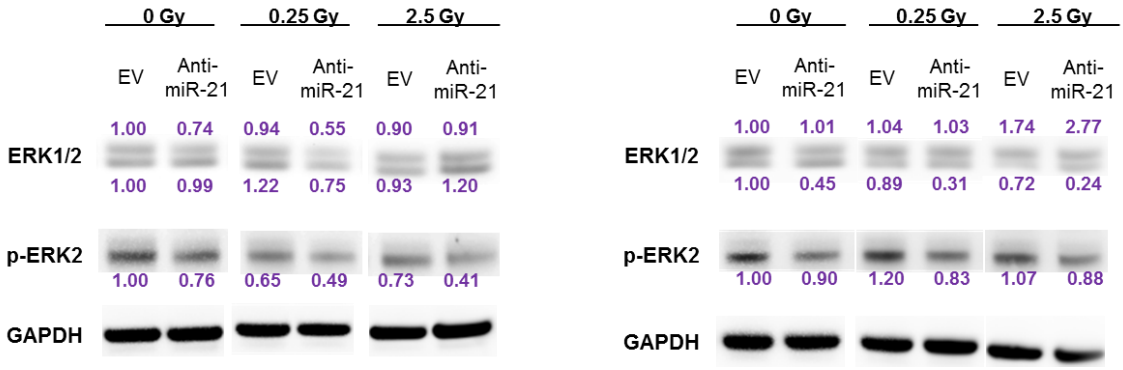

Figure 59. Representative blots of ERK1/2 and p-ERK2 proteins after radiation. Representative blots of ERK1/2 (44 and 42 kDa) and phospho-ERK2 (42 kDa) protein changes in EV and anti-miR-21 treated MCF-10A cells after low and medium dose of radiation 4 (left) and 24 (right) hours after radiation. Expressed fold changes are calculated by normalization to the value of EV 0 Gy sample. GAPDH (37 kDa) is used as endogenous control.

The expression of ERK1/2 and phospho-ERK1/2 was done for 6 biological replicates and these data are presented in Figure 60. Expression of ERK1 and ERK2 and phospho-ERK2 confirmed same trend of changes as previously presented and described in Figure 59.

Second part of integrin pathway is JNK1/2 kinase activity according to the previously published data [211].

MiR-21 knockdown affected the expression of total JNK1 and JNK2 and also its phosphorylated forms 4 hours and 24 hours after exposure to radiation. The expression of JNK1 in anti-miR-21 treated cells was downregulated compared to EV cells, in sham-irradiated and cells exposed to 0.25 Gy and 2.5 Gy. Total JNK2 was also significantly downregulated in cells with miR-21 knockdown. Exposure to radiation also contributed to further downregulation of JNK1/2 protein expressions, compared to the levels in sham-irradiated anti-miR-21 treated MCF-10A cells.

Expression of phospho-JNK1 and phospho-JNK2 was extremely lowered after miR-21 knockdown compared to EV treated cells, the radiation did have moderate but significant additional effect on their expression levels (Figure 61). The expression of JNK1/2 and phospho-JNK1/2 was done for 4 biological replicates and these data are presented in Figure 62. Data showed that miR-21 knockdown downregulates the expression of total JNK1 and JNK2, 4 hours and 24 hours after radiation while this effect was more prominent for phospho-JNK1 and phospho-JNK2 at both time points. Dose of 2.5 Gy had additional effect on phospho-JNK1 after 4 hours and on phospho-JNK2 24 hours after exposure.

The expected downregulation of the downstream targets of integrin signaling pathway (according to the predictions) is shown only with JNK1/2 and its phosphorylated forms. Expression of these proteins was significantly downregulated at both time points.

Interestingly, for the first time, it is presented that miR-21 knockdown has the selective influence on JNK activity, with small changes also seen in ERK1/2 activity. According to *in silico* predictions, JNK1/2 and ERK1/2 are not direct targets of miR-21 but the MAP3K1, as upstream regulator of JNK1/2 and ERK1/2, can be. MiR-21 could possibly

influence the activity of MAPK pathway with the potent selection of JNK1/2 as it is documented in our work.

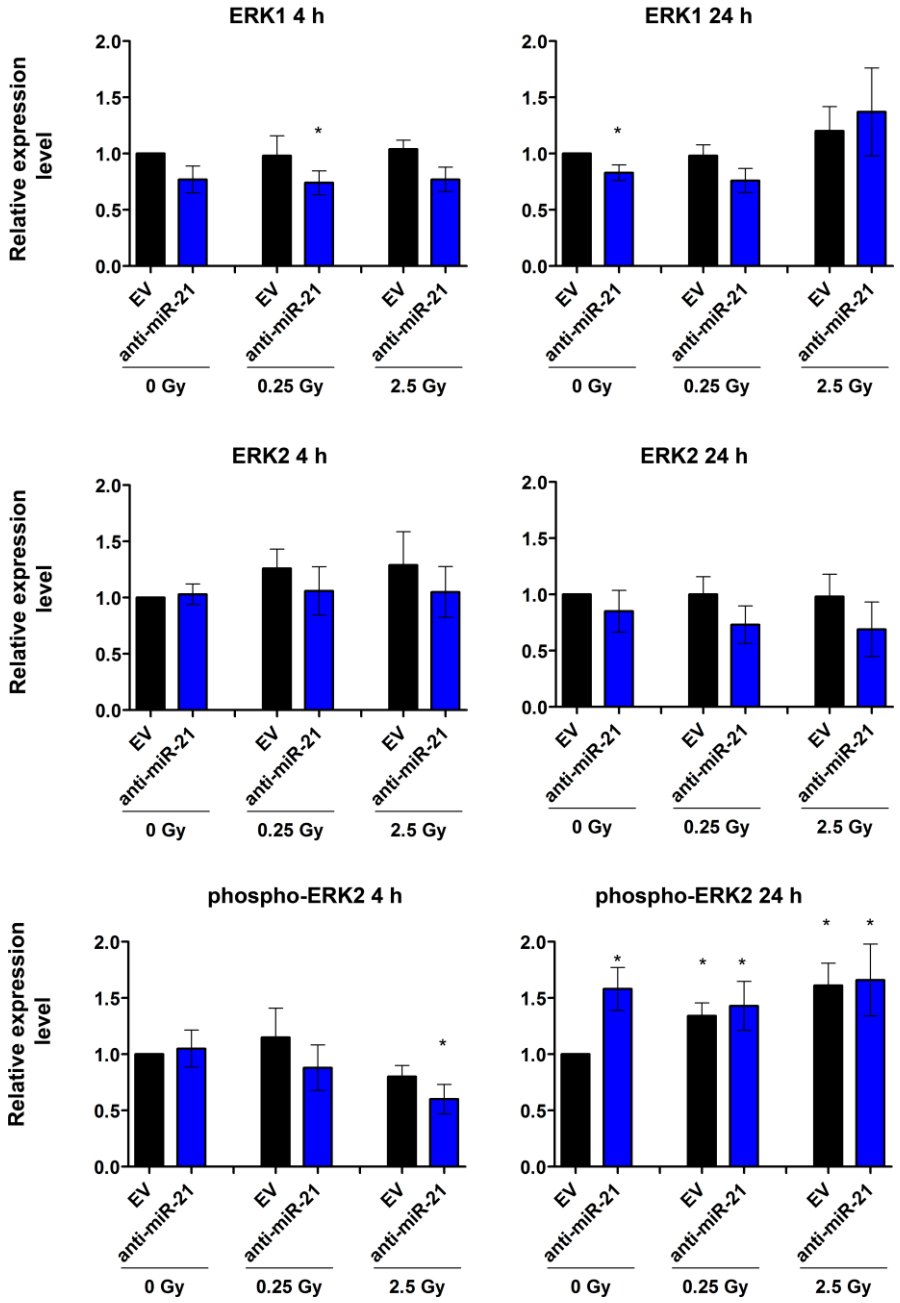

Figure 60. Western blot analysis of ERK1/2 and phospho-ERK2 4 and 24 hours after radiation in MCF-10A cells. Quantification of Western blots for ERK1/2 (upper and middle row) and phospho-ERK2 (lower row) protein expression 4 (left) and 24 hours (right) after radiation of MCF-10A cells. Graphs represent quantification of proteins relative to GAPDH. Expressed fold changes are calculated by normalization to the value of EV 0 Gy sample. Mean values and standard error of mean (SEM) are shown (n=6). The Student's t-test was used for statistical analysis.*p <0.05, **p <0.01.

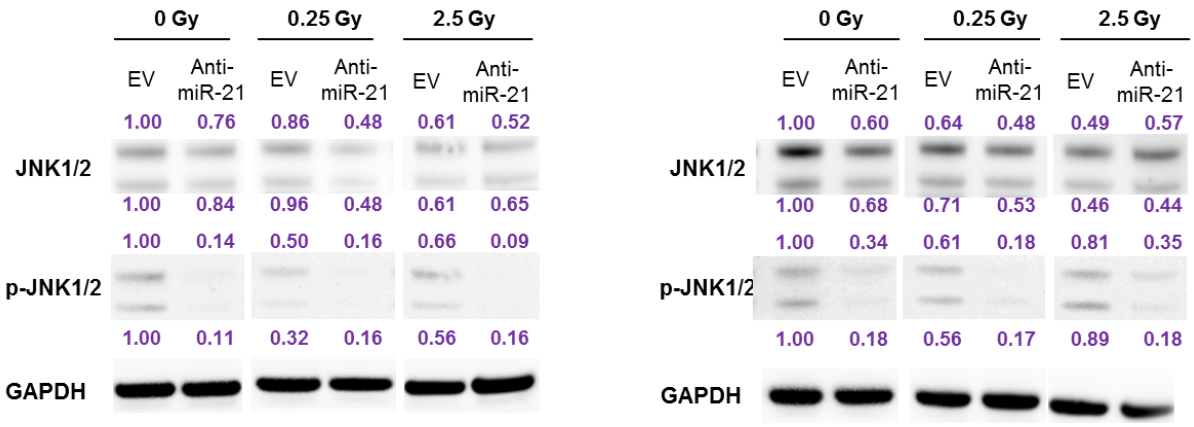

Figure 61. Representative blots of JNK1/2 and p-JNK1/2 proteins after radiation. Representative blots of JNK1/2 (54 and 46 kDa) and phospho-JNK1/2 (54 and 46 kDa) in EV and anti-miR-21 treated MCF-10A cells after low and medium dose of radiation 4 (left) and 24 (right) hours after radiation. Expressed fold changes are calculated by normalization to the value of EV 0 Gy sample. GAPDH (37 kDa) is used as endogenous control.

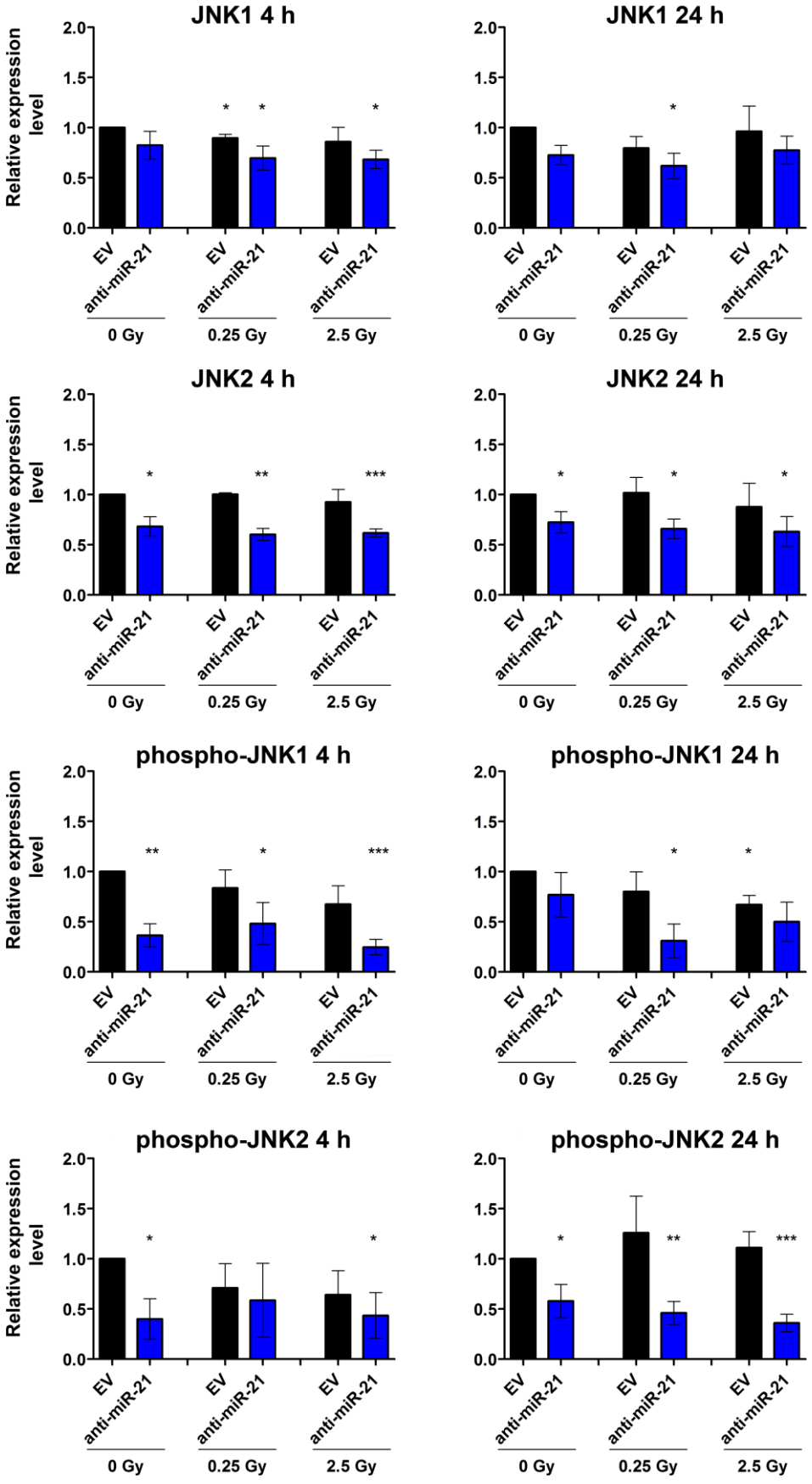
JNK1 4 h
JNK1 24 h
JNK2 4 h
JNK2 24 h
phospho-JNK1 4 h
phospho-JNK1 24 h
phospho-JNK2 4 h
phospho-JNK2 24 h
Relative expression level
2.0
1.5
1.0
0.5
0.0
EV
anti-miR-21
0 Gy
0.25 Gy
2.5 Gy

Figure 62. Western blot analysis of JNK1/2 and phospho-JNK1/2 4 and 24 hours after radiation in MCF-10A cells. Quantification of Western blots for JNK1/2 (upper two rows) and phospho-JNK1/2 (lower two rows) protein expression 4 (left) and 24 hours (right) after radiation of MCF-10A cells. Graphs represent quantification of proteins relative to GAPDH. Expressed fold changes are calculated by normalization to the value of EV 0 Gy sample. Mean values and standard error of mean (SEM) are shown (n= 4). The Student's t-test was used for statistical analysis.*p <0.05, **p <0.01, ***p<0.001.

5 DISCUSSION

MiRNAs are key molecular components of the cell in both normal and pathologic states [212]. They regulate the translation of broad set of mRNAs and therefore hold a great potential as targets for cancer therapy [213, 214]. At the same time, the dysregulation of miRNAs present an emerging hallmark of cancer, in the tumour itself as well as in the surrounding microenvironment [215, 216]. Exposure to ionizing radiation may also be monitored by the changes in expression of certain miRNAs which have been proven in recent studies in humans and mice (such as members of let-7 family, miR-21, miR-125a, miR-22, miR-222) but a regulatory role of these miRNAs in the radiation response still remains unclear [63, 66, 217, 218]. Certain miRNAs, named oncomiRs, play a role in promoting the onset and growth of cancers when overexpressed [219]. MiR-21, as one of the first described oncomiRs [34], has a crucial role in tumour cell proliferation [111], apoptosis [220], invasion, and metastasis [221] as well as also promoting radioresistance [195, 222, 223]. Inhibition of oncomiRs using antisense oligomers currently presents an evolving therapeutic strategy [35, 107]. The tissue-specific delivery of siRNAs to the cancer cells still presents big challenge, therefore it is of great importance to understand the effects of miR-21 inhibition on healthy tissue surrounding the cancer.

In the present study we have investigated the hypothesis that exposure to low and medium dose of radiation will result in miRNA profile changes. We also wanted to investigate how treatment with anti-miR-21 in combination with radiation might affect breast cancer (MDA-MB-361) and non-transformed mammary epithelial cells (MCF-10A).

The goal of this study was therefore to determine whether there are differences in the response of MCF-10A to radiation after miR-21 inhibition and to elucidate if combination of anti-miR-21 treatment with radiation is a potential breast cancer therapeutical strategy without serious side-effects on healthy surrounding tissue.

5.1 Upregulated miRNAs after low dose and medium dose of irradiation in MCF-10A cells

The first part of the project was designed to detect changes in miRNAs expression profiles in MCF-10A cell line 4 hours and 24 hours after exposure to low dose (0.25 Gy) and medium dose of radiation (2.5 Gy). MiRNA array analyses established that ~ 30 % of 384 analysed miRNAs was detectable in MCF-10A cells (Table 16). Differences in miRNAs expression after radiation were evident. The early response to radiation exposure is mainly a decrease in miRNA levels after both doses (Figure 11 and Figure 12) followed by the increase in individual miRNA levels 24 hours post-irradiation (Figure 13 and Figure 14). After 24 hours post irradiation, most of detected miRNAs were upregulated compared to 4 hour time point, which led to conclusion that later time point might be more suitable for tracking the changes. These obtained data correlate with previously published data in human fibroblasts where the early response to radiation exposure was a decrease of miRNA levels followed by increase at later time points [224].

Seven miRNAs were selected for further validation according to their expression changes obtained with Low density array analyses and their role in breast cancer (tumorigenesis). Two additional miRNAs (not present on array) were also selected: miR-335* (added in order to check expression of both miR-335 products) and miR-1226 (according to previously published data [92]). In order to validate changes seen in arrays, total of nine miRNAs were analysed in details with single qRT-PCR assay analyses using MCF-10A cells after irradiation. With single assays, we were able to validate changes detected in Low density arrays of 4 miRNAs: miR-21, miR-221, miR-335 and miR-494 (Table 18). For 3 miRNAs we have performed the time line analysis after radiation to investigate if other time points should also be considered for further experiments (Figure 16). MiR-21 and miR-221 expression was not significantly changed after low dose (0.25 Gy) radiation but after 2.5 Gy dose changes were more prominent. Significant changes in miRNA expressions were detected at later time points (from 6 hour on). Lower dose did not have such strong impact on miR-21 and miR-221 expression (particular in early time points) as it is detected after exposure to 2.5 Gy. This observation is not in correlation with published data [217] where miR-21 expression

was increased 3 and 8 hours after exposure to low dose of 0.1 and 0.4 Gy in fibroblast (AG1522) cell line. In HUVEC cells [225] miR-221 expression showed transient increase 1 hour after exposure to 0.25 Gy which, at 2 and 4 hour time points, was reduced to normal levels which is also seen in our data.

To investigate if these miRNA expression changes are characteristic only for non-tumorigenic mammary epithelial cells, we had tested expression of the same 9 miRNAs in breast cancer cell line MDA-MB-361 (Figure 17). Expression profiles of miR-21, miR-221 and miR-891 were opposite to the changes detected in MCF-10A which suggest that these miRNAs can potentially be considered as breast cancer markers. Differential miR-21 response to radiation is detected between MCF-10A and MDA-MB-361 cells and possible explanation could be dependent on higher endogenous (~ 4 fold) miR-21 expression levels in cancer cells (Figure 18) and correlates with previously published data that miR-21 is overexpressed in most human cancers [34, 226-229]. Observed increase in miR-21 expression 24 hours after irradiation in MCF-10A is in correlation with previous work showing that miR-21 is upregulated in different cell types of mammalian cells in response to ionizing radiation [66, 230-232]. Over-expression of miR-21, as consequence of irradiation, can lead to transforming non-tumorigenic cells into tumorigenic ones as it was proved for hepatocytes [233].

Because miR-21 has a major role in cancer progression [132, 221, 226, 227] it represents a strong candidate target for cancer therapy and its downregulation is of promising therapeutic importance.

It has been shown that treatment with anti-miR-21 oligonucleotides reduced breast cancer growth, decreased the viability of hepatocellular carcinoma (HCC) [228], and colon cancer cells [229] by inducing apoptosis [234]. The use of antisense based oligonucleotide (anti-miR-21) in therapy is still challenging due to their suboptimal delivery and low scalability [235] and there is still no clear evidences for or against a lack of potentially damaging anti-miR-21 effects on normal, cancer-surrounding tissue. We decided to investigate these effects in MCF-10A cells which were not described till now.

5.2 MiR-21 knockdown does not significantly influence cell viability, 2D or 3D growth, colony formation ability or the cell cycle of MCF-10A cells

We have detected endogenous levels of miR-21 to be higher in MDA-MB-361 cells compared to MCF-10a (Figure 18) which is in relation with the data obtained in previous studies stating that the overexpression of miR-21 is one characteristic of breast cancer cells compared to normal adjacent cancer tissues [95, 236].

Inhibition of miR-21 is performed using the lentiviral vector-mediated transfer [237] in order to enable long-term miR-21 downregulation and was successful in both cell lines (Figure 19). The colony formation assay showed that after anti-miR-21 treatment MCF-10A cells do not show significant changes in proliferation compared to EV treated cells. This is unlike the MDA-MB-361 breast cancer cells whose proliferation ability was tremendously affected by it (Figure 23, Figure 24). Cell viability analyses also showed that MCF-10A cells express the increase in number of viable cells at later time points indicating that they still retain the ability to proliferate which was not detected with cancer cell line. All this indicates that anti-miR-21 treatment has strong effect on breast cancer cell line MDA-MB-361. The effect of anti-miR-21 mediated cell growth and proliferation inhibition in cancer cells was also confirmed for MCF-7 [95] and T47D [195] breast cancer cell line. Therefore, our data suggest the possibility that use of anti-miR-21 treatment can have strong inhibitory effect on proliferation and growth of breast cancers with less possibility to damage surrounding normal cells.

Next to noticing the effect of miR-21 inhibition as delayed growth of MDA-MB-361 but not of MCF-10A cells, we also wanted to see if this is present in a 3D spheroid models as they mimic better the *in vivo* conditions [238, 239]. Monitoring the growth of 3D microtissues over 13 days, we detected that MDA-MB-361 cells after miR-21 inhibition are smaller in size compared to EV treated cells. The sizes of MCF-10A 3D microtissues (EV or anti-miR-21) were similar in the beginning, but they show the tendency to slightly shrink during the period of growth and particular after being exposed to 2.5 Gy dose of radiation (Figure 43). Anti-miR-21 treated MCF-10A cells exposed to 0.25 Gy did not show growth delay compared to EV treated cells, but the dose of 2.5 Gy seemed to influence the growth of EV and anti-miR-21 treated cells 9

days after treatment (Figure 44). On the other side, the size of anti-miR-21 sham-irradiated MDA-MB-361 3D microtissues was reduced to half, compared to EV treated cells. The size of anti-miR-21 3D microtissues did not change from day 0 to day 13, possibly due to already strong inhibitory effect of miR-21 knockdown. Dose of 2.5 Gy had additional effect on growth delay in EV and anti-miR-21 treated cells at day 9 (Figure 45). The growth delay effect of combined anti-miR-21 and radiation treatment in 3D-microtissue analysis of MDA-MB-361 cells is in correlation with results obtained in 2D cell culture.

All above mentioned results for the MDA-MB-361 cell line correlate to the previously described suppression of cell growth and proliferation after miR-21 knockdown in another breast cancer cell lines (MCF-7, MDA-MB-231) *in vitro* as well as suppression of its xenograft growth [95, 109]. For MDA-MB-231 breast cancer cell line opposing results exist, showing that their cell growth is not changed with this treatment which could be explained by efficiency of transfection using siRNA oligonucleotide method [99].

5.3 Anti-miR-21 treatment increases apoptosis and reduce the G2 cell fraction in MDA-MB-361 cells but not in MCF-10A cells

Since we have noticed that anti-miR-21 has a strong effect on MDA-MB-361 cells and that their cell viability was affected, we decided to analyse the cell cycle of both cell lines. The differences in cell cycle distribution between MCF-10A (Figure 27) and MDA-MB-361 (Figure 28) after miR-21 inhibition were detected. Significant increase in subG1 population of MDA-MB-361 cells was detected after miR-21 inhibition compared to EV cells, whereas MCF-10A cells did not show any changes in their subG1 fraction. Radiation did not influence further fluctuations in the subG1 cell cycle analysis. As a result of increased subG1 population in breast cancer cell line, prominent reduction in number of cells in S and G2 phase were noticed while that was not visible with MCF-10A cells. Previous studies have shown that G2/M cell cycle arrest upon irradiation can predict the level of radioresistance of tumor cells [213]. Reduced cell viability as well as induction of apoptosis, as a result of miR-21 knockdown in breast cancer cells, were also previously described in MDA-MB-231 cell line [240]. The observed reduction in G2

phase correlates further with observed reduced cell viability of tumour cells. Such effect resulting in changes of G2 block in cancer cells confirms the results previously reported for breast cancer, colon cancer and glioblastoma cell lines [109, 195, 241].

Possible explanation why non-tumorigenic mammary epithelial MCF-10A cells react differently than MDA-MB-361 breast cancer cells to the combined treatment of anti-miR-21 and radiation could be the oncomiR addiction of cancer cells [100, 242]. Due to the fact that miR-21 is already overexpressed in the MDA-MB-361 cells and that it may enable cancerous features [132, 221, 226], its inhibition has potent effect on survival of cancer cells and exactly this disparity between tumorigenic and non-tumorigenic cells can further support the idea of using miR-21 inhibitors in future designs of cancer treatments [163, 234, 243]. MiR-21 represents a potent oncomiR and numerous studies showed that the miR-21-initiated malignancy can be stopped or reversed, with the depletion of miR-21. It was published in *in vivo* mouse model that overexpression of miR-21 led to a pre-B malignant lymphoid-like phenotype while its inactivation resulted in the tumours regression as a result of apoptosis [100]. Since miR-21 knockdown had strong inhibitory effect on proliferation and cell cycle of MDA-MB-361 breast cancer cell line, but not on the MCF-10A cell line, suggest that this treatment could be used in order to stop or reverse cancerous features without having negative impact on normal cells.

5.4 Anti-miR-21 treatment in MCF-10A cells results in absence of phosphorylated JNK1/2 protein

Since the effects of combined anti-miR-21 and radiation treatment are not previously described in non-cancerous cells, we investigated what kind of changes miR-21 inhibition in MCF-10A cells can trigger on protein level. For this purpose, proteins after each radiation treatment were isolated, labelled and further analysed using ICPL labelling. Changes between anti-miR-21 and EV treated cells were detected and compared amongst samples exposed to low (0.25 Gy) and medium dose (2.5 Gy) of radiation.

The number of significantly upregulated proteins in anti-miR-21 treated sham-irradiated and cells exposed to 0.25 Gy dose of radiation after 24 hours (Table 22) is higher than in group of samples analysed 4 hours post-irradiation (Table 21). After dose of 2.5 Gy,

the increase in significantly downregulated proteins is noticeable after 24 hours. This could indicate the importance of this time point for monitoring changes not only on miRNA but also on protein level. Using the bioinformatics and Ingenuity pathway analysis, the changes in MCF-10A proteomes after miR-21 knockdown and radiation suggest that integrin pathway activation is decreased with radiation and miR-21 inhibition. We have detected 5 integrin subunits, including β1 and β4 that have an important role in directing polarity and breast non-cancerous tissue structure while its expressions are usually altered in cancer cells [244]. For the validation of integrin changes after radiation, we decided to check if the downstream targets are also influenced and if yes, in which way. The decreased activation of selected downstream pathway members was expected, according to predictions, after combination of miR-21 knockdown and 2.5 Gy dose of irradiation. We detected changes in total JNK1/2 and phospho-JNK1/2 in sham-irradiated cells as well as after exposure to radiation where this was primarily the effect of miR-21 knockdown. Previously it has been described in prostate cancer that β1 downregulation increases activation of MAP2K4 (upstream regulator of JNK1), and that as a response to irradiation (*in vivo* and *in vitro*) JNK1 is being activated [245]. Since this effect was only seen in cells treated with anti-miR-21 we concluded that it could be the consequence of miR-21 inhibition (Figure 62).

JNK activation by phosphorylation can have both pro-proliferative and antiproliferative role in human cancers, dependent on cell type and on crosstalk with other kinases. Decreased phospho-JNK1/2 expression is shown to be associated with a better overall survival of patients with breast infiltrating ductal carcinoma [246]. In cancer cells, JNKs can act as “oncokinases” transducing signals that lead to cell survival and proliferation or as tumor suppressor kinases enabling the apoptosis of cancer cells. Inhibition of JNKs activity can cause the growth arrest and apoptosis of some cancer cells [137, 247].

Since we postulated that downregulation of phospho-JNK1/2 is a consequence of miR-21 knockdown and that MAP3K1 is listed as target of miR-21-5p in *in silico* predictions, we suggest that miR-21 can affect activation of JNK1/2 via its MAP3K1 upstream regulator. MAP3K1 is described as the activator of MAP2K4, further activating JNK1/2

pathway whereas MAP2K3/6 is responsible for p38 activation [248]. This could possibly be the explanation why we could see changes in JNK but not so prominent changes in ERK pathway (although the phospho-ERK1 is slightly downregulated 4 hours after irradiation) in MCF-10A cells after miR-21-5p knockdown.

Previously it has been described that downregulation of miR-21 blocks activation of JNK/c-jun or ERK/NF-κB pathways in human embryo lung fibroblasts via Pdcd4 and Spry1 (validated targets of miR-21) implying the existence of feedback regulation between miR-21 and MAPKs [249]. In our project, blocking of JNK pathway (lower expression of JNK1/2 and its phosphorylated forms in anti-miR-21 treated cells compared to EV cells) (Figure 62) was more prominent and significant then the control of ERK pathway.

Further investigations of this mechanism must be performed for the elucidation of how and if miR-21 is influencing other members of MAPK cascade.

5.5 Predicted changes in Nrf2 after anti-miR-21 treatment in MCF-10A cells

According to detected changes in proteomes, Ingenuity Pathway analysis suggested that the Nrf2 pathway is important in cell response to radiation (in parallel to detected p53 changes as standard effect of radiation [250]). Predicted changes in expression of Nrf2 can be explained as a result of exposure to ionizing radiation, during which ROS is formed [251]. Nrf2 promotes a prosurvival response in irradiated cells by ROS detoxification and promotion of DNA repair [252]. Recent studies have demonstrated that hyperactivation of the Nrf2 pathway favors the survival of not only normal but malignant cells too, enabling protection against oxidative stress [253] and radiotherapy [187]. Hyperactivation of this pathway can enable cancer cells to escape oxidative stress by expressing antioxidant target genes, phase II detoxifying enzymes and transporters promoting tumor growth and cell survival [254, 255]. Understanding the mechanisms of how Nrf2 performs its dual role might be important for developing effective strategies against cancer.

Nrf2 can be downregulated in a significant number of breast cancer patients which indicates that its expression can be different between cancer and normal cells [256].

Increased expression of Nrf2 after miR-21 inhibition in MCF-10A by Western blot analysis was seen only in one of two biological replicates without significant detected changes in total Nrf2 or its phosphorylation status (Figure 53, Figure 54). Our data do not show changes in Nrf2 expression, but due to only two biological replicates method for better and more sensitive detection of this protein needs to be established.

Nrf2 is the key transcription factor responsible for expression of cytoprotective genes. The expression of genes that are regulated by Nrf2, has been analysed by RT^2 Profiler PCR Assay. The decision to check gene expression only after 2.5 Gy was made since the low dose of radiation (0.25 Gy) did not show any differences in expression of Nrf2 in Western blot analyses (compared to sham-irradiated cells). Most of the genes were not changed in anti-miR-21 treated MCF-10A cells (when compared to EV treated) sham-irradiated cells at 24 hour time point. After combined treatment of radiation and miR-21 inhibition most dysregulated genes were downregulated, contrary to expected increase according to the IPA prediction. For the validation with the single assays 4 genes and *Nrf2* were selected. Increase in mRNA expression levels for *Nrf2* and *HMOX1* genes after combined miR-21 inhibition and 2.5 Gy dose of radiation was detected. Both Nrf2 and HMOX-1 have dual role in cells. HMOX-1 may decrease tumor initiation through the detoxification and ROS scavenging [257] but this system can also have stimulatory effect on the progression of tumors due to its anti-apoptotic and pro-migratory modulatory influence [258, 259].

Even though, according the IPA prediction, Nrf2 should be more activated in tumors after radiation, we only could confirm this tendency at the gene expression levels, but not on the protein levels, perhaps due to the too early or too late time checkpoint (24 hours) or potentially as effect of miR-21 induced translation blockage.

Till now, many alternative pathways of Nrf2 activation are described and one plausible reason for this is that all these pathways ensure the proper activation of Nrf2 under stress conditions or prevention of its constitutive activation that leads to cancer resistance to different treatments. This is a possible explanation why, after miR-21 knockdown, the absence of phospho-JNK1/2 does not result in reduced activation of Nrf2, as the other pathways (p38 or ERK1/2) can take over the regulation of Nrf2. Even

though, JNK is suggested to phosphorylate and therefore activate the Nrf2 it is not the only kinase able to do this and therefore the lack of activation by JNK can be taken over by other kinases such as ERK, PI3K, PKC and similar (Figure 5).

5.6 Conclusion

The effects of radiotherapy on the tumor adjacent healthy tissue in combination with different breast cancer treatments (including novel anti-oncomiRs) are still not well established. In order to ensure the safety of targeted anti-miR-21 treatment we designed the study to investigate combined effects using different cellular models *in vitro*. One of the goals was to detect how miRNAs expression is changed after radiation analysing non-tumorigenic mammary epithelial cells (MCF-10A) and breast cancer cells (MDA-MB-361). The differences in miRNA expressions should qualify them as specific radiation exposure markers in the future. Human miR-21 is well-known oncomiR that was differentially expressed between MCF-10A and MDA-MB-361 cells after radiation and therefore selected for further analysis.

As a novelty, in this study we show the influence of the miR-21 knockdown on 3D microtissue formation ability with increased apoptosis rate for MDA-MB-361 but not for MCF-10A cells. Non tumorigenic mammary epithelial cells were not as sensitive to the combined treatment as cancer cells and were able to overcome any obstacles caused by miR-21 knockdown and to continue with proliferation.

For the first time, in our study the regulation of JNK1/2 phosphorylation is observed after miR-21 knockdown in MCF-10A cells. We have suggested potentially new way of regulation of JNK1/2 expression and phosphorylation in mammary epithelial cells. Upregulation of Nrf2-regulated genes in MCF-10A cells 24 hours after 2.5 Gy dose was detected as a response to the radiation, which confirms protective cellular role of Nrf2 against oxidative stress.

Inhibition of miR-21 in breast cancer cells could hold a significant value for the breast cancer patients. Our findings encourage the potential future use of anti-miR-21 treatment in combination with radiation, as a novel breast cancer therapeutical strategy.

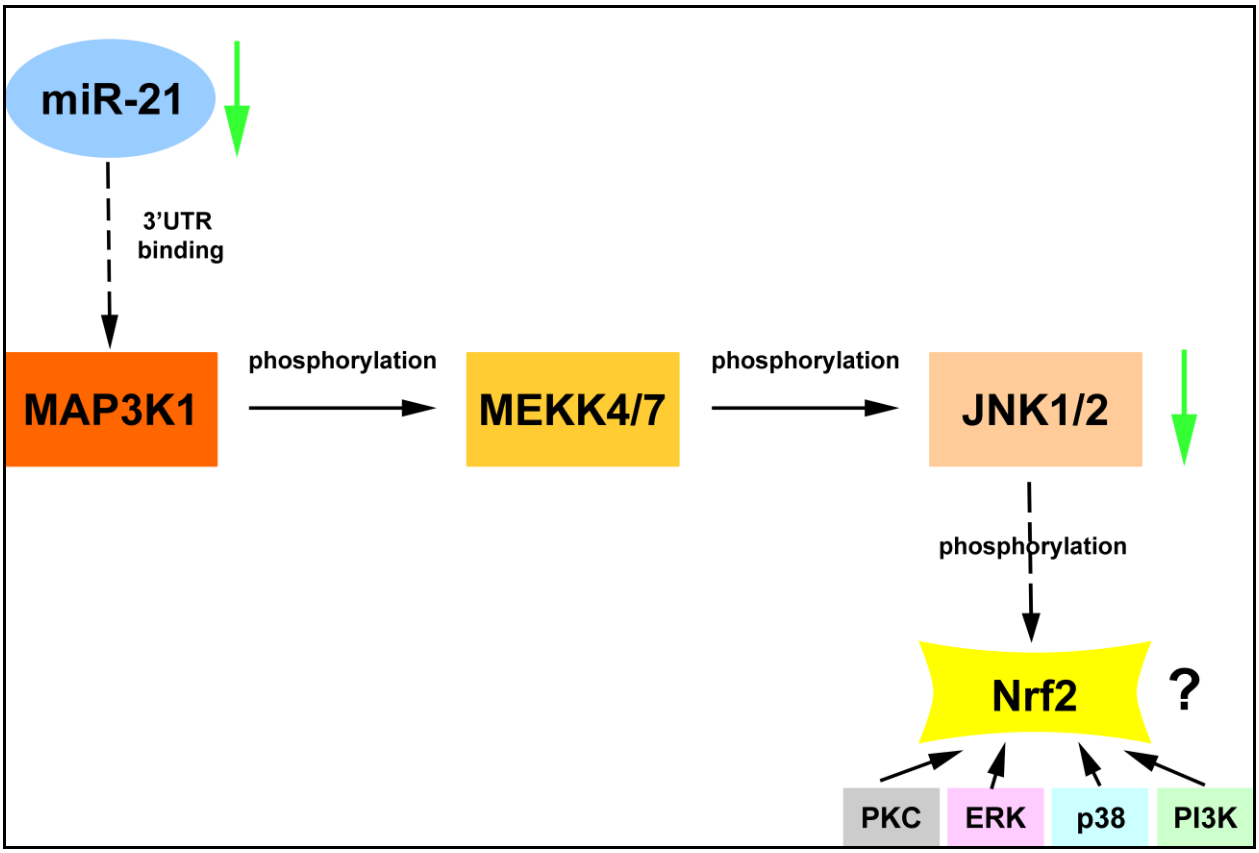
miR-21
3'UTR
binding
MAP3K1
phosphorylation
MEKK4/7
phosphorylation
JNK1/2
phosphorylation
Nrf2
?
PKC
ERK
p38
PI3K

5.7 Outlook

Due to its role in cancer biology, miR-21 has a potential of being a diagnostic and prognostic biomarker for breast cancers and its accurate profiling favors the chances for future therapies. Benefits of using miRNA inhibitory approach compared to the current strategies targeting specific genes and proteins are becoming more evident. The problem of efficient delivery is still a major obstacle and lentiviral approaches could be beneficial in future.

In this study we have shown that combination of miR-21 knockdown and radiation induces differential cellular response between non-transformed mammary epithelial cells and breast cancer cells in 2D and *3D in vitro* cellular cultures. Our findings encourage the potential future use of miR-21 as a main target in novel breast cancer therapies, in particular when combined with radiation.

Detected absence of phosphorylated forms of JNK1/2 (members of MAPK pathway) in MCF-10A cells after anti-miR-21 treatment suggests that miR-21 could be potent regulator of MAPK pathway activity. Further investigations of signaling pathways that are mediated with miR-21 will help in promotion of using miR-21 in targeted therapy approach.

REFERENCES

1. Birney, E., Stamatoyannopoulos, J.A., Dutta, A.*, et al.* Identification and analysis of functional elements in 1% of the human genome by the ENCODE pilot project. *Nature,* 447: 799-816, 2007.

2. de Hoon, M., Shin, J.W., and Carninci, P. Paradigm shifts in genomics through the FANTOM projects. *Mammalian Genome,* 26: 391-402, 2015.

3. Carninci, P., Kasukawa, T., Katayama, S.*, et al.* The transcriptional landscape of the mammalian genome. *Science,* 309: 1559-1563, 2005.

4. Djebali, S., Davis, C.A., Merkel, A.*, et al.* Landscape of transcription in human cells. *Nature,* 489: 101-108, 2012.

5. Esteller, M. Non-coding RNAs in human disease. *Nature reviews. Genetics,* 12: 861-874, 2011.

6. Bissels, U., Wild, S., Tomiuk, S.*, et al.* Absolute quantification of microRNAs by using a universal reference. *RNA,* 15: 2375-2384, 2009.

7. David, R. Non-coding RNAs: PIWI's new assistant. *Nature reviews. Molecular cell biology,* 14: 544-545, 2013.

8. Carthew, R.W. and Sontheimer, E.J. Origins and Mechanisms of miRNAs and siRNAs. *Cell,* 136: 642-655, 2009.

9. Castle, J.C., Armour, C.D., Lower, M.*, et al.* Digital genome-wide ncRNA expression, including SnoRNAs, across 11 human tissues using polyA-neutral amplification. *PLoS ONE,* 5: e11779, 2010.

10. Lai, F., Orom, U.A., Cesaroni, M.*, et al.* Activating RNAs associate with Mediator to enhance chromatin architecture and transcription. *Nature,* 494: 497-501, 2013.

11. Andersson, R., Gebhard, C., Miguel-Escalada, I.*, et al.* An atlas of active enhancers across human cell types and tissues. *Nature,* 507: 455-461, 2014.

12. Lasda, E. and Parker, R. Circular RNAs: diversity of form and function. *RNA,* 20: 1829-1842, 2014.

13. Mercer, T.R., Dinger, M.E., and Mattick, J.S. Long non-coding RNAs: insights into functions. *Nature reviews. Genetics,* 10: 155-159, 2009.

14. Wilusz, J.E., Sunwoo, H., and Spector, D.L. Long noncoding RNAs: functional surprises from the RNA world. *Genes & Development,* 23: 1494-1504, 2009.

15. Ponting, C.P., Oliver, P.L., and Reik, W. Evolution and functions of long noncoding RNAs. *Cell,* 136: 629-641, 2009.

16. Kozomara, A. and Griffiths-Jones, S. miRBase: integrating microRNA annotation and deep-sequencing data. *Nucleic Acids Research,* 39: D152-157, 2011.

17. Friedman, R.C., Farh, K.K., Burge, C.B.*, et al.* Most mammalian mRNAs are conserved targets of microRNAs. *Genome Research,* 19: 92-105, 2009.

18. MacFarlane, L.-A. and Murphy, P.R. MicroRNA: Biogenesis, Function and Role in Cancer. *Current Genomics,* 11: 537-561, 2010.

19. Bartel, D.P. MicroRNAs. *Cell,* 116: 281-297, 2004.

20. He, L. and Hannon, G.J. MicroRNAs: small RNAs with a big role in gene regulation. *Nature reviews. Genetics,* 5: 522-531, 2004.

21. Meister, G., Landthaler, M., Patkaniowska, A.*, et al.* Human Argonaute2 mediates RNA cleavage targeted by miRNAs and siRNAs. *Molecular Cell,* 15: 185-197, 2004.

22. Valencia-Sanchez, M.A., Liu, J., Hannon, G.J.*, et al.* Control of translation and mRNA degradation by miRNAs and siRNAs. *Genes & Development,* 20: 515-524, 2006.

23. Hausser, J., Syed, A.P., Bilen, B.*, et al.* Analysis of CDS-located miRNA target sites suggests that they can effectively inhibit translation. *Genome Research,* 23: 604-615, 2013.

24. Brummer, A. and Hausser, J. MicroRNA binding sites in the coding region of mRNAs: extending the repertoire of post-transcriptional gene regulation. *Bioessays,* 36: 617-626, 2014.

25. Calin, G.A. and Croce, C.M. MicroRNA signatures in human cancers. *Nature reviews. Cancer,* 6: 857-866, 2006.

26. Ha, M. and Kim, V.N. Regulation of microRNA biogenesis. *Nature reviews. Molecular cell biology,* 15: 509-524, 2014.

27. Lee, Y., Kim, M., Han, J.*, et al.* MicroRNA genes are transcribed by RNA polymerase II. *The EMBO Journal,* 23: 4051-4060, 2004.

28. Denli, A.M., Tops, B.B.J., Plasterk, R.H.A.*, et al.* Processing of primary microRNAs by the Microprocessor complex. *Nature,* 432: 231-235, 2004.

29. Bohnsack, M.T., Czaplinski, K., and Gorlich, D. Exportin 5 is a RanGTP-dependent dsRNA-binding protein that mediates nuclear export of pre-miRNAs. *RNA,* 10: 185-191, 2004.

30. Kim, V.N., Han, J., and Siomi, M.C. Biogenesis of small RNAs in animals. *Nature reviews. Molecular cell biology,* 10: 126-139, 2009.

31. Chendrimada, T.P., Gregory, R.I., Kumaraswamy, E., *et al.* TRBP recruits the Dicer complex to Ago2 for microRNA processing and gene silencing. *Nature,* 436: 740-744, 2005.

32. Winter, J., Jung, S., Keller, S., *et al.* Many roads to maturity: microRNA biogenesis pathways and their regulation. *Nature Cell Biology,* 11: 228-234, 2009.

33. Davis, B.N. and Hata, A. Regulation of MicroRNA Biogenesis: A miRiad of mechanisms. *Cell communication and signalling,* 7: 18, 2009.

34. Folini, M., Gandellini, P., Longoni, N., *et al.* miR-21: an oncomir on strike in prostate cancer. *Molecular Cancer,* 9: 1-12, 2010.

35. Kasinski, A.L. and Slack, F.J. Epigenetics and genetics. MicroRNAs en route to the clinic: progress in validating and targeting microRNAs for cancer therapy. *Nature Reviews Cancer,* 11: 849-864, 2011.

36. Hayes, J., Peruzzi, P.P., and Lawler, S. MicroRNAs in cancer: biomarkers, functions and therapy. *Trends in Molecular Medicine,* 20: 460-469, 2014.

37. Hata, A. and Lieberman, J. Dysregulation of microRNA biogenesis and gene silencing in cancer. *Science signalling,* 8: re3, 2015.

38. Jemal, A., Siegel, R., Xu, J., *et al.* Cancer statistics, 2010. *CA: A Cancer Journal for Clinicians,* 60: 277-300, 2010.

39. *American Cancer Society: Cancer Facts and Figures 2016. Atlanta, Ga: American Cancer Society* 2016; Available from: http://www.cancer.org/cancer/breastcancer/detailedguide/breast-cancer-key-statistics.

40. Blows, F.M., Driver, K.E., Schmidt, M.K., *et al.* Subtyping of Breast Cancer by Immunohistochemistry to Investigate a Relationship between Subtype and Short and Long Term Survival: A Collaborative Analysis of Data for 10,159 Cases from 12 Studies. *PLoS Medicine,* 7: e1000279, 2010.

41. Perou, C.M., Sorlie, T., Eisen, M.B., *et al.* Molecular portraits of human breast tumours. *Nature,* 406: 747-752, 2000.

42. Zhao, X., Rødland, E.A., Tibshirani, R., *et al.* Molecular subtyping for clinically defined breast cancer subgroups. *Breast Cancer Research,* 17: 29, 2015.

43. Skibinski, A. and Kuperwasser, C. The origin of breast tumor heterogeneity. *Oncogene,* 34: 5309-5316, 2015.

44. Bernardi, R. and Gianni, L. Hallmarks of triple negative breast cancer emerging at last? *Cell Research,* 24: 904-905, 2014.

45. Carey, L., Winer, E., Viale, G.*, et al.* Triple-negative breast cancer: disease entity or title of convenience? *Nature reviews. Clinical oncology,* 7: 683-692, 2010.

46. Visvader, J.E. Cells of origin in cancer. *Nature,* 469: 314-322, 2011.

47. Clarke, M.F., Dick, J.E., Dirks, P.B.*, et al.* Cancer stem cells--perspectives on current status and future directions: AACR Workshop on cancer stem cells. *Cancer Research,* 66: 9339-9344, 2006.

48. Wang, L.B., He, Y.Q., Wu, L.G.*, et al.* Isolation and characterization of human breast tumor stem cells. *Chinese journal of cellular and molecular immunology,* 28: 1261-1264, 2012.

49. Bozorgi, A., Khazaei, M., and Khazaei, M.R. New Findings on Breast Cancer Stem Cells: A Review. *Journal of Breast Cancer,* 18: 303-312, 2015.

50. Thariat, J., Hannoun-Levi, J.M., Sun Myint, A.*, et al.* Past, present, and future of radiotherapy for the benefit of patients. *Nature reviews. Clinical oncology,* 10: 52-60, 2013.

51. Early Breast Cancer Trialists' Collaborative, G. Effect of radiotherapy after breast-conserving surgery on 10-year recurrence and 15-year breast cancer death: meta-analysis of individual patient data for 10 801 women in 17 randomised trials. *Lancet,* 378: 1707-1716, 2011.

52. Ragaz, J., Olivotto, I.A., Spinelli, J.J.*, et al.* Locoregional radiation therapy in patients with high-risk breast cancer receiving adjuvant chemotherapy: 20-year results of the British Columbia randomized trial. *Journal of the National Cancer Institute,* 97: 116-126, 2005.

53. Salvo, N., Barnes, E., van Draanen, J.*, et al.* Prophylaxis and management of acute radiation-induced skin reactions: a systematic review of the literature. *Current oncology,* 17: 94-112, 2010.

54. Bray, F.N., Simmons, B.J., Wolfson, A.H.*, et al.* Acute and Chronic Cutaneous Reactions to Ionizing Radiation Therapy. *Dermatology and Therapy,* 6: 185-206, 2016.

55. Hill, R.P., Rodemann, H.P., Hendry, J.H.*, et al.* Normal tissue radiobiology: from the laboratory to the clinic. *International Journal of Radiation Oncology, Biology, and Physics,* 49: 353-365, 2001.

56. West, C.M. and Barnett, G.C. Genetics and genomics of radiotherapy toxicity: towards prediction. *Genome Medicine,* 3: 52-52, 2011.

57. Glaysher, S., Bolton, L.M., Johnson, P.*, et al.* Activity of EGFR, mTOR and PI3K inhibitors in an isogenic breast cell line model. *BMC Research Notes,* 7: 397, 2014.

58. Barnett, G.C., West, C.M.L., Dunning, A.M.*, et al.* Normal tissue reactions to radiotherapy: towards tailoring treatment dose by genotype. *Nature reviews. Cancer,* 9: 134-142, 2009.

59. Bentzen, S.M. Preventing or reducing late side effects of radiation therapy: radiobiology meets molecular pathology. *Nature reviews. Cancer,* 6: 702-713, 2006.

60. Combs, S.E., Thilmann, C., Debus, J.*, et al.* Precision radiotherapy for hemangiopericytomas of the central nervous system. *Cancer,* 104: 2457-2465, 2005.

61. Tinoco, G., Warsch, S., Gluck, S.*, et al.* Treating breast cancer in the 21st century: emerging biological therapies. *Journal of Cancer,* 4: 117-132, 2013.

62. Camphausen, K. and Tofilon, P.J. Combining radiation and molecular targeting in cancer therapy. *Cancer biology & therapy,* 3: 247-250, 2004.

63. Metheetrairut, C. and Slack, F.J. MicroRNAs in the ionizing radiation response and in radiotherapy. *Current Opinion in Genetics & Development,* 23: 12-19, 2013.

64. Zhang, B., Chen, J., Ren, Z.*, et al.* A specific miRNA signature promotes radioresistance of human cervical cancer cells. *Cancer Cell International,* 13: 118-118, 2013.

65. Li, G., Qiu, Y., Su, Z.*, et al.* Genome-Wide Analyses of Radioresistance-Associated miRNA Expression Profile in Nasopharyngeal Carcinoma Using Next Generation Deep Sequencing. *PLoS ONE,* 8: e84486, 2013.

66. Wagner-Ecker, M., Schwager, C., Wirkner, U.*, et al.* MicroRNA expression after ionizing radiation in human endothelial cells. *Radiation Oncology,* 5: 25, 2010.

67. Palayoor, S.T., John-Aryankalayil, M., Makinde, A.Y.*, et al.* Differential expression of stress and immune response pathway transcripts and miRNAs in normal human endothelial cells subjected to fractionated or single-dose radiation. *Molecular Cancer Research,* 12: 1002-1015, 2014.

68. Korpela, E. and Liu, S.K. Endothelial perturbations and therapeutic strategies in normal tissue radiation damage. *Radiation oncology* 9: 266, 2014.

69. Peng, Y. and Croce, C.M. The role of MicroRNAs in human cancer. *Signal Transduction And Targeted Therapy,* 1: 15004, 2016.

70. Han, M., Liu, M., Wang, Y.*, et al.* Antagonism of miR-21 Reverses Epithelial-Mesenchymal Transition and Cancer Stem Cell Phenotype through AKT/ERK1/2 Inactivation by Targeting PTEN. *PLoS ONE,* 7: e39520, 2012.

71. Ma, L., Teruya-Feldstein, J., and Weinberg, R.A. Tumour invasion and metastasis initiated by microRNA-10b in breast cancer. *Nature,* 449: 682-688, 2007.

72. Huang, Q., Gumireddy, K., Schrier, M.*, et al.* The microRNAs miR-373 and miR-520c promote tumour invasion and metastasis. *Nature Cell Biology,* 10: 202-210, 2008.

73. Svoronos, A.A., Engelman, D.M., and Slack, F.J. OncomiR or Tumor Suppressor? The Duplicity of MicroRNAs in Cancer. *Cancer Research,* 76: 3666, 2016.

74. Eastlack, C.S. and Alahari, K.S. MicroRNA and Breast Cancer: Understanding Pathogenesis, Improving Management. *Non-Coding RNA,* 1, 2015.

75. Tang, J., Ahmad, A., and Sarkar, F.H. The role of microRNAs in breast cancer migration, invasion and metastasis. *International journal of molecular sciences,* 13: 13414-13437, 2012.

76. van Schooneveld, E., Wildiers, H., Vergote, I.*, et al.* Dysregulation of microRNAs in breast cancer and their potential role as prognostic and predictive biomarkers in patient management. *Breast Cancer Research,* 17: 21, 2015.

77. van Schooneveld, E., Wouters, M.C., Van der Auwera, I.*, et al.* Expression profiling of cancerous and normal breast tissues identifies microRNAs that are differentially expressed in serum from patients with (metastatic) breast cancer and healthy volunteers. *Breast Cancer Research,* 14: R34, 2012.

78. Blenkiron, C., Goldstein, L.D., Thorne, N.P.*, et al.* MicroRNA expression profiling of human breast cancer identifies new markers of tumor subtype. *Genome Biology,* 8, 2007.

79. Ward, A., Balwierz, A., Zhang, J.D.*, et al.* Re-expression of microRNA-375 reverses both tamoxifen resistance and accompanying EMT-like properties in breast cancer. *Oncogene,* 32, 2013.

80. He, Y.J., Wu, J.Z., Ji, M.H.*, et al.* miR-342 is associated with estrogen receptor-α expression and response to tamoxifen in breast cancer. *Experimental and Therapeutic Medicine,* 5, 2013.

81. Gan, R., Yang, Y., Yang, X.*, et al.* Downregulation of miR-221/222 enhances sensitivity of breast cancer cells to tamoxifen through upregulation of TIMP3. *Cancer Gene Therapy,* 21, 2014.

82. Jung, E.J., Santarpia, L., Kim, J.*, et al.* Plasma microRNA 210 levels correlate with sensitivity to trastuzumab and tumor presence in breast cancer patients. *Cancer,* 118, 2012.

83. Wang, H., Tan, G., Dong, L.*, et al.* Circulating MiR-125b as a marker predicting chemoresistance in breast cancer. *PLoS ONE,* 7, 2012.

84. Mei, M., Ren, Y., Zhou, X.*, et al.* Downregulation of miR-21 enhances chemotherapeutic effect of taxol in breast carcinoma cells. *Technology in Cancer Research & Treatment,* 9, 2010.

85. Stankevicins, L., Silva Ap, A., Ventura Dos Passos, F.*, et al.* MiR-34a is up-regulated in response to low dose, low energy X-ray induced DNA damage in breast cells. *Radiation Oncology,* 8, 2013.

86. Miller, T.E., Ghoshal, K., Ramaswamy, B.*, et al.* MicroRNA-221/222 confers tamoxifen resistance in breast cancer by targeting p27Kip1. *The Journal of biological chemistry,* 283: 29897-29903, 2008.

87. Stinson, S., Lackner, M.R., Adai, A.T.*, et al.* TRPS1 targeting by miR-221/222 promotes the epithelial-to-mesenchymal transition in breast cancer. *Science signaling,* 4: ra41, 2011.

88. Scott, G.K., Goga, A., Bhaumik, D.*, et al.* Coordinate suppression of ERBB2 and ERBB3 by enforced expression of micro-RNA miR-125a or miR-125b. *The Journal of biological chemistry,* 282: 1479-1486, 2007.

89. He, H., Xu, F., Huang, W.*, et al.* miR-125a-5p expression is associated with the age of breast cancer patients. *Genetics and Molecular Research,* 14: 17927-17933, 2015.

90. Min, W., Wang, B., Li, J.*, et al.* The expression and significance of five types of miRNAs in breast cancer. *Medical science monitor basic research,* 20: 97-104, 2014.

91. Gao, Y., Zeng, F., Wu, J.Y.*, et al.* MiR-335 inhibits migration of breast cancer cells through targeting oncoprotein c-Met. *Tumour biology,* 36: 2875-2883, 2015.

92. Jin, C., Rajabi, H., and Kufe, D. miR-1226 targets expression of the mucin 1 oncoprotein and induces cell death. *International Journal of Oncology,* 37: 61-69, 2010.

93. Chen, P.Y., Manninga, H., Slanchev, K.*, et al.* The developmental miRNA profiles of zebrafish as determined by small RNA cloning. *Genes & Development,* 19: 1288-1293, 2005.

94. Hayashi, T., Koyama, N., Azuma, Y.*, et al.* Mesenchymal miR-21 regulates branching morphogenesis in murine submandibular gland in vitro. *Developmental Biology,* 352: 299-307, 2011.

95. Si, M.L., Zhu, S., Wu, H.*, et al.* miR-21-mediated tumor growth. *Oncogene,* 26: 2799-2803, 2007.

96. Huang, T.H., Wu, F., Loeb, G.B.*, et al.* Up-regulation of miR-21 by HER2/neu signaling promotes cell invasion. *The Journal of Biological Chemistry,* 284: 18515-18524, 2009.

97. Lee, J.A., Lee, H.Y., Lee, E.S.*, et al.* Prognostic Implications of MicroRNA-21 Overexpression in Invasive Ductal Carcinomas of the Breast. *Journal of breast cancer,* 14: 269-275, 2011.

98. Song, B., Wang, C., Liu, J.*, et al.* MicroRNA-21 regulates breast cancer invasion partly by targeting tissue inhibitor of metalloproteinase 3 expression. *Journal of experimental & clinical cancer research,* 29: 29, 2010.

99. Zhu, S., Wu, H., Wu, F.*, et al.* MicroRNA-21 targets tumor suppressor genes in invasion and metastasis. *Cell Research,* 18: 350-359, 2008.

100. Medina, P.P., Nolde, M., and Slack, F.J. OncomiR addiction in an in vivo model of microRNA-21-induced pre-B-cell lymphoma. *Nature,* 467: 86-90, 2010.

101. Bouchie, A. First microRNA mimic enters clinic. *Nature Biotechnology,* 31: 577-577, 2013.

102. Christopher, A.F., Kaur, R.P., Kaur, G.*, et al.* MicroRNA therapeutics: Discovering novel targets and developing specific therapy. *Perspectives in Clinical Research,* 7: 68-74, 2016.

103. Johar, R., Sharma, R., Kaur, A.*, et al.* Role of Reactive Oxygen Species in Estrogen Dependant Breast Cancer Complication. *Anti-Cancer Agents in Medicinal Chemistry,* 16: 190-199, 2015.

104. Liu, Q., Zou, R., Zhou, R.*, et al.* miR-155 Regulates Glioma Cells Invasion and Chemosensitivity by p38 Isforms In Vitro. *Journal of Cellular Biochemistry,* 116: 1213-1221, 2015.

105. Wang, S., Zhang, R., Claret, F.X.*, et al.* Involvement of microRNA-24 and DNA methylation in resistance of nasopharyngeal carcinoma to ionizing radiation. *Molecular Cancer Therapeutics,* 13: 3163-3174, 2014.

106. Yuan, W., Xiaoyun, H., Haifeng, Q.*, et al.* MicroRNA-218 enhances the radiosensitivity of human cervical cancer via promoting radiation induced apoptosis. *International journal of medical sciences,* 11: 691-696, 2014.

107. Stenvang, J., Petri, A., Lindow, M.*, et al.* Inhibition of microRNA function by antimiR oligonucleotides. *Silence,* 3: 1, 2012.

108. Cheng, C.J., Bahal, R., Babar, I.A.*, et al.* MicroRNA silencing for cancer therapy targeted to the tumour microenvironment. *Nature,* 518: 107-110, 2015.

109. Yan, L.X., Wu, Q.N., Zhang, Y.*, et al.* Knockdown of miR-21 in human breast cancer cell lines inhibits proliferation, in vitro migration and in vivo tumor growth. *Breast cancer research,* 13: R2, 2011.

110. Zhu, S., Si, M.L., Wu, H.*, et al.* MicroRNA-21 targets the tumor suppressor gene tropomyosin 1 (TPM1). *The Journal of biological chemistry,* 282: 14328-14336, 2007.

111. Meng, F., Henson, R., Wehbe-Janek, H.*, et al.* MicroRNA-21 regulates expression of the PTEN tumor suppressor gene in human hepatocellular cancer. *Gastroenterology,* 133: 647-658, 2007.

112. O'Day, E. and Lal, A. MicroRNAs and their target gene networks in breast cancer. *Breast cancer research,* 12: 201, 2010.

113. Qi, L., Bart, J., Tan, L.P.*, et al.* Expression of miR-21 and its targets (PTEN, PDCD4, TM1) in flat epithelial atypia of the breast in relation to ductal carcinoma in situ and invasive carcinoma. *BMC Cancer,* 9, 2009.

114. Dhillon, A.S., Hagan, S., Rath, O.*, et al.* MAP kinase signalling pathways in cancer. *Oncogene,* 26: 3279-3290, 2007.

115. Yang, S.H., Sharrocks, A.D., and Whitmarsh, A.J. MAP kinase signalling cascades and transcriptional regulation. *Gene,* 513: 1-13, 2013.

116. Haagenson, K.K. and Wu, G.S. Mitogen activated protein kinase phosphatases and cancer. *Cancer biology & therapy,* 9: 337-340, 2010.

117. Hanahan, D. and Weinberg, Robert A. Hallmarks of Cancer: The Next Generation. *Cell,* 144: 646-674, 2011.

118. Boutros, T., Chevet, E., and Metrakos, P. Mitogen-activated protein (MAP) kinase/MAP kinase phosphatase regulation: roles in cell growth, death, and cancer. *Pharmacological Reviews,* 60: 261-310, 2008.

119. Zhou, J.Y., Liu, Y., and Wu, G.S. The role of mitogen-activated protein kinase phosphatase-1 in oxidative damage-induced cell death. *Cancer Research,* 66: 4888-4894, 2006.

120. Chen, Z., Gibson, T.B., Robinson, F.*, et al.* MAP kinases. *Chemical reviews,* 101: 2449-2476, 2001.

121. Kyriakis, J.M. and Avruch, J. Mammalian mitogen-activated protein kinase signal transduction pathways activated by stress and inflammation. *Physiological Reviews,* 81: 807-869, 2001.

122. Kim, E.K. and Choi, E.J. Pathological roles of MAPK signaling pathways in human diseases. *Biochimica et biophysica acta,* 1802: 396-405, 2010.

123. Whyte, J., Bergin, O., Bianchi, A.*, et al.* Key signalling nodes in mammary gland development and cancer. Mitogen-activated protein kinase signalling in experimental models of breast cancer progression and in mammary gland development. *Breast Cancer Research* 11: 209-209, 2009.

124. Lee, S.H., Jaganath, I.B., Atiya, N.*, et al.* Suppression of ERK1/2 and hypoxia pathways by four Phyllanthus species inhibits metastasis of human breast cancer cells. *Journal of Food and Drug Analysis,* 24: 855-865, 2016.

125. Santen, R.J., Song, R.X., McPherson, R.*, et al.* The role of mitogen-activated protein (MAP) kinase in breast cancer. *The Journal of steroid biochemistry and molecular biology,* 80: 239-256, 2002.

126. Navolanic, P.M., Steelman, L.S., and McCubrey, J.A. EGFR family signaling and its association with breast cancer development and resistance to chemotherapy (Review). *International Journal of Oncology,* 22: 237-252, 2003.

127. Marampon, F., Ciccarelli, C., and Zani, B.M. Down-regulation of c-Myc following MEK/ERK inhibition halts the expression of malignant phenotype in rhabdomyosarcoma and in non muscle-derived human tumors. *Molecular cancer,* 5: 31, 2006.

128. McGlynn, L.M., Kirkegaard, T., Edwards, J.*, et al.* Ras/Raf-1/MAPK pathway mediates response to tamoxifen but not chemotherapy in breast cancer patients. *Clinical Cancer Research,* 15: 1487-1495, 2009.

129. Whelan, J.T., Hollis, S.E., Cha, D.S.*, et al.* Post-transcriptional regulation of the Ras-ERK/MAPK signaling pathway. *Journal of cellular physiology,* 227: 1235-1241, 2012.

130. Liu, F., Zheng, S., Liu, T.*, et al.* MicroRNA-21 promotes the proliferation and inhibits apoptosis in Eca109 via activating ERK1/2/MAPK pathway. *Molecular and Cellular Biochemistry,* 381: 115-125, 2013.

131. Huang, T.H., Wu, F., Loeb, G.B.*, et al.* Up-regulation of miR-21 by HER2/neu signaling promotes cell invasion. *The Journal of Biological Chemistry,* 284, 2009.

132. Liu, L.Z., Li, C., Chen, Q.*, et al.* MiR-21 induced angiogenesis through AKT and ERK activation and HIF-1alpha expression. *PLoS ONE,* 6: e19139, 2011.

133. Weston, C.R. and Davis, R.J. The JNK signal transduction pathway. *Current Opinion in Genetics & Development,* 12: 14-21, 2002.

134. Davis, R.J. Signal transduction by the c-Jun N-terminal kinase. *Biochemical Society symposium,* 64: 1-12, 1999.

135. Yang, M. and Huang, C.-Z. Mitogen-activated protein kinase signaling pathway and invasion and metastasis of gastric cancer. *World Journal of Gastroenterology,* 21: 11673-11679, 2015.

136. Bogoyevitch, M.A., Ngoei, K.R., Zhao, T.T.*, et al.* c-Jun N-terminal kinase (JNK) signaling: recent advances and challenges. *Biochimica et biophysica acta,* 1804: 463-475, 2010.

137. Bode, A.M. and Dong, Z. The functional contrariety of JNK. *Molecular Carcinogenesis,* 46: 591-598, 2007.

138. Chen, Y.R., Meyer, C.F., and Tan, T.H. Persistent activation of c-Jun N-terminal kinase 1 (JNK1) in gamma radiation-induced apoptosis. *The Journal of biological chemistry,* 271: 631-634, 1996.

139. Dhanasekaran, D.N. and Reddy, E.P. JNK Signaling in Apoptosis. *Oncogene,* 27: 6245-6251, 2008.

140. Ebelt, N.D., Cantrell, M.A., and Van Den Berg, C.L. c-Jun N-Terminal Kinases Mediate a Wide Range of Targets in the Metastatic Cascade. *Genes & Cancer,* 4: 378-387, 2013.

141. Mingo-Sion, A.M., Marietta, P.M., Koller, E.*, et al.* Inhibition of JNK reduces G2/M transit independent of p53, leading to endoreduplication, decreased proliferation, and apoptosis in breast cancer cells. *Oncogene,* 23: 596-604, 2004.

142. Bubici, C. and Papa, S. JNK signalling in cancer: in need of new, smarter therapeutic targets. *British Journal of Pharmacology,* 171: 24-37, 2014.

143. Echevarría-Vargas, I.M., Valiyeva, F., and Vivas-Mejía, P.E. Upregulation of miR-21 in Cisplatin Resistant Ovarian Cancer via JNK-1/c-Jun Pathway. *PLoS ONE,* 9: e97094, 2014.

144. Xu, G., Zhang, Y., Wei, J.*, et al.* MicroRNA-21 promotes hepatocellular carcinoma HepG2 cell proliferation through repression of mitogen-activated protein kinase-kinase 3. *BMC Cancer,* 13: 469, 2013.

145. Jia, M., Souchelnytskyi, N., Hellman, U.*, et al.* Proteome profiling of immortalization-to-senescence transition of human breast epithelial cells identified MAP2K3 as a senescence-promoting protein which is downregulated in human breast cancer. *PROTEOMICS - Clinical Applications,* 4: 816-828, 2010.

146. Peng, J. and Andersen, J.K. The role of c-Jun N-terminal kinase (JNK) in Parkinson's disease. *IUBMB Life,* 55: 267-271, 2003.

147. Humphries, J.D., Byron, A., and Humphries, M.J. INTEGRIN LIGANDS. *Journal of Cell Science,* 119: 3901-3903, 2006.

148. Hynes, R.O. Integrins: bidirectional, allosteric signaling machines. *Cell,* 110: 673-687, 2002.

149. Calderwood, D.A., Shattil, S.J., and Ginsberg, M.H. Integrins and actin filaments: reciprocal regulation of cell adhesion and signaling. *The Journal of biological chemistry,* 275: 22607-22610, 2000.

150. Guan, J.L. Role of focal adhesion kinase in integrin signaling. *The International Journal of Biochemistry & Cell Biology,* 29: 1085-1096, 1997.

151. Alberts, B., Johnson, A., Lewis, J., Morgan, D., Raff, M., Roberts, K., Walter, P, *Molecular Biology of the Cell*. 6th edition ed. 2014.

152. Kim, S.H. and Kim, S.H. Antagonistic effect of EGF on FAK phosphorylation/dephosphorylation in a cell. *Cell Biochemistry and Function,* 26: 539-547, 2008.

153. Kim, S.H., Turnbull, J., and Guimond, S. Extracellular matrix and cell signalling: the dynamic cooperation of integrin, proteoglycan and growth factor receptor. *Journal of Endocrinology,* 209: 139-151, 2011.

154. Sulzmaier, F.J., Jean, C., and Schlaepfer, D.D. FAK in cancer: mechanistic findings and clinical applications. *Nature Reviews Cancers,* 14: 598-610, 2014.

155. Luo, M. and Guan, J.-L. Focal adhesion kinase: a prominent determinant in breast cancer initiation, progression and metastasis. *Cancer Letters,* 289: 127-139, 2010.

156. Alexopoulou, A.N., Ho-Yen, C.M., Papalazarou, V.*, et al.* Tumour-associated endothelial-FAK correlated with molecular sub-type and prognostic factors in invasive breast cancer. BMC Cancer, 2014. **14**, 237 DOI: 10.1186/1471-2407-14-237.

157. Tamura, M., Gu, J., Takino, T.*, et al.* Tumor Suppressor PTEN Inhibition of Cell Invasion, Migration, and Growth: Differential Involvement of Focal Adhesion Kinase and p130<sup>Cas</sup&gt. *Cancer Research,* 59: 442, 1999.

158. Meng, F., Henson, R., Wehbe-Janek, H.*, et al.* MicroRNA-21 Regulates Expression of the PTEN Tumor Suppressor Gene in Human Hepatocellular Cancer. *Gastroenterology,* 133: 647-658, 2007.

159. Park, M.J., Kim, M.S., Park, I.C.*, et al.* PTEN suppresses hyaluronic acid-induced matrix metalloproteinase-9 expression in U87MG glioblastoma cells through focal adhesion kinase dephosphorylation. *Cancer Research,* 62: 6318-6322, 2002.

160. Al-Gubory, K.H. Environmental pollutants and lifestyle factors induce oxidative stress and poor prenatal development. *Reproductive BioMedicine Online,* 29: 17-31, 2014.

161. Misawa, M. and Takahashi, J. Generation of reactive oxygen species induced by gold nanoparticles under x-ray and UV Irradiations. *Nanomedicine,* 7: 604-614, 2011.

162. Hecht, F., Pessoa, C.F., Gentile, L.B.*, et al.* The role of oxidative stress on breast cancer development and therapy. *Tumour Biology,* 37: 4281-4291, 2016.

163. Sicard, F., Gayral, M., Lulka, H.*, et al.* Targeting miR-21 for the Therapy of Pancreatic Cancer. *Molecular Therapy,* 21: 986-994, 2013.

164. Teodoro, J.S., Gomes, A.P., Varela, A.T.*, et al.* Uncovering the beginning of diabetes: the cellular redox status and oxidative stress as starting players in hyperglycemic damage. *Molecular and Cellular Biochemistry,* 376: 103-110, 2013.

165. Reuter, S., Gupta, S.C., Chaturvedi, M.M.*, et al.* Oxidative stress, inflammation, and cancer: how are they linked? *Free radical biology & medicine,* 49: 1603-1616, 2010.

166. Trachootham, D., Alexandre, J., and Huang, P. Targeting cancer cells by ROS-mediated mechanisms: a radical therapeutic approach? *Nature reviews. Drug discovery,* 8: 579-591, 2009.

167. Jezierska-Drutel, A., Rosenzweig, S.A., and Neumann, C.A. Role of Oxidative Stress and the Microenvironment in Breast Cancer Development and Progression. *Advances in Cancer Research,* 119: 107-125, 2013.

168. Storz, P. Reactive oxygen species in tumor progression. *Frontiers in bioscience,* 10: 1881-1896, 2005.

169. Reddy, K.B. and Glaros, S. Inhibition of the MAP kinase activity suppresses estrogen-induced breast tumor growth both in vitro and in vivo. *International Journal of Oncology,* 30: 971-975, 2007.

170. Roberts, P.J. and Der, C.J. Targeting the Raf-MEK-ERK mitogen-activated protein kinase cascade for the treatment of cancer. *Oncogene,* 26: 3291-3310, 2007.

171. Ostrakhovitch, E.A. and Cherian, M.G. Inhibition of extracellular signal regulated kinase (ERK) leads to apoptosis inducing factor (AIF) mediated apoptosis in epithelial breast cancer cells: the lack of effect of ERK in p53 mediated copper induced apoptosis. *Journal of Cellular Biochemistry,* 95: 1120-1134, 2005.

172. Gorrini, C., Harris, I.S., and Mak, T.W. Modulation of oxidative stress as an anticancer strategy. *Nature Reviews. Drug Discovery,* 12: 931-947, 2013.

173. Kumar, H., Kim, I.-S., More, S.V.*, et al.* Natural product-derived pharmacological modulators of Nrf2/ARE pathway for chronic diseases. *Natural Product Reports,* 31: 109-139, 2014.

174. Nguyen, T., Sherratt, P.J., Nioi, P.*, et al.* Nrf2 controls constitutive and inducible expression of ARE-driven genes through a dynamic pathway involving nucleocytoplasmic shuttling by Keap1. *The Journal of biological chemistry,* 280: 32485-32492, 2005.

175. Nguyen, T., Nioi, P., and Pickett, C.B. The Nrf2-Antioxidant Response Element Signaling Pathway and Its Activation by Oxidative Stress. *The Journal of biological chemistry,* 284: 13291-13295, 2009.

176. Taguchi, K., Motohashi, H., and Yamamoto, M. Molecular mechanisms of the Keap1-Nrf2 pathway in stress response and cancer evolution. *Genes to Cells,* 16: 123-140, 2011.

177. Bryan, H.K., Olayanju, A., Goldring, C.E.*, et al.* The Nrf2 cell defence pathway: Keap1-dependent and -independent mechanisms of regulation. *Biochemical Pharmacology,* 85: 705-717, 2013.

178. Kansanen, E., Kivela, A.M., and Levonen, A.L. Regulation of Nrf2-dependent gene expression by 15-deoxy-Delta12,14-prostaglandin J2. *Free Radical Biology & Medicine,* 47: 1310-1317, 2009.

179. Sun, Z., Huang, Z., and Zhang, D.D. Phosphorylation of Nrf2 at multiple sites by MAP kinases has a limited contribution in modulating the Nrf2-dependent antioxidant response. *PLoS ONE,* 4: e6588, 2009.

180. Rojo, A.I., Medina-Campos, O.N., Rada, P.*, et al.* Signaling pathways activated by the phytochemical nordihydroguaiaretic acid contribute to a Keap1-independent regulation of Nrf2 stability: Role of glycogen synthase kinase-3. *Free radical biology & medicine,* 52: 473-487, 2012.

181. Ramos-Gomez, M., Dolan, P.M., Itoh, K.*, et al.* Interactive effects of nrf2 genotype and oltipraz on benzo[a]pyrene-DNA adducts and tumor yield in mice. *Carcinogenesis,* 24: 461-467, 2003.

182. Rachakonda, G., Sekhar, K.R., Jowhar, D.*, et al.* Increased cell migration and plasticity in Nrf2-deficient cancer cell lines. *Oncogene,* 29: 3703-3714, 2010.

183. Jaramillo, M.C. and Zhang, D.D. The emerging role of the Nrf2-Keap1 signaling pathway in cancer. *Genes & Development,* 27: 2179-2191, 2013.

184. Singh, A., Misra, V., Thimmulappa, R.K.*, et al.* Dysfunctional KEAP1-NRF2 interaction in non-small-cell lung cancer. *PLoS Medicine,* 3: e420, 2006.

185. Wang, X.-J., Sun, Z., Villeneuve, N.F.*, et al.* Nrf2 enhances resistance of cancer cells to chemotherapeutic drugs, the dark side of Nrf2. *Carcinogenesis,* 29: 1235-1243, 2008.

186. Kim, Y.R., Oh, J.E., Kim, M.S.*, et al.* Oncogenic NRF2 mutations in squamous cell carcinomas of oesophagus and skin. *The Journal of pathology,* 220: 446-451, 2010.

187. Zhang, P., Singh, A., Yegnasubramanian, S.*, et al.* Loss of Kelch-like ECH-associated protein 1 function in prostate cancer cells causes chemoresistance and radioresistance and promotes tumor growth. *Molecular Cancer Therapeutics,* 9: 336-346, 2010.

188. No, J.H., Kim, Y.-B., and Song, Y.S. Targeting Nrf2 Signaling to Combat Chemoresistance. *Journal of Cancer Prevention,* 19: 111-117, 2014.

189. Na, H.K. and Surh, Y.J. Oncogenic potential of Nrf2 and its principal target protein heme oxygenase-1. *Free radical biology & medicine,* 67: 353-365, 2014.

190. Soule, H.D., Maloney, T.M., Wolman, S.R.*, et al.* Isolation and Characterization of a Spontaneously Immortalized Human Breast Epithelial Cell Line, MCF-10. *Cancer Research,* 50: 6075-6086, 1990.

191. Imbalzano, K.M., Tatarkova, I., Imbalzano, A.N.*, et al.* Increasingly transformed MCF-10A cells have a progressively tumor-like phenotype in three-dimensional basement membrane culture. *Cancer Cell International,* 9: 7-7, 2009.

192. Tiscornia, G., Singer, O., and Verma, I.M. Production and purification of lentiviral vectors. *Nature Protocols,* 1: 241-245, 2006.

193. Hofig, I., Atkinson, M.J., Mall, S.*, et al.* Poloxamer synperonic F108 improves cellular transduction with lentiviral vectors. *Journal of Gene Medicine,* 14: 549-560, 2012.

194. Anastasov, N., Hofig, I., Mall, S.*, et al.* Optimized Lentiviral Transduction Protocols by Use of a Poloxamer Enhancer, Spinoculation, and scFv-Antibody Fusions to VSV-G. *Methods Mol Biol,* 1448: 49-61, 2016.

195. Anastasov, N., Hofig, I., Vasconcellos, I.G.*, et al.* Radiation resistance due to high expression of miR-21 and G2/M checkpoint arrest in breast cancer cells. *Radiation Oncology,* 7: 206, 2012.

196. Kutner, R.H., Zhang, X.-Y., and Reiser, J. Production, concentration and titration of pseudotyped HIV-1-based lentiviral vectors. *Nature Protocols,* 4: 495-505, 2009.

197. Franken, N.A., Rodermond, H.M., Stap, J.*, et al.* Clonogenic assay of cells in vitro. *Nature proocols,* 1: 2315-2319, 2006.

198. Rafehi, H., Orlowski, C., Georgiadis, G.T.*, et al.* Clonogenic Assay: Adherent Cells. *Journal of Visualized Experiments : JoVE*: 2573, 2011.

199. Puck, T.T. and Marcus, P.I. Action of x-rays on mammalian cells. *The Journal of experimental medicine,* 103: 653-666, 1956.

200. Nusse, M., Beisker, W., Kramer, J.*, et al.* Measurement of micronuclei by flow cytometry. *Methods in cell biology,* 42 Pt B: 149-158, 1994.

201. Anastasov, N., Hofig, I., Radulovic, V.*, et al.* A 3D-microtissue-based phenotypic screening of radiation resistant tumor cells with synchronized chemotherapeutic treatment. *BMC Cancer,* 15: 466, 2015.

202. Falkenberg, N., Hofig, I., Rosemann, M.*, et al.* Three-dimensional microtissues essentially contribute to preclinical validations of therapeutic targets in breast cancer. *Cancer medicine,* 5: 703-710, 2016.

203. Livak, K.J. and Schmittgen, T.D. Analysis of Relative Gene Expression Data Using Real-Time Quantitative PCR and the 2−ΔΔCT Method. *Methods,* 25: 402-408, 2001.

204. Peterson, S.M., Thompson, J.A., Ufkin, M.L.*, et al.* Common features of microRNA target prediction tools. *Frontiers in Genetics,* 5: 23, 2014.

205. Yentrapalli, R., Azimzadeh, O., Sriharshan, A.*, et al.* The PI3K/Akt/mTOR Pathway Is Implicated in the Premature Senescence of Primary Human Endothelial Cells Exposed to Chronic Radiation. *PLoS ONE,* 8: e70024, 2013.

206. Bakshi, M.V., Barjaktarovic, Z., Azimzadeh, O.*, et al.* Long-term effects of acute low-dose ionizing radiation on the neonatal mouse heart: a proteomic study. *Radiation and Environmental Biophysics,* 52: 451-461, 2013.

207. Mann, M. and Kelleher, N.L. Precision proteomics: the case for high resolution and high mass accuracy. *Proceedings of the National Academy of Sciences of the United States of America,* 105: 18132-18138, 2008.

208. Yentrapalli, R., Azimzadeh, O., Barjaktarovic, Z.*, et al.* Quantitative proteomic analysis reveals induction of premature senescence in human umbilical vein endothelial cells exposed to chronic low-dose rate gamma radiation. *Proteomics,* 13: 1096-1107, 2013.

209. Krämer, A., Green, J., Pollard, J.*, et al.* Causal analysis approaches in Ingenuity Pathway Analysis. *Bioinformatics,* 30: 523-530, 2014.

210. Betel, D., Wilson, M., Gabow, A.*, et al.* The microRNA.org resource: targets and expression. *Nucleic Acids Research,* 36: D149-D153, 2008.

211. Eke, I. and Cordes, N. Focal adhesion signaling and therapy resistance in cancer. *Seminars in Cancer Biology,* 31: 65-75, 2015.

212. Ebert, M.S. and Sharp, P.A. Roles for microRNAs in conferring robustness to biological processes. *Cell,* 149: 515-524, 2012.

213. Liu, J., Zhu, H., Yang, X.*, et al.* MicroRNA-21 is a novel promising target in cancer radiation therapy. *Tumour biology,* 35: 3975-3979, 2014.

214. Price, C. and Chen, J. MicroRNAs in Cancer Biology and Therapy: Current Status and Perspectives. *Genes & Diseases,* 1: 53-63, 2014.

215. McManus, M.T. MicroRNAs and cancer. *Seminars in Cancer Biology,* 13: 253-258, 2003.

216. Lu, J., Getz, G., Miska, E.A.*, et al.* MicroRNA expression profiles classify human cancers. *Nature,* 435, 2005.

217. Chaudhry, M.A., Omaruddin, R.A., Kreger, B.*, et al.* Micro RNA responses to chronic or acute exposures to low dose ionizing radiation. *Molecular Biology Reports,* 39: 7549-7558, 2012.

218. Dickey, J.S., Zemp, F.J., Martin, O.A.*, et al.* The role of miRNA in the direct and indirect effects of ionizing radiation. *Radiation and Environmental Biophysics,* 50: 491-499, 2011.

219. Esquela-Kerscher, A. and Slack, F.J. Oncomirs - microRNAs with a role in cancer. *Nature reviews. Cancer,* 6: 259-269, 2006.

220. Chan, J.A., Krichevsky, A.M., and Kosik, K.S. MicroRNA-21 is an antiapoptotic factor in human glioblastoma cells. *Cancer Research,* 65: 6029-6033, 2005.

221. Asangani, I.A., Rasheed, S.A., Nikolova, D.A.*, et al.* MicroRNA-21 (miR-21) post-transcriptionally downregulates tumor suppressor Pdcd4 and stimulates invasion, intravasation and metastasis in colorectal cancer. *Oncogene,* 27: 2128-2136, 2008.

222. Gwak, H.S., Kim, T.H., Jo, G.H.*, et al.* Silencing of microRNA-21 confers radio-sensitivity through inhibition of the PI3K/AKT pathway and enhancing autophagy in malignant glioma cell lines. *PLoS ONE,* 7: e47449, 2012.

223. Summerer, I., Unger, K., Braselmann, H.*, et al.* Circulating microRNAs as prognostic therapy biomarkers in head and neck cancer patients. *British Journal of Cancer,* 113: 76-82, 2015.

224. Maes, O.C., An, J., Sarojini, H.*, et al.* Changes in MicroRNA expression patterns in human fibroblasts after low-LET radiation. *Journal of Cellular Biochemistry,* 105: 824-834, 2008.

225. Vincenti, S., Brillante, N., Lanza, V.*, et al.* HUVEC respond to radiation by inducing the expression of pro-angiogenic microRNAs. *Radiation Research,* 175: 535-546, 2011.

226. Jiang, L.-H., Ge, M.-H., Hou, X.-X.*, et al.* miR-21 regulates tumor progression through the miR-21-PDCD4-Stat3 pathway in human salivary adenoid cystic carcinoma. *Laboratory Investigation,* 95: 1398-1408, 2015.

227. Özgün, A., Karagoz, B., Bilgi, O.*, et al.* MicroRNA-21 as an Indicator of Aggressive Phenotype in Breast Cancer. *Oncology Research and Treatment,* 36: 115-118, 2013.

228. Bonci, D. MicroRNA-21 as therapeutic target in cancer and cardiovascular disease. *Recent patents on cardiovascular drug discovery,* 5: 156-161, 2010.

229. Song, M.-S. and Rossi, J.J. The anti-miR21 antagomir, a therapeutic tool for colorectal cancer, has a potential synergistic effect by perturbing an angiogenesis-associated miR30. *Frontiers in Genetics,* 4: 301, 2013.

230. Shi, Y., Zhang, X., Tang, X.*, et al.* MiR-21 is continually elevated long-term in the brain after exposure to ionizing radiation. *Radiation Research,* 177: 124-128, 2012.

231. Cellini, F., Morganti, A.G., Genovesi, D.*, et al.* Role of microRNA in response to ionizing radiations: evidences and potential impact on clinical practice for radiotherapy. *Molecules,* 19: 5379-5401, 2014.

232. Chaudhry, M.A., Sachdeva, H., and Omaruddin, R.A. Radiation-induced micro-RNA modulation in glioblastoma cells differing in DNA-repair pathways. *DNA and Cell Biology,* 29: 553-561, 2010.

233. Zhu, Y., Yu, X., Fu, H.*, et al.* MicroRNA-21 is involved in ionizing radiation-promoted liver carcinogenesis. *International Journal of Clinical and Experimental Medicine,* 3: 211-222, 2010.

234. Najafi, Z., Sharifi, M., and Javadi, G. Degradation of miR-21 induces apoptosis and inhibits cell proliferation in human hepatocellular carcinoma. *Cancer Gene Therapy,* 22: 530-535, 2015.

235. Castanotto, D. and Rossi, J.J. The promises and pitfalls of RNA-interference-based therapeutics. *Nature,* 457: 426-433, 2009.

236. Yan, L.-X., Huang, X.-F., Shao, Q.*, et al.* MicroRNA miR-21 overexpression in human breast cancer is associated with advanced clinical stage, lymph node metastasis and patient poor prognosis. *RNA,* 14: 2348-2360, 2008.

237. Anastasov, N., Klier, M., Koch, I.*, et al.* Efficient shRNA delivery into B and T lymphoma cells using lentiviral vector-mediated transfer. *Journal of Hematopathology,* 2: 9-19, 2009.

238. Yamada, K.M. and Cukierman, E. Modeling tissue morphogenesis and cancer in 3D. *Cell,* 130: 601-610, 2007.

239. Abbott, A. Cell culture: Biology's new dimension. *Nature,* 424: 870-872, 2003.

240. Motamed N, Z.M., Heidarian Y. miR-21 Knockdown Reduces Cell Viability and Induces Cell Apoptosis in Breast Cancer Cell Line MDA-MB-231. *Academia Journal of Scientific Research,* 4: 355-360, 2016.

241. Wang, P., Zou, F., Zhang, X.*, et al.* microRNA-21 negatively regulates Cdc25A and cell cycle progression in colon cancer cells. *Cancer Research,* 69: 8157-8165, 2009.

242. Sharma, S.V. and Settleman, J. Oncogene addiction: setting the stage for molecularly targeted cancer therapy. *Genes & Development,* 21: 3214-3231, 2007.

243. Cheng, C.J. and Slack, F.J. The duality of oncomiR addiction in the maintenance and treatment of cancer. *Cancer Journal,* 18: 232-237, 2012.

244. Nistico, P., Di Modugno, F., Spada, S.*, et al.* beta1 and beta4 integrins: from breast development to clinical practice. *Breast cancer research,* 16: 459, 2014.

245. Goel, H.L., Sayeed, A., Breen, M.*, et al.* beta1 integrins mediate resistance to ionizing radiation in vivo by inhibiting c-Jun amino terminal kinase 1. *Journal of Cellular Physiology,* 228: 1601-1609, 2013.

246. Yeh, Y.T., Hou, M.F., Chung, Y.F.*, et al.* Decreased expression of phosphorylated JNK in breast infiltrating ductal carcinoma is associated with a better overall survival. *International Journal of Cancer,* 118: 2678-2684, 2006.

247. Potapova, O., Gorospe, M., Dougherty, R.H.*, et al.* Inhibition of c-Jun N-terminal kinase 2 expression suppresses growth and induces apoptosis of human tumor cells in a p53-dependent manner. *Molecular and Cellular Biology,* 20: 1713-1722, 2000.

248. Roux, P.P. and Blenis, J. ERK and p38 MAPK-activated protein kinases: a family of protein kinases with diverse biological functions. *Microbiology and Molecular Biology Reviews,* 68: 320-344, 2004.

249. Shen, L., Ling, M., Li, Y.*, et al.* Feedback Regulations of miR-21 and MAPKs via Pdcd4 and Spry1 Are Involved in Arsenite-Induced Cell Malignant Transformation. *PLoS ONE,* 8: e57652, 2013.

250. Fei, P. and El-Deiry, W.S. P53 and radiation responses. *Oncogene,* 22: 5774-5783, 2003.

251. Yamamori, T., Yasui, H., Yamazumi, M.*, et al.* Ionizing radiation induces mitochondrial reactive oxygen species production accompanied by upregulation of mitochondrial electron transport chain function and mitochondrial content

under control of the cell cycle checkpoint. *Free radical biology & medicine,* 53: 260-270, 2012.

252. Sekhar, K.R. and Freeman, M.L. Nrf2 promotes survival following exposure to ionizing radiation. *Free radical biology & medicine,* 88: 268-274, 2015.

253. Ma, Q. Role of Nrf2 in Oxidative Stress and Toxicity. *Annual Review of Pharmacology and Toxicology,* 53: 401-426, 2013.

254. Lau, A., Villeneuve, N.F., Sun, Z.*, et al.* Dual roles of Nrf2 in cancer. *Pharmacological Research,* 58: 262-270, 2008.

255. Menegon, S., Columbano, A., and Giordano, S. The Dual Roles of NRF2 in Cancer. *Trends in Molecular Medicine,* 22: 578-593, 2016.

256. Loignon, M., Miao, W., Hu, L.*, et al.* Cul3 overexpression depletes Nrf2 in breast cancer and is associated with sensitivity to carcinogens, to oxidative stress, and to chemotherapy. *Molecular Cancer Therapeutics,* 8: 2432-2440, 2009.

257. Loboda, A., Damulewicz, M., Pyza, E.*, et al.* Role of Nrf2/HO-1 system in development, oxidative stress response and diseases: an evolutionarily conserved mechanism. *Cellular and Molecular Life Sciences,* 73: 3221-3247, 2016.

258. Gozzelino, R., Jeney, V., and Soares, M.P. Mechanisms of cell protection by heme oxygenase-1. *Annual Review of Pharmacology and Toxicology,* 50: 323-354, 2010.

259. Was, H., Dulak, J., and Jozkowicz, A. Heme oxygenase-1 in tumor biology and therapy. *Current Drug Targets,* 11: 1551-1570, 2010.

LIST OF FIGURES

ACKNOWLEDGMENTS

First of all, I would like to thank Prof. Dr. Michael J. Atkinson for opportunity to be a member of the Institute of Radiation Biology (ISB) and for all the support and guidance during the PhD thesis. His advices helped me to further improve myself in a scientific world and I am very grateful for the mentorship.

I would like to extend my great gratitude to my mentor Dr. Nataša Anastasov for giving me opportunity to work on a very exciting and challenging project in her group. Under Dr. Anastasov mentorship I have expand my knowledge on the topic of miRNAs, breast cancer, and lentiviruses and learned about scientific writing and data presentation.

I would also like to thank Prof. Dr. Jochen Graw, as my thesis committee member and second supervisor, for his constructive advices and feedback during thesis committee meetings.

I would like to especially thank Dr. Omid Azimzadeh for his constant help in the field of proteomics, scientific suggestions and helpful advices that were useful for the writing of the thesis.

My special thanks go to all members of the Dark.Risk project, group of extraordinary scientists who I was honored to meet and it was my great pleasure to take part in scientific discussions at annual meetings.

I thank all past and present members of Institute of Radiation Biology for their co-operation, all necessary help and wonderful memories. I would especially like to thank Theresa Heider who helped me in every aspect and without whose support the PhD experience would not be the same. I am very grateful to Sabine Richter, Lisa Mutschelknaus, Dr. Isolde Summerer, Rosi Kell and Klaudia Winkler for all the collaborations, support, great memories and lots of fun times spent in shared office.

I would like to especially thank Dr. Branka Kolundžija and Dr Vedran Bandalo for all support and advices during the writing of this thesis.

Thanks a lot to Maja Miloradović, Dr. Mayur Bakshi, and Dr. Arjen van Doorn for lots of support, help and exciting and adventurous social time that we spent in last four years.

Most of all, I would like to thank my family for lots of support during all these years.

Велику захвалност дугујем својој породици која ме је увек подржавала током свих ових година. Хвала пуно!

Thank you so much!